RESULTS

OBJECTIVE 1 : To decipher, understand and manipulate the role of microtubule-trafficking in the cell.

a. **To investigate the role of microtubules in the intracellular movement of p53 and HIF-1α.**
b. **To investigate the effects of microtubule-targeting drugs on the movement and activity of p53 and HIF-1α.**

p53

The *p53* (or *TP53*) gene was discovered in 1979 and has emerged as one of the most important cancer-related genes to date. The gene, located on chromosome 17, produces a protein product that functions as a transcription factor. The genes controlled by p53 are involved in cell division and viability. It is estimated that p53 mutations are the most frequent genetic event in human cancers, accounting for more than 50% of cases (146) **(Figure 12)**. It is predicted that in the majority of the remaining tumors, the p53 signaling pathway is inactivated by up-regulation of p53 inhibitors, such as Mdm2, or by down-regulation of p53 cooperators, such as ARF (147-149). Wt p53 is a labile protein with a short half-life. Accumulation and activation of the protein can be triggered by a variety of stress signals including DNA damage, hypoxia, nucleotide deprivation, viral infection, heat shock, and mitogenic or oncogenic activation (150-152). The specific activity of p53 is further enhanced by post-translational modifications and by a variety of positive and negative regulators (153-155). Activated p53 elicits cellular responses that ultimately lead to growth arrest and/or programmed cell death (apoptosis) (156, 157).

Figure 12. World wide distribution of cancers and p53 mutations. *Inactivation of the p53 gene is essentially due to small mutations (missense and nonsense mutations or insertions/deletions of several nucleotides), which lead to either expression of a mutant protein (90% of cases) or absence of protein (10% of cases) No inactivation of p53 gene expression by hypermethylation of transcription promoters has been demonstrated at the present time, which supports the hypothesis of a function for p53 mutants. In many cases, these mutations are associated with loss of the wild-type allele of the p53 gene located on the short arm of chromosome 17, which is why the p53 gene is said to behave like a classical tumour suppressor gene with a mutation on one allele and loss of heterozygosity (LOH) of the second allele.* http://p53.free.fr

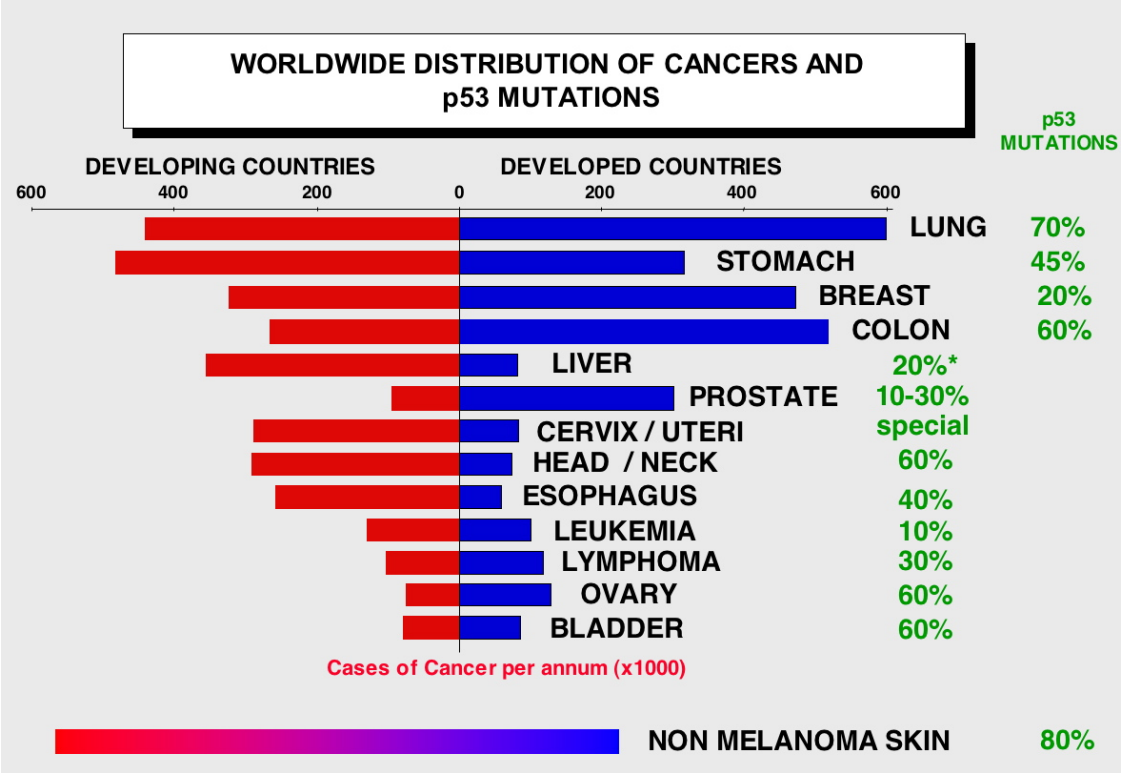

The regulation of p53 functions is tightly controlled through several mechanisms including p53 transcription and translation, protein stability, post-translational modifications, and subcellular localization. Despite intensive study of p53, the regulation of p53 subcellular localization although important for its function is still poorly understood. The regulation of p53 localization depends on factors that influence its nuclear import and export, subnuclear localization and cytoplasmic tethering and sequestration (158). Cytoplasmic p53 associates with the microtubule cytoskeleton and the dynein family of motor proteins (57, 159); while Parc (160), mot2 (161, 162) and adenovirus E1B (163) are involved in its cytoplasmic sequestration. Finally, a portion of p53 is localized to the mitochondria as part of the non-transcriptional apoptotic response (164, 165).

It has been previously shown that p53 associates with microtubules and uses the microtubule-dependent motor complex dynein-dynactin for nuclear targeting, e.g., after DNA damage (57). Disruption of the microtubule network by polymerization with high concentrations of taxol or depolymerization with vincristine impedes p53 translocation to the nucleus and in turn inhibits activation of downstream targets by p53. **Although an intact microtubule network is required for p53 trafficking, we sought to understand the effect of lower concentrations of microtubule-targeting agents on the p53 protein to better understand how proteins traffic on the microtubules (159)**.

Low concentrations of taxol or vincristine enhance p53 nuclear accumulation and result in transcriptional activation of mdm2. To assess the effects of the microtubule-stabilizing drug taxol and the microtubule-destabilizing drug vincristine on p53 cellular localization, A549 human lung carcinoma cells (with wt p53) were treated with low (6 nM) and high (100 nM) concentrations of each drug for 18 hr. At low concentrations, both the microtubule-stabilizing drug taxol and the microtubule-destabilizing drug vincristine cause suppression of microtubule dynamics (166-171). The subcellular localization of p53 was monitored by indirect immunofluorescence followed by confocal laser scanning microscopy (**Figure. 13A**). Cells treated with the DNA-damaging drug ADR readily accumulated p53 in the nucleus, as expected (154). Treatment with 6 nM

taxol or 6 nM vincristine (without ADR) resulted in enhanced p53 nuclear accumulation (red p53 staining), similar to the ADR-treated cells. In agreement with previous reports (171, 172), these low concentrations of taxol and vincristine had no apparent effects on microtubules or the organization of the microtubule network (**Figure 13A**). In contrast, treatment with higher taxol concentrations (100 nM) resulted in extensive stabilization of microtubules, as evidenced by tubulin bundling, whereas treatment with 100 nM vincristine resulted in microtubule depolymerization (**Figure 13A)**. Low concentrations of taxol (3–25nM) enhanced p53 nuclear accumulation and induced mdm2, a surrogate marker of p53 nuclear accumulation (**Figure 13B**). Higher doses of taxol (50 and 100 nM), however, failed to induce mdm2, consistent with a lack of p53 in the nucleus. Similar to the taxol treatment, 3–12 nM vincristine resulted in induction of mdm2, whereas higher concentrations had no effect on mdm2 expression levels, consistent with the loss of the microtubule network and a lack of p53 nuclear accumulation. To investigate whether the above findings were specific to the A549 human lung carcinoma cells, we performed a similar experiment by using the 1A9 human ovarian carcinoma cells containing wt p53 (173). The results confirmed the enhanced p53 nuclear accumulation seen after treatment with low concentrations of either taxol or vincristine (**Figure 14A-B**).

P53 nuclear accumulation by anti-microtubule agents requires drug-tubulin interaction. We next tested whether the effects of low concentrations of taxol and vincristine on p53 nuclear accumulation were microtubule dependent. We used a subclone of 1A9 cells (1A9/Epo B) that harbors an acquired β-tubulin mutation at residue Arg-282 to Gln (R282Q). This mutation is located near the taxane-binding site on tubulin (79). It impairs the taxol-tubulin interaction, thus conferring 10- to 15-fold cross-resistance to taxol, but has no effect on vincristine's interaction with tubulin (142). Treatment of 1A9/Epo B cells with 3 nM taxol had no effect on p53 nuclear accumulation, whereas treatment with 3 nM vincristine resulted in increased p53 nuclear accumulation (**Figure 14C**). As expected, 100 nM vincristine resulted in the complete depolymerization of the microtubule network and did not enhance p53 nuclear accumulation. Interestingly, treatment with 100 nM taxol slightly increased p53 nuclear

staining in 1A9/Epo B cells. This observation is in agreement with the impaired taxol-tubulin interaction. As a consequence, much higher concentrations of taxol are required to mimic the effect of low taxol concentrations in a wt cell line. Together, these results suggest that suppression of microtubule dynamics by low concentrations of anti-microtubule agents enhances the nuclear accumulation of p53 and activates the p53 target gene, *mdm2*.

Low concentrations of other anti-microtubule agents enhance p53 nuclear accumulation. To further test the above hypothesis, the effects of other microtubule-stabilizing compounds, Epo A and B, or destabilizing compounds, Nococodazole and colchicine, on p53 nuclear accumulation were examined. The results shown in **Figure 15A-B** reveal that treatment of A549 cells with a low concentration (3 nM) of each of these compounds enhanced p53 nuclear accumulation (**Figure 15A** red p53 staining) and increased the transactivation of mdm2 (**Figure 15B**).

Potentiation of apoptotic cell death in cells treated with low concentrations of taxol or vincristine followed by ADR. Because p53 exerts many of its effects by transcriptional regulation (174), its translocation from cytoplasmic sites of synthesis to nuclear target genes is critical to elicit biological responses. To further investigate the biological effects of enhanced p53 nuclear targeting by low doses of anti-microtubule agents, we performed the experiment shown in **Figure 16**. A549 cells were first treated with 3, 6, or 100 nM of either taxol (**Figure 16A**) or vincristine **Figure 16B**) for 18 hr and then exposed to ADR (200 ng_ml) for another 6 hr. When 3 or 6 nM of each drug was combined with ADR (taxol 3→ADR, taxol 6→ADR, vincristine 3→ADR, and vincristine 6→ADR), apoptosis was observed. As a marker of apoptosis, the p85 cleaved epitope of poly(ADPribose) polymerase (PARP) (exposed only after it is cleaved in cells undergoing apoptosis) was detected (175). The results with PARP cleavage were confirmed with caspase-3 activation assay and the sulforhodamine-B cell survival assay (**Figure 17A-B**). Although lower concentrations of anti-microtubule agents did not induce caspase-3 activation and were only marginally cytotoxic, they rendered cells sensitive to posttreatment with ADR (**Figure 17**). In the samples where PARP cleavage

was observed (taxol 3→ADR, taxol 6→ADR, vincristine 3→ADR, and vincristine 6→ADR), induction of p53 and mdm2 was also observed. This finding is consistent with enhanced p53 nuclear accumulation and activation of apoptotic responses (176). Although treatment with higher concentrations of taxol (100 nM) alone or in combination with ADR induced PARP cleavage, it did not increase p53 or mdm2 levels. Similar results were observed with high concentrations of vincristine. These results suggest that, at higher drug concentrations, anti-microtubule agents induce cell death independently of p53-nuclear targeting. To further tighten the correlation between enhanced p53 nuclear accumulation and p53-mediated apoptosis, we performed a Northern blot analysis for an apoptotic p53 target gene, the *PUMA* (**Figure 17C**). *PUMA* is induced by both high levels of exogenous p53 and elevated endogenous p53 and results in apoptosis (177, 178)) Increased *PUMA* levels were observed in cells treated with taxol 3→ADR, taxol 6→ADR but not with taxol 100, taxol 100→ADR, suggesting that the apoptosis induced by high concentrations of taxol is p53-independent. These data confirm and extend the notion that low concentrations of anti-microtubule agents enhance p53 nuclear accumulation and lead to apoptosis on short exposure to ADR.

Figure 13. Low concentrations of PTX or VCR enhance p53 nuclear accumulation in A549 cells. (A) *A549 cells were treated with the indicated drugs for 18 hr and processed for double immunofluorescence labeling with antibodies against p53 (red, labeled with Rhodamine red) or a-tubulin (green, labeled with FITC). Untreated A549 cells were included as control (CTRL). (Bar = 10 μm.)* ***(B)*** *Low concentrations of PTX or VCR induce mdm2 in A549 cells. Untreated A549 cells (0) or cells treated for 18 hr were processed for Western blotting. Cells treated with 400 ng/ml of ADR for 18 hr are included as a positive control for p53 and mdm2 increased levels. Thirty micrograms of total cellular protein from each sample were resolved in a 10% SDS/PAGE, transferred, and immunoblotted with antibodies against p53 and mdm2.*

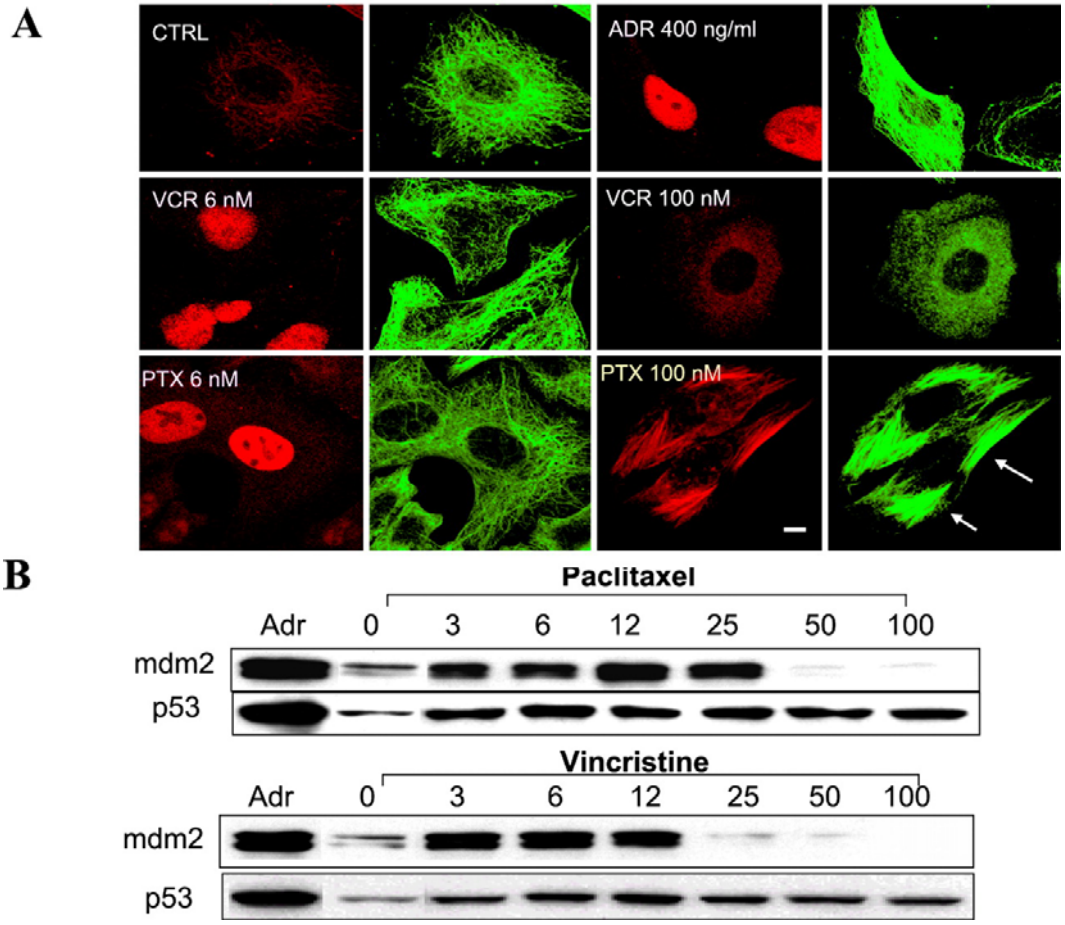

Figure 14. Low concentrations of Taxol or Vincristine enhance p53 nuclear accumulation, and induce mdm2 in 1A9 cells in a tubulin-dependent manner. *1A9 cells were plated in duplicate, subjected to the indicated drug treatments, and processed either for immunofluorescence* ***(A)*** *or Western blotting* ***(B).*** ***(A)*** *Cells are stained with antibodies against p53 (red) or α -tubulin (green).* ***(B)*** *Thirty micrograms of total cell protein were probedby Western with antibodies against p53 and mdm2. Induction of mdm2 is consistent with enhanced p53 nuclear accumulation* ***(A).*** ***(C)*** *The tubulin mutant 1A9/Epo B cells were treated with the indicated drugs for 18 hr and processed for double immunofluorescence labeling with antibodies against p53 (red) or α -tubulin (green).*

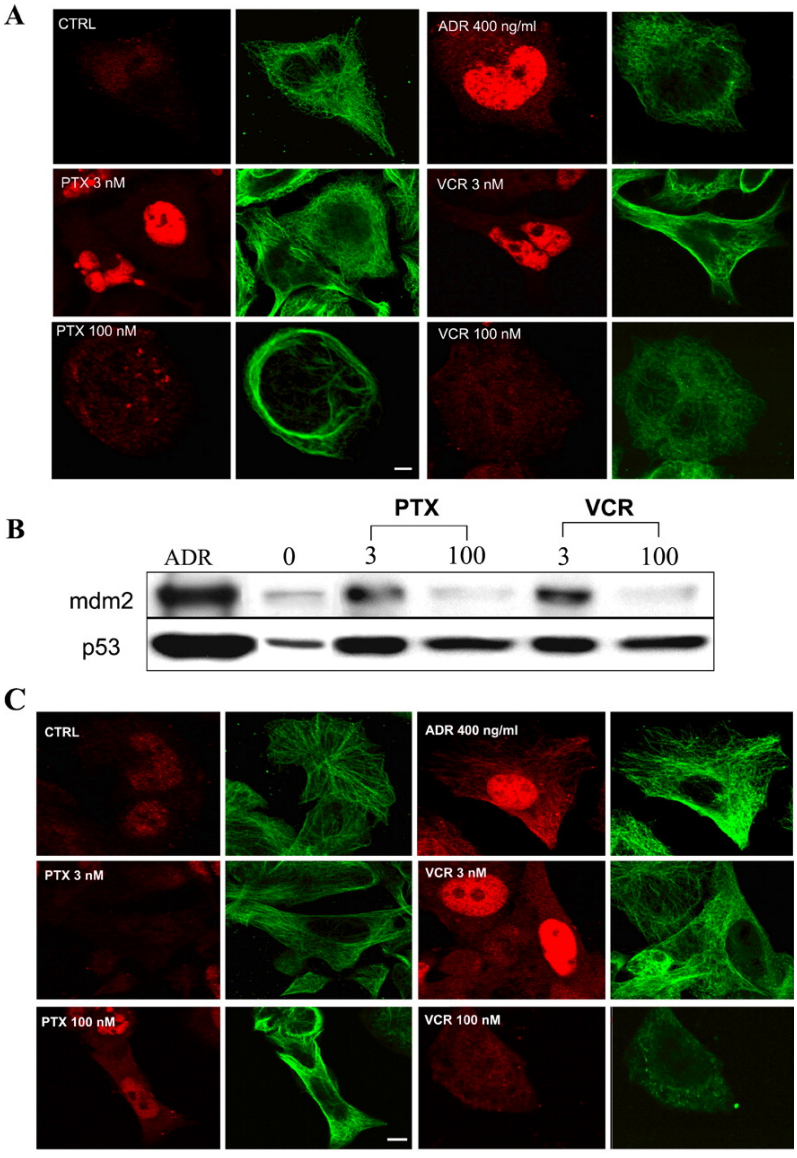

Figure 15. Low concentrations of other anti-microtubule agents enhance p53 nuclear accumulation and induce mdm2 in A549 cells. *A549 cells were plated in duplicate, subjected to the indicated drug treatments, and processed either for immunofluorescence* ***(A)*** *or Western blotting* ***(B).*** *Arrows in A point to either bundled microtubules (Epo A, Epo B) or depolymerized tubulin network (colchicine, Nocodazole). (Bar = 10 µm.)*

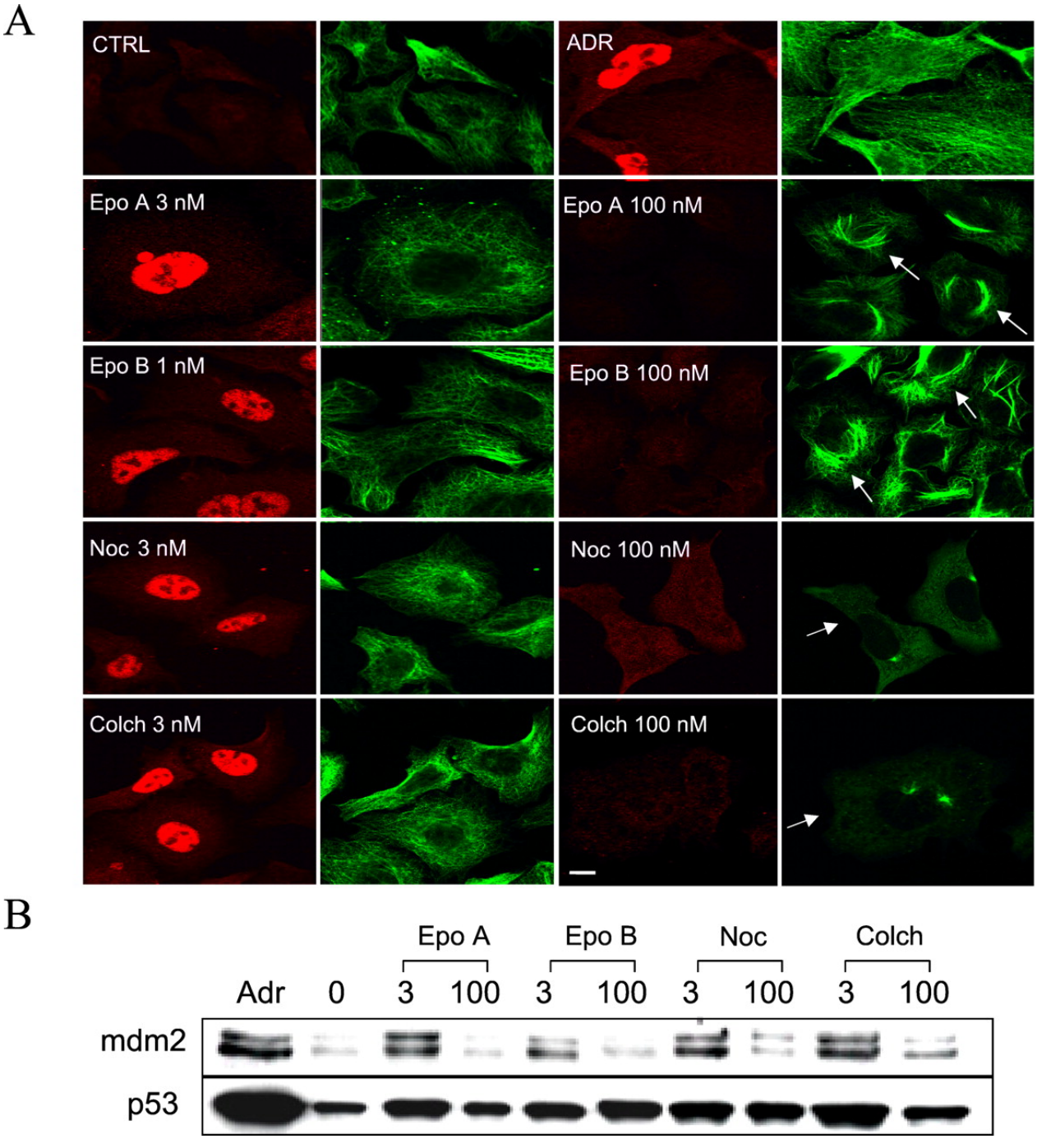

Fig 16. Treatment with low concentrations of PTX or VCR followed by ADR enhances apoptosis in A549 cells. A-B) *A549 cells were treated with 3, 6, or 100 nM of PTX or VCR for 18 hr followed by treatment with 200 ng/ml of ADR for an additional 6 hr (PTX3 ADR, PTX6 ADR, PTX100 ADR, and VCR3 ADR, VCR6 ADR, VCR100 ADR). ADR was added to the medium containing PTX or VCR at the indicated concentrations. Western blots were probed with antibodies against the cleaved (p85) form of PARP, p53, mdm2, and actin as a loading control. C) A549 cells were treated with 3, 6, or 100 nM PTX for 18 hr, followed by treatment with 200 ng/ml of ADR for an additional 6 hr (PTX3 ADR, PTX6 ADR, PTX100 ADR. Ten micrograms of total RNA from each sample were analyzed by Northern blotting for PUMA. Ethidium bromide staining of 28S RNA is shown as loading control.*

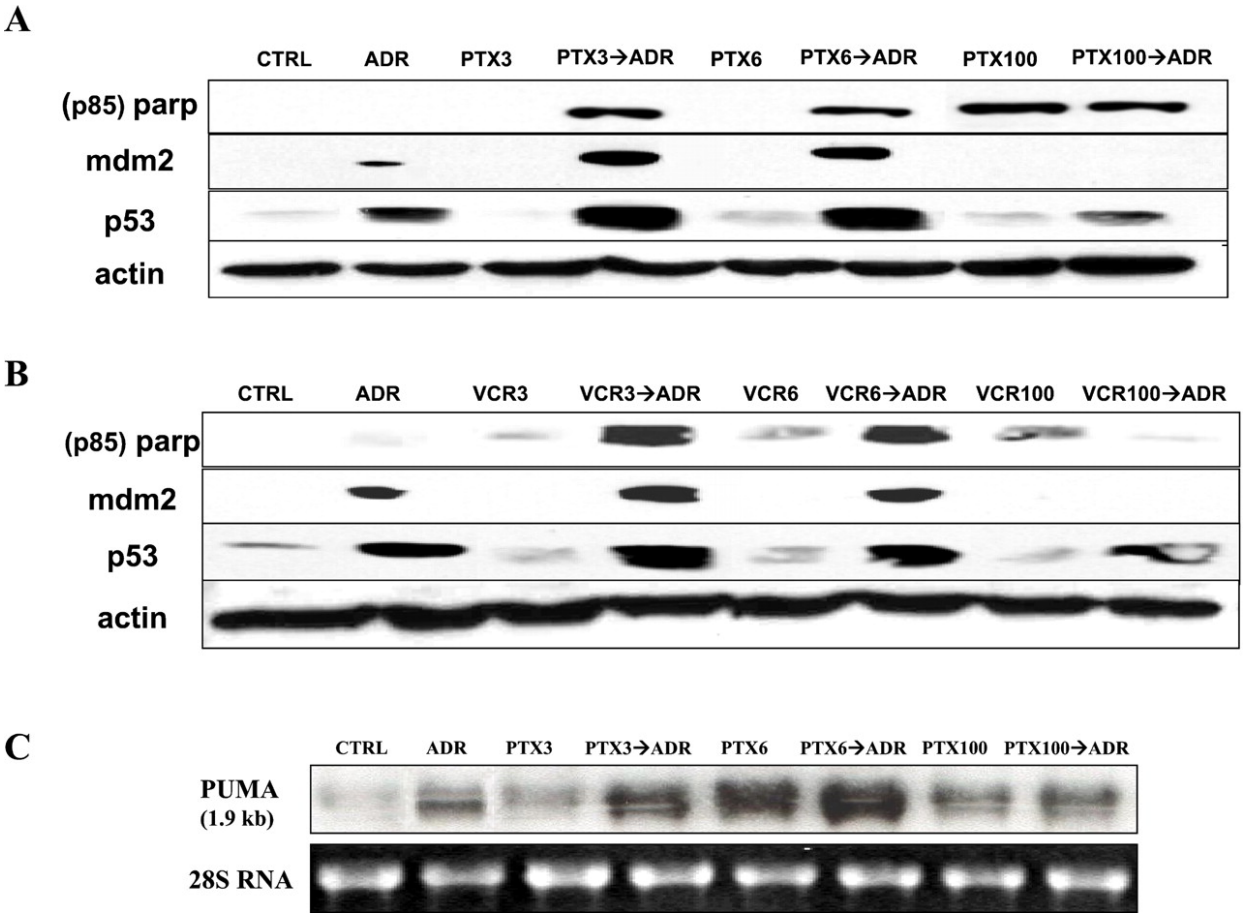

Figure 17. Effect of taxol and adriamycin combination on cell survival. A) *A549 cells were plated in 96-well plates in triplicate and treated with a fixed concentration of PTX at 3 nM, or 6 nM for 24 hr followed by 400 ng/ml of ADR for another 4 days. Cell survival was determined with the sulforhodamine-B assay, and the OD564 was measured in a microplate reader. The bar graph represents percent survival as determined by the OD value of the treated cells divided by the OD value of untreated cells. The mean OD values were determined from three independent experiments. Error bars represent standard error of the mean.* ***B)*** *Effect of PTX and ADR combination on caspase-3 activation. A549 cells were plated in 96-well plates in sextuplet and treated with 3 nM or 6 nM PTX overnight followed by 400 ng/ml of ADR for an additional 6 hr. After drug treatment, cells were tested for caspase-3 activity by the HTS Caspase-3 Activity Fluorometric Assay (Oncogene Science), according to the manufacturer's instructions. The values of the y axis (random fluorescent units) represent the mean of two independent experiments where cells were plated in sextuplet each time (mean of 12 values). Error bars represent SEM. Control is arbitrarily assigned the value of 10, and the data presented are normalized to the value of the control.*

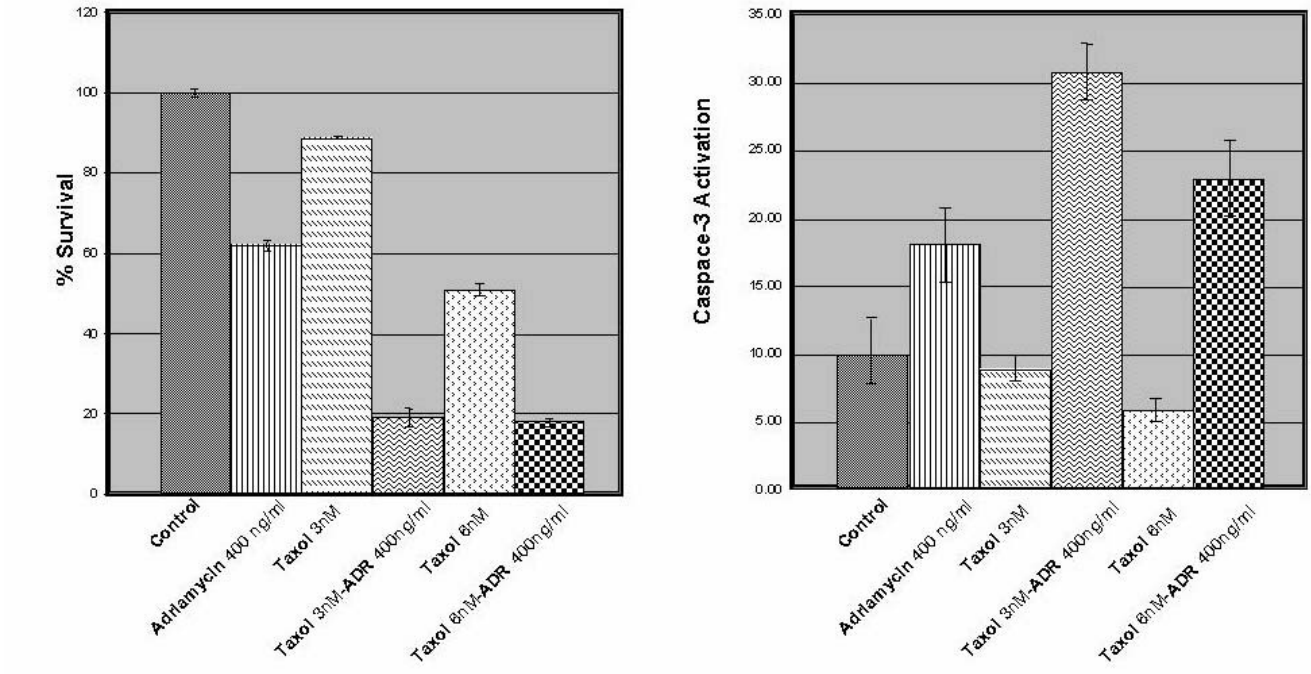

Discussion

It had been previously shown that the tumor suppressor protein p53 is associated with the microtubule cytoskeleton and, in response to DNA damage, is transported toward the nucleus via the minus-end microtubule-associated motor protein dynein (57). Microtubule dynamics are essential for many microtubule-dependent cellular processes and in particular for mitosis, which is very sensitive to alteration of microtubule dynamics (56, 179-181). Both microtubule-stabilizing and -destabilizing agents at very low concentrations potently suppress microtubule dynamics, leading to kinetic stabilization of the mitotic spindle (167-169, 171). In addition, microtubules provide tracks or scaffolds for the directional vesicle transport as well as organelle positioning. Suppression of the dynamics of interphase microtubules may actually enhance their functions in transporting molecules (159). Low concentrations of taxol or vincristine (3 and 6 nM) enhance the nuclear accumulation of p53 and induce activation of the p53-dependent gene, mdm2. Furthermore, we showed that p53 nuclear accumulation depended on the ability of anti-microtubule agents to bind tubulin, as evidenced by the lack of response of a cell line with a mutant beta-tubulin (R282Q mutation located at the taxol-binding pocket) to low doses of taxol. These findings favor the notion that suppression of microtubule dynamics leads to enhanced p53 nuclear targeting and is in concert with published reports showing that very low concentration of microtubule-targeting agents suppress microtubule dynamics both *in vitro* and in cells (56, 167-169, 171).

This correlation raises the possibility that the microtubule-stabilizing effects of MAPs and the suppression of microtubule dynamics by low concentrations of microtubule targeting agents could elicit similar cellular effects, such as enhanced microtubule-dependent transport. The involvement of microtubules in signal transduction and the relationship between microtubules and transcription factors in human cancer have only recently started to attract attention (for reviews, see refs. (32, 182). For example, p53 function depends on its nuclear localization, and both p53 nuclear import and export are cellular processes tightly regulated (158, 183). We showed here that enhanced p53 nuclear accumulation with low concentrations of taxol or vincristine before short exposure to low concentrations of ADR resulted in apoptotic cell death in A549 cells, as

evidenced by the induction of PARP cleavage and caspase-3 activation. This finding may be important in a clinical setting, as the taxanes are often combined with ADR or radiation for the treatment of different types of cancer (184, 185). Our findings demonstrate that pretreatment with low concentrations of microtubule targeting agents (which do not induce either mitotic arrest or change tubulin polymerization) sensitizes cells to the effects of ADR, including induction of *PUMA* and apoptosis. This effect may be the result of additive phosphorylation of p53, as anti-microtubule agents and DNA damage have been shown to induce p53 phosphorylation at distinct residues (186). Our results demonstrate that drugs like taxol alter p53 nuclear trafficking at therapeutically relevant drug exposure and that combination therapies with known p53-dependent agents such as ADR can be potentiated by p53-enhancing concentrations of taxol. This conclusion supports the notion that lower doses of anti-microtubule agents can be therapeutically more attractive than higher doses (186). Finally, although disruption of microtubule functions by anti-microtubule agents is well known and is the basis of mitosis arrest and of inhibition of microtubule-mediated trafficking, very low concentrations of anti-microtubule agents can increase some functions of microtubules in interphase cells. Our data demonstrate that microtubule-mediated trafficking in interphase cells can be regulated and enhanced above physiological levels. It is possible that the manipulation of microtubule dynamics by microtubule-interacting compounds can be exploited to enhance cell death in human cancer cells.

HIF-α

Hypoxia is a hallmark of solid human tumors, as the microenvironment of rapidly growing solid tumors is associated with increased energy demands and diminished vascular supply, thus, resulting in focal areas of prominent hypoxia (reduced oxygen tension). It has been demonstrated that hypoxia in tumors tends to select for a more malignant phenotype associated with increased mutation rates, and increased expression of genes promoting angiogenesis and tumor invasion, leading to a more metastatic phenotype of human cancers (187). In addition, hypoxic tumors are resistant to both chemotherapy and radiation. The effectiveness of chemothrerapy is hampered as hypoxia selects for cells with a very aggressive and often metastatic phenotype, in addition to the fact that hypoxic areas lack functional vessels, inhibiting the delivery of chemotherapy drugs. Moreover, the multidrug resistance (MDR1) gene product P-glycoprotein is induced by ambient hypoxia (188), contributing to the overall drug-resistance phenotype of hypoxic tumors. Radiotherapy on the other hand, is severely compromised because oxygen is necessary to produce the reactive oxygen species that mediate the secondary toxic effects produced by ionizing radiation. Consequently, hypoxia is a major reason for the failure of cancer therapy and hypoxic tumors are therefore associated with poor patient out come. The main mechanism of tumor cell response to reduced oxygen levels is via activation of hypoxia-inducible transcription factors (HIF), which are critically important in tumor progression and angiogenesis as its transcriptional activity promotes induction of genes involved in angiogenesis, glycolysis, growth-factor signaling, immortalization, genetic instability, tissue invasion and metastasis, apoptosis and pH regulation.

Hypoxia Inducible Factor 1 (HIF-1) is a transcriptional factor that plays a key role in adaptation to hypoxia and therefore in tumor progression and angiogenesis. HIF is a heterodimer composed of HIF-1α and HIF-1β (also known as ARNT –aryl hydrocarbon receptor nuclear translocator) subunits, both of which belong to basic helix-loop-helix (bHLH)/PAS domain transcription. The human HIF-1α gene is located on chromosome 14 (14q21-q24) whereas the HIF-1β gene is located on chromosome 1 (1q21). Homology is relatively well conserved for the HIF-1α and HIF-1β subunits, with over a 90% similarity between human, rat and mouse. HIF-1α and HIF-1β are relatively large

proteins in size, being comprised of 826 and 789 amino acids, respectively. HIF-1β is constitutively expressed, whereas HIF-1α is maintained at low steady-state levels under normoxia through controlled degradative processes in the presence of oxygen. (**Figure 18**)

HIF-1 is a critical, genome-wide transcription regulator identified for oxygen homeostasis responsive to hypoxic stress. HIF-1 controls the expression of >80 genes involved in angiogenesis, metabolic adaptation to hypoxia, tumor survival and invasion (189). Several lines of evidence show clearly that overexpression of HIF-1α and HIF-1 dependent genes contribute to the lethal phenotype of many solid tumors. As a consequence of HIF-1 transcriptional activation an increasing number of genes is transcribed. Many of the proteins encoded by these genes are involved in adaptive responses counteracting a detrimental impact of hypoxia. Coordination towards hypoxia comprises erythropoiesis, angiogenesis, iron homeostasis, glucose and energy metabolism, as well as cell proliferation and survival decisions. Four groups of direct HIF-1 target genes that are particularly relevant to cancer encode angiogenic factors, including VEGF, glucose transporters and all the glycolytic enzymes, survival factors and invasion factors (**Figure 19**)

Seventy percent of human cancers overexpress HIF-1α protein, with the highest levels observed in metastases as compared to adjacent normal tissues (190, 191), making HIF-1α a prime target for anticancer therapy. Several strategies have been employed by several groups most of which focus on the identification of small molecules that specifically inhibit HIF-1 protein and the HIF-transcriptome (192), such as topoisomerase I inhibitors (193), Hsp90 inhibitors (194-197), YC-1 (198-200), nonsteroidal anti-inflammatory drugs (NSAIDS) (201, 202), gene therapy (203-206) and anti-microtubule agents such as 2ME2 (61).

Figure 18. HIF-1 pathway. *Under normoxic conditions HIF-1α is post-transcriptionally modified by specific prolyl-4-hydroxylases allowing its interaction with a complex containing the von Hippel-Lindau protein. pVHL ubiquitinates HIF-1α and targeting it for proteasomal degradation. In the absence of oxygen, HIF-1α is stabilized allowing HIF-1α to heterodimerize with its partner HIF-1β and bind to the hypoxia response element, therefore activating the transcription of several genes implicated in the response to hypoxia.*

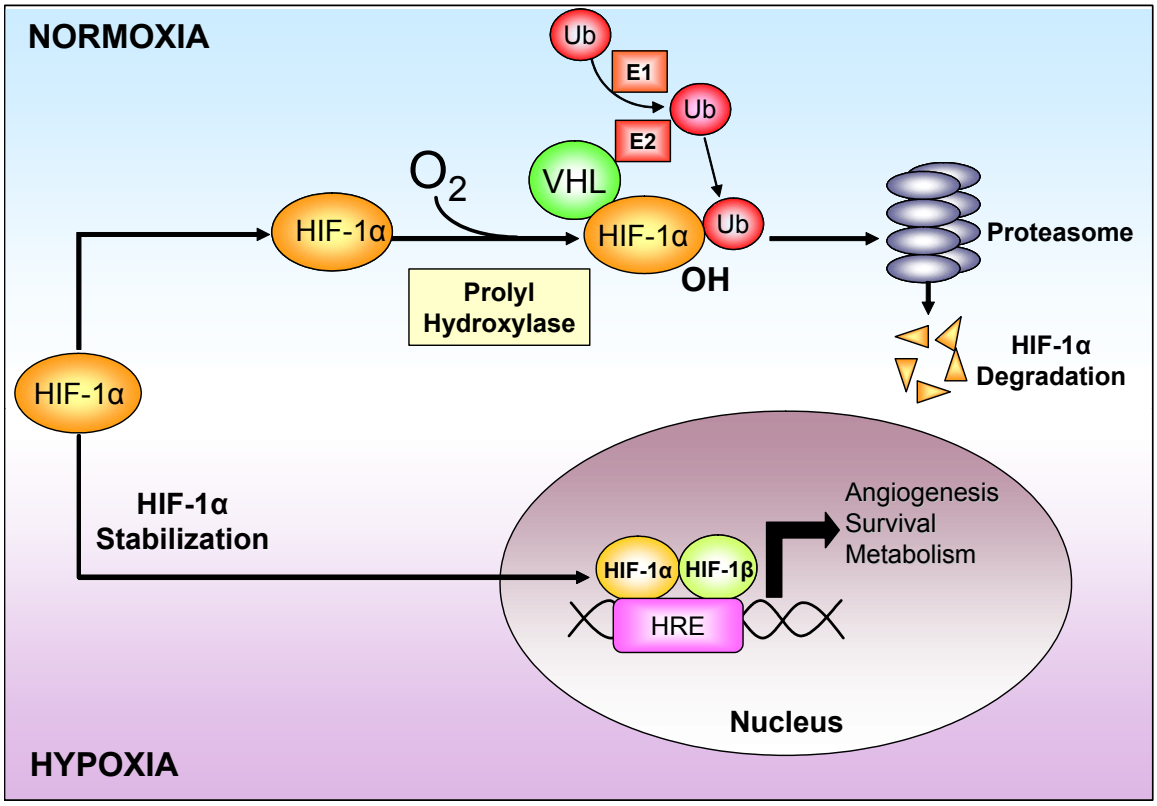

Figure 19. Genes that are transcriptional activated by HIF-1. *HIF-1 is a transcription factor that controls the expression of a battery of more than 80 target genes whose protein products control oxygen delivery (via angiogenesis), metabolic adaptation to hypoxia (via glycolysis) and cell survival (via induction of growth factors) (189) .*

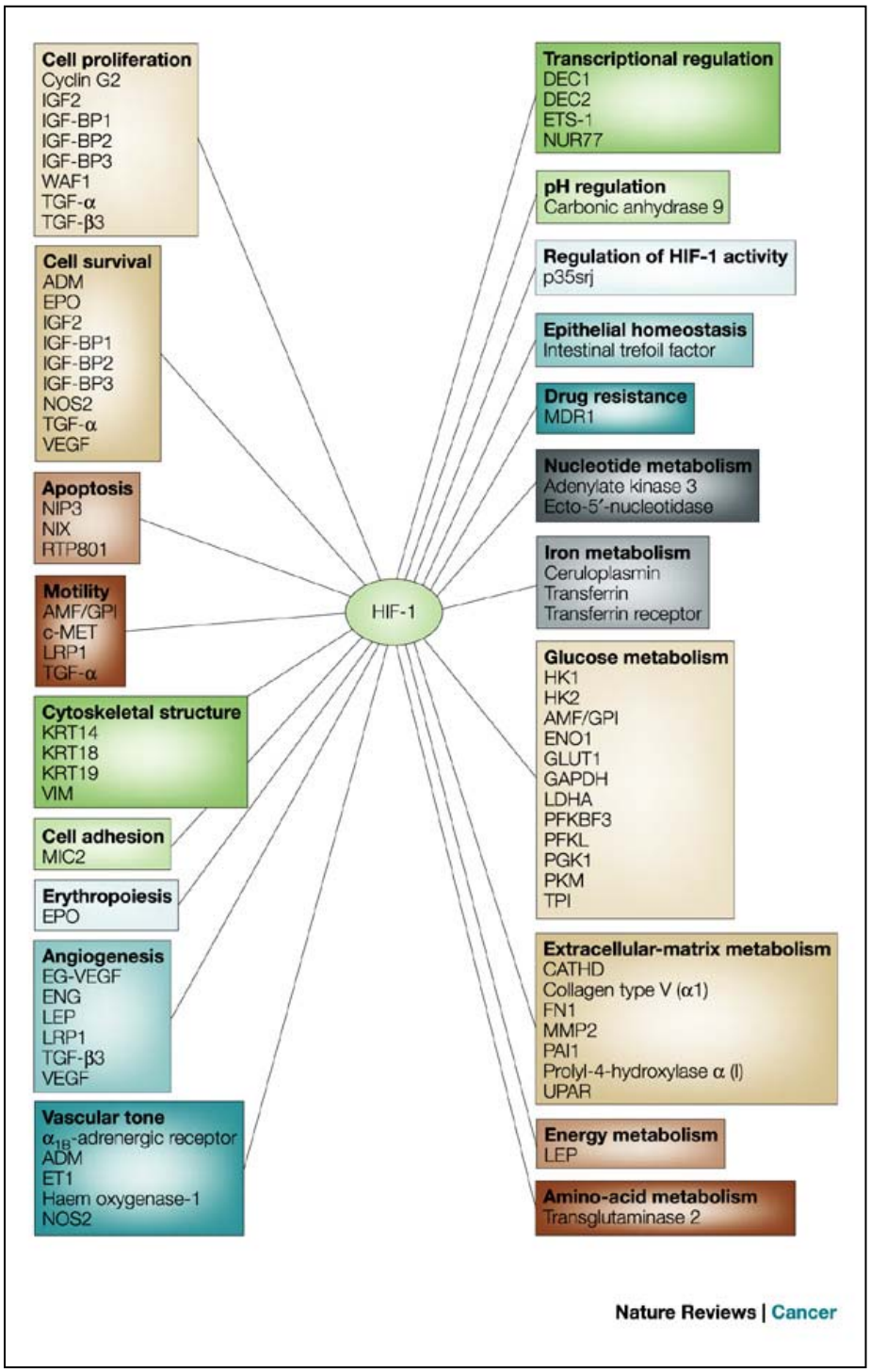

2ME2 is an antiproliferative molecule that effectively induces apoptosis in actively proliferating cells *in vitro* and *in vivo*. 2ME2 is emerging as an attractive drug candidate because of its unique characteristics: (*a*) nontoxic (207, 208); (*b*) it is orally available (207, 209-212) and (*c*) no effect on several responses normally associated with estrogens (213-215). The antitumor and antiangiogenic effects of 2ME2 are well reported. 2ME2 has been shown to inhibit tumor growth in a variety of different cell lines and solid tumors. The ability of this compound to target endothelial cells was first identified by its antiproliferative activity against microvascular and large vessel endothelial cells (207). Additional studies showed that 2ME2 inhibits the migration and invasion of capillary endothelial cells and their ability to form capillary-like structures on collagen gels (207, 216). 2ME2 has been shown *in vitro* to bind at the colchicine-binding site of microtubules and inhibit tubulin polymerization by interacting at the colchicine binding site (87, 217, 218). *In vivo*, 2ME2 has been shown to depolymerize endothelial (207) as well as in tumor cells (219). One of the hallmarks of microtubule-disrupting drugs is their ability to induce G2/M arrest. In agreement with that, 2ME2 was shown in the earliest studies to arrest MCF-7 breast cancer cells in G2/M arrest with malformed spindles (220). 2ME2 is an effective inhibitor of tumor growth and angiogenesis in numerous *in vivo* models (101, 207, 212). Mabjeesh et al. (61) showed that regulation of the HIF-1 pathway contributed to the antiangiogenic effects of 2ME2.

Downregulation of HIF-1 pathway is linked to microtubule integrity due to the association of HIF-1α with microtubules. The inhibition of HIF-1 occurred downstream of the 2ME2/tubulin interaction, as disruption of interphase microtubules was shown to be required for HIF-α downregulation. To investigate whether microtubules are involved in directed HIF-1α protein trafficking towards the nucleus, we performed the experiment shown in **Figure 20**. Prostate cancer cells, PC3, were subjected to hypoxia (to induce and stabilize HIF-1α protein) and fixed and stained for tubulin and HIF-1α for visualization by immunofluorescence. Upon higher magnification we were able to see a colocalization of the two antibodies, indicating colocalization of the two proteins. We hypothesized that HIF-1α could use the microtubule network for its trafficking needs within the cell, in a similar manner as we had seen with p53 (159). To

further probe this hypothesis we performed the experiment detailed in **Figure 21.** In this experiment, PC3 cells are treated with 100 μM 2ME2 for 6 hours only while they are concomitantly exposed to hypoxia. We rationalized that since hypoxic exposure leads to rapid (within minutes) HIF-1α protein stabilization (due to inhibition of its proteasomal degradation in the cytoplasm) and subsequent translocation to the nucleus; microtubule disruption would result in impaired nuclear accumulation of HIF-1α if indeed functional microtubules mediate HIF intracellular trafficking (**Figure 22)**. Indeed, 2ME2 treatment at concentrations that depolymerized microtubules impaired HIF-1α nuclear accumulation and resulted in significant retention of HIF-1α protein in the cytoplasm compared to untreated control cells (**Figure 20**). This result strongly suggested that microtubules are involved in HIF-1α trafficking (**Figure 21).** Thus, 2ME2 by depolymerizing interphase microtubules impairs HIF-1α nuclear transport and activity. To further study this association we performed transmission electron microscopy (TEM) to confirm at high resolution the co-localization of HIF-1α with the microtubule cytoskeleton. In preliminary experiments shown in **Figure 23**, PC3 cells were exposed to 1% oxygen for 6 hr, and processed for double-labeling TEM microscopy with antibodies against tubulin and HIF-1α. This analysis revealed co-localization of HIF-1α labeled with 6 nm gold particles and microtubules labeled with 12 nm gold particles.

Microtubule-disruption inhibits HIF-1α protein translation. We have also investigated the potential association of HIF-1α mRNA with microtubules by using fluorescent molecular beacons (MBs), specific for HIF-1α mRNA **(Figure 24)**. MBs are oligonucleotides (ONDs) with a stem-loop hairpin structure, dual labeled with a fluorophore at one end and a quencher at the other **(Figure 24A)**. Delivering MBs into cells results in a fluorescent signal only if the MB hybridize to target mRNAs **(Figure 24B)**. Using this experimental approach, we first confirmed *in vitro* that our MB hybridizes specifically to a synthesized HIF-1α oligonucleotide target, by measuring the fluorescence intensity of the reaction in a fluorescence microplate reader. As a negative control, an unrelated oligonucleotide target (survivin) was mixed with the HIF-1α MB *in vitro*, and as expected, no hybridization was observed as evidenced by a lack of fluorescence emission. We then transfected the HIF-1α MB into untreated or 2ME2-treated MCF-7 cells that stably express GFP-tubulin. These samples were processed by

confocal microscopy. As shown in **Figures 24C-D**, in untreated MCF-7: GFP-tubulin cells, the HIF-1α molecular beacon (**Figure 24C,** middle panel **Figure 24D**) hybridized with HIF-1α mRNA and exhibited a microtubule-like pattern of fluorescence staining. The co-localization between the GFP-tubulin and the red fluorescent HIF-1α MB staining, is shown in the merged image (third panel **Figure 24D**). The 2ME2 treatment resulted in mis-localization of the HIF-1α MB from microtubules, consistent with the extended microtubule depolymerization (first panel) caused by this drug (yellow arrows). As a result, no co-localization is observed between the GFP-tubulin and the red MB after 2ME2 treatment (third panel). We have also performed a live-cell imaging experiment using the MCF-7:GFP-tubulin cells, following transfection with the red HIF-1α MB, for real time observation of the intracellular movement of HIF-1α mRNA and its relationship with a functional microtubule network. **These results support our hypothesis that 2ME2 inhibits HIF-1α translation by affecting the localization of HIF-1α mRNA complexes with the microtubule cytoskeleton, thus impairing efficient HIF-1α translation**.

Figure 20. *PC3 (prostate cancer) cells were subjected to hypoxia for 6 hrs and cells were fixed and processed for double immunofluorescence labeling with anti-HIF-1α (red) and anti-α-tubulin (shown in white) antibodies. Staining was analyzed by confocal laser scanning microscopy and merged images are shown. Solid arrows point to nuclear HIF-1α. Right panel shows magnification of the marked cytoplasmic area. Dashed arrows point to areas clearly depicting HIF-1α staining co-localizing with microtubules.*

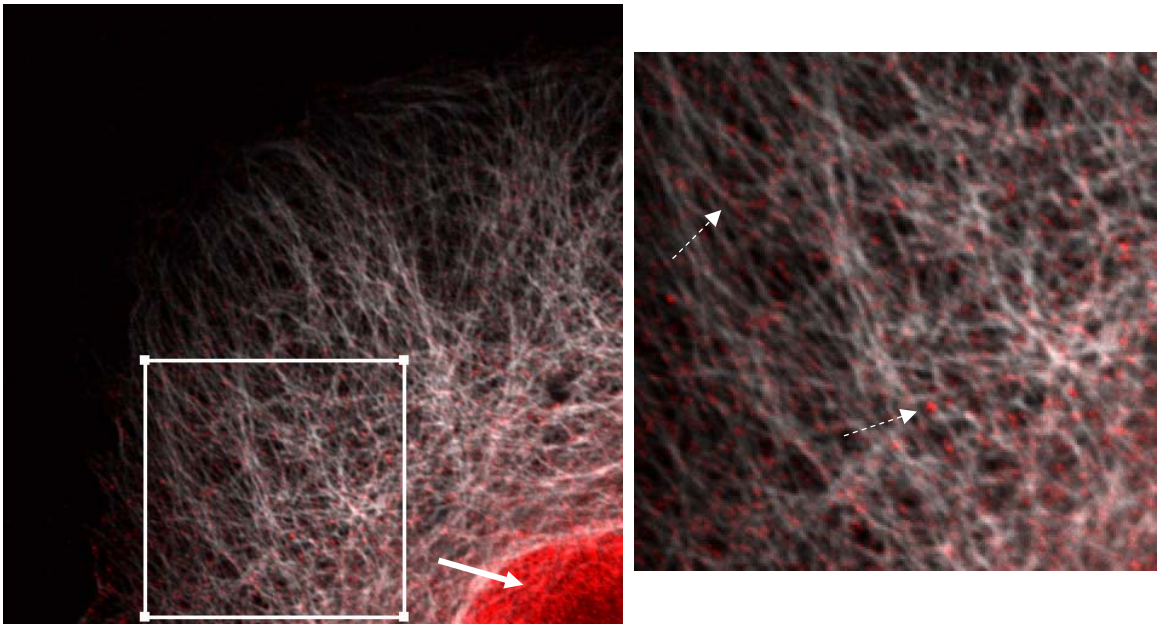

Figure 21: *PC-3 cells were subjected to hypoxia for 6 hrs in the absence or presence of 100 μM 2ME2 and cells were fixed and processed for double immunofluorescence labeling with anti-HIF-1α (green) and anti-α-tubulin (red) antibodies. Staining was analyzed by confocal laser scanning microscopy*

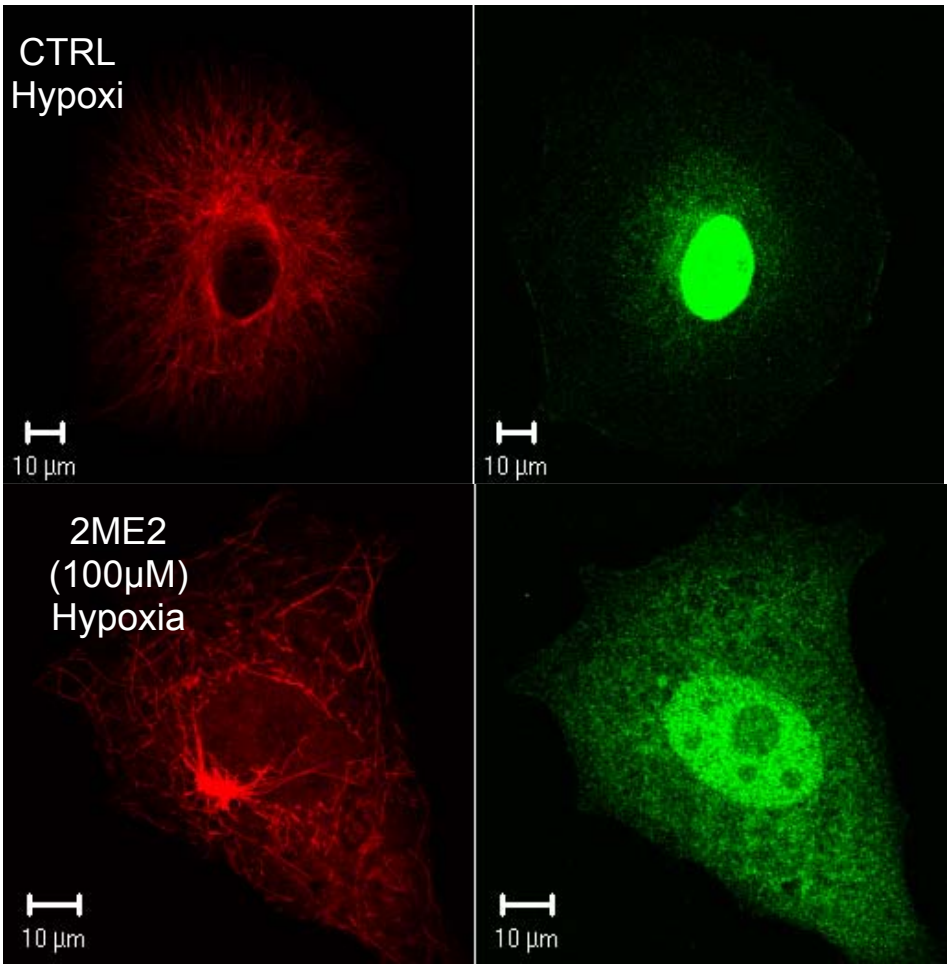

Figure 22. Microtubule-Dependent HIF-1a Translocation. *HIF-1a traffics along microtubules via an unknown motor to reach the nucleus.*

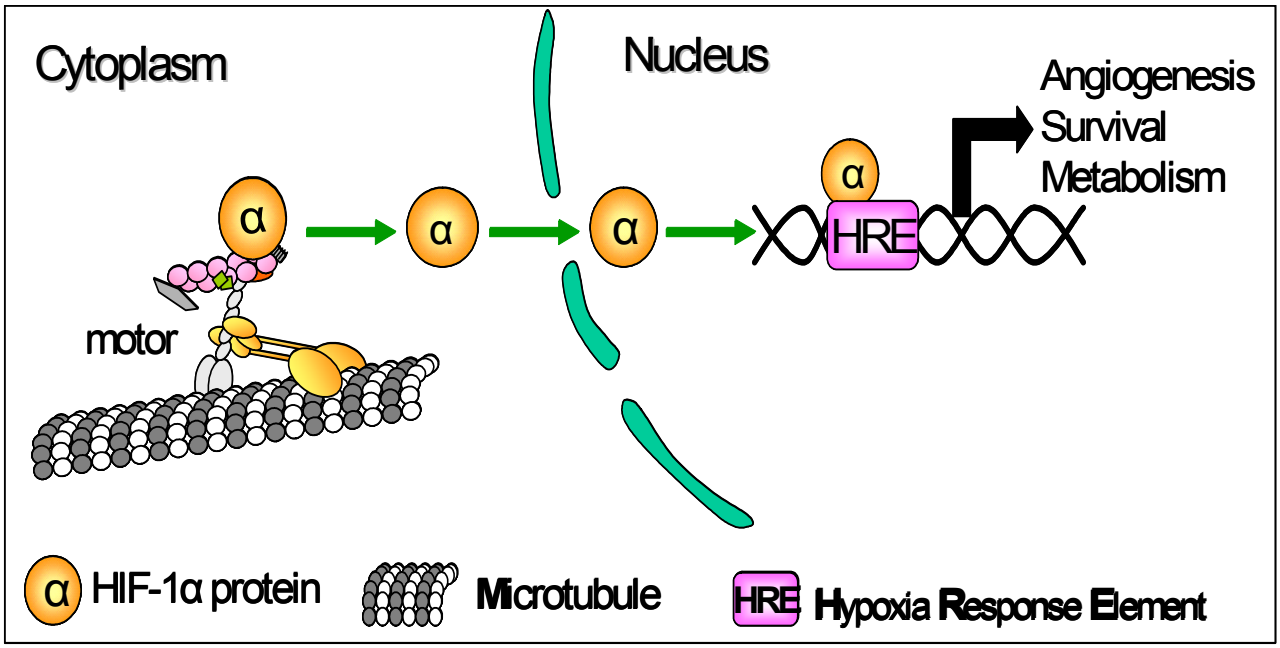

Figure 23. TEM shows HIF-1α on Microtubules. *PC3 cells were subjected to hypoxia, fixed with PHEMO buffer and processed for double-labeling immuno-fluorescence using antibodies against HIF-1α (6 nm colloidal gold secondary Ab,* ***red arrows****) and α-tubulin rat (12 nm colloidal gold secondary antibody,* ***black arrows****). Cells were further fixed in 1% glutaraldehyde and processed for transmission electron microscope. C:cytoplasm, N:Nucleus*

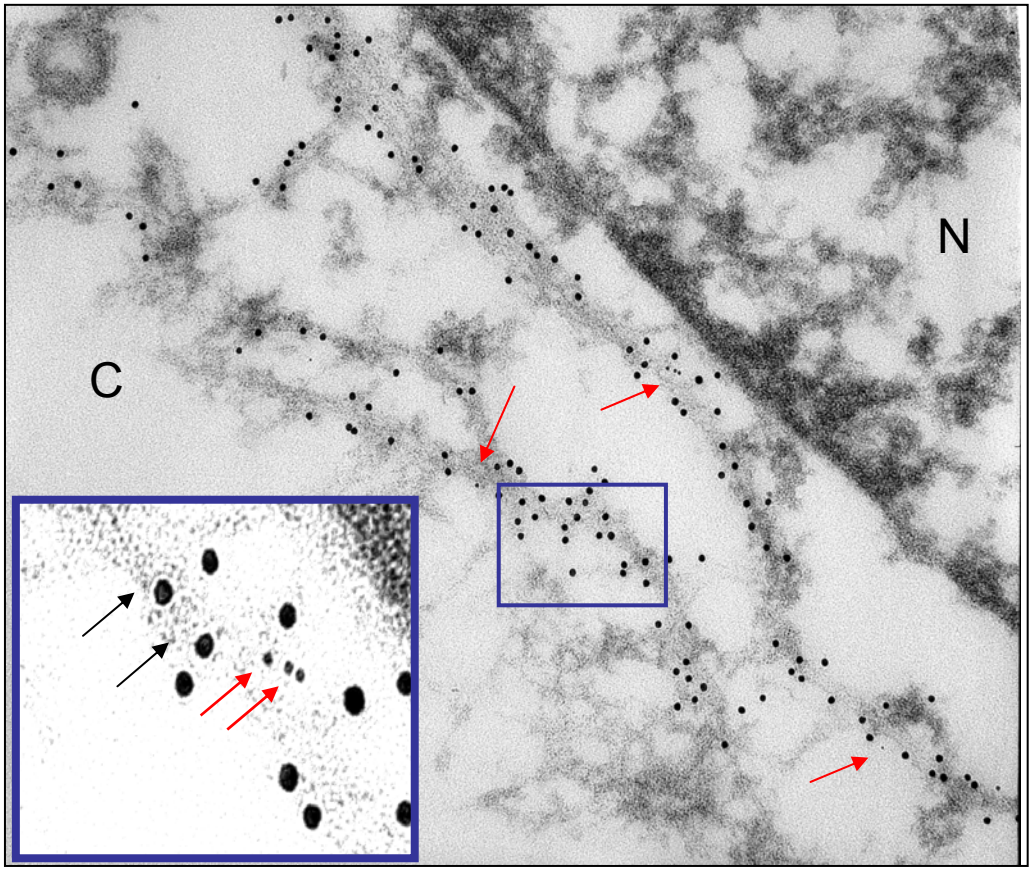

Figure 24. HIF-1a molecular beacons associate with microtubules. *A) Molecular beacons (MB) are dual labeled single-stranded oligonucleotides (ONDs) with a hairpin structure and with a fluorophore on one end and a quencher on the other end.* ***B)*** *Delivering molecular beacons into cells can result in a fluorescent signal due to hybridization of the probe with a target mRNA.* ***C)*** *HIF-1a MBs in MCF-7 cells show a microtubule pattern.* ***D)*** *Molecular Beacons specific for HIF-1a label RNA in MDA-MB-231 cells treated with 2Me2.*

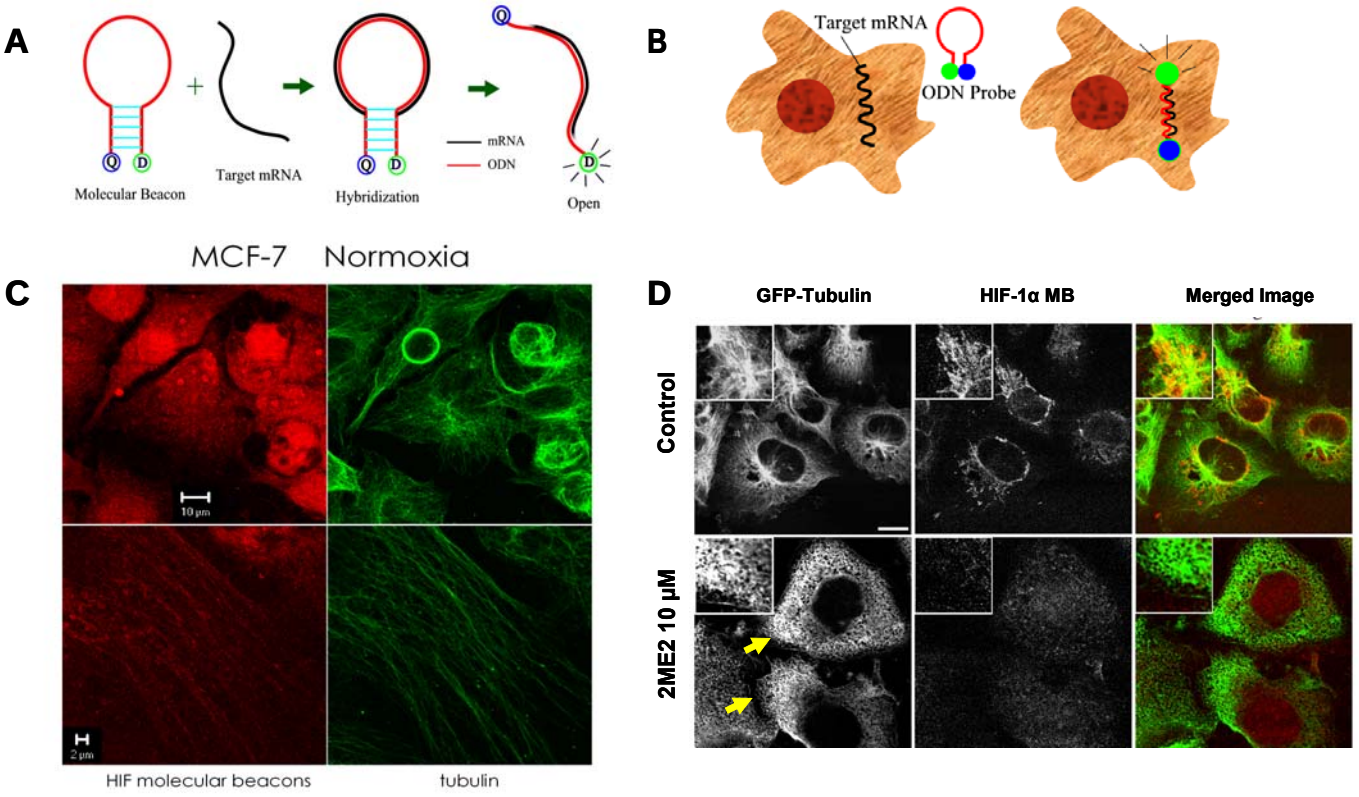

Methods for Objective 1

Materials and Methods for p53

Cell Lines and Antibodies. Human lung cancer A549 cells were obtained from the National Cancer Institute Drug Anticancer Drug Screen and the human cervical cancer HeLa cells from American Type Culture Collection. A2780 (1A9) human ovarian carcinoma cells and their epothilone (Epo)-resistant subline, A2780/Epo B, were a generous gift from Craig Fairchild (Bristol-Myers Squibb). Mouse monoclonal antibodies against p53(Ab 6: Mab Do1) and mdm2 (Ab-2) were purchased from Oncogene Science. The sheep polyclonal antibody against p53 (Ab-7) was from Oncogene Science. The mouse monoclonal anti-α-tubulin (DM1α) antibody and the rabbit polyclonal anti-actin antibody were from Sigma. The antibody against the cleaved epitope of poly(ADP-ribose)polymerase (PARP) (p85) was from Upstate Biotechnology (Lake Placid, NY). PTX was purchased from Bristol-Myers Squibb, VCR from Eli Lilly, and colchicine, Noc, and adriamycin (ADR) were from Sigma.

Western and Northern Blot Analysis. 30 μg of total cell protein was resolved by 10% SDS_PAGE and immunoblotted with the indicated antibodies. Northern blot analysis for the p53-up-regulated modulator of apoptosis (PUMA) mRNA was performed as previously described (177).

Immunofluorescence and Microscopy. Exponentially growing cells were plated on 12-mm glass coverslips (A. Daigger, Vernon Hills, IL) and incubated overnight. The next day, after drug treatment, cells were fixed and processed for double immunofluorescence labeling.. The primary antibodies used were the mouse monoclonal anti-α-tubulin (DM1α) antibody for tubulin/MT staining and the sheep polyclonal (Ab-7) antibody for p53 staining. The coverslips were examined on a Zeiss axioplasm microscope by using a Zeiss 100 /1.3 oil immersion objective. Confocal images were obtained on an LSM 510 laser scanning (Zeiss) microscope (Zeiss axioplasm).

MATERIALS AND METHODS FOR HIF-1A

Cell lines. Human breast cancer MDA-MB-231 cells were maintained in DMEM and human prostate cancer PC-3 cells, human lung cancer A549 cells, human breast cancer MCF-7:GFP-alpha tubulin were cultured in RPMI 1640; All media were supplemented with 10% FBS and antibiotics. Cells were cultured at 37ºC in a humidified atmosphere and 5% CO_2 in air. For hypoxic exposure, cells were placed in a sealed modular incubator chamber (Billups-Rothenberg, Del Mar, California) flushed with 1% O_2, 5% CO_2 and 94% N_2

Drug treatment of Cells. Cells were seeded in culture dishes and grown overnight until 70% confluence. The medium was then replaced with a new medium containing either vehicle (0.1% DMSO) or drug at the concentrations indicated in the figures for overnight at 37ºC. The following day, cells were exposed to hypoxia or left under normoxia for 6 hours. The cells were then washed twice with ice-cold PBS, harvested whole cell extract (WCE) was prepared by lysing the cells with 100mM potassium phosphate (pH 7.8) and 0.2% Triton X-100 supplemented with protease and phosphatase inhibitors.

Immunofluorescence and Confocal Microscopy. Exponentially growing cells were plated on 12-mm glass coverslips (Fisher Scientific, Pittsburgh, Pennsylvania) into 24-well plates and cells were allowed to attach overnight. The following day, cells were treated with the indicated drugs for 16 h and subjected to hypoxia for an additional 6 hours. Cells were fixed with PHEMO buffer (PIPES 0.068M, HEPES 0.025 M, EGTA 0.015 M, MgCl2 0.003 M, 10% DMSO, pH, 6.8) containing 3.7 % formaldehyde, 0.05% glutaraldehyde, 0.5 % Triton X-100, for 10min at room temperature. Coverslips were blocked in 10% goat serum in PBS for 10min and processed for double-labeling immunofluorescence with rat anti-α-tubulin (Covagen) and mouse anti HIF-1α (BD Biosciences). The secondary antibodies were Alexa Fluor 488 goat anti-mouse antibody and Alexa Fluor 568 goat anti-rat antibody antibodies (Molecular Probes). Coverslips were then mounted onto glass slides and examined with a LSM510 META Zeiss axioplasm laser scanning confocal microscope.

Transmission electron microscopy (TEM). PC3 cells were plated on Thermanox cover slips (Electron Microscopy Sciences #72280) in 24 well plates and grown overnight to 60% confluency. Cells were then exposed to 1% oxygen for 6 hr, and processed for double-labeling TEM microscopy with antibodies against tubulin (12 nm gold particles) and HIF-1α. (6 nm gold particles). They were initially fixed in 2% glutaraldelhyde for 4 hours at room temperature, rinsed in distilled water twice, post-fixed in 1% OsO4 in 0.1M sodium cacodylate buffer (pH 7.4) at 4°C for 1 hour and finally rinsed in distilled water as above. Samples were then dehydrated through an ethanol series (30, 50, 60, 80, 90, 100, 100%) followed by 2 changes of propylene oxide (PPO; 10 minutes each). Then samples were infiltrated with Embed 812 (Electron Microscopy Sciences) for 3 days according to the manufacturer's instructions. Each block was cut at 1mm x 1mm using a diamond knife and RMC MT-7000 ultramicrotome, and thin sections were made and collected onto 200 mesh copper grids. Grids were post stained with 10% uranyl acetate in distilled water and then 2% lead citrate in distilled water for 20 minutes in each treatment.

Molecular Beacons for HIF-1α. MBs were custom synthesized by Integrated DNA Technologies, Inc (IDT). For detection of gene expression in fixed cells, the cells were plated on glass coverslips overnight, after drug treatment they were fixed with ice-cold acetone for 5 minutes. After air drying, the slides were stained with MBs diluted in RPMI 1640 media at 100nM and then incubated on the slides at 37^0C for 60 minutes. The slides were washed with PBS and subjected to immunofluorescence staining or were counterstained with Sytox Green (Molecular Probes, Eugene, Oregon, USA) and mounted on a slide for visualization on a LSM 510 laser scanning (Zeiss) microscope (Zeiss axioplasm). For live cell imaging, the MBs were transfected with Oligofectamine (Invitrogen) according to the manufacturer's indications at a final concentration of 100nM and visualized with the Ultraview microscope (Perkin Elmer)

OBJECTIVE 2: Elucidate the details of the mechanism of action of agents that target the microtubules.

a. To investigate the proteins and signals involved in the step leading from mitotic arrest to apoptosis.
b. To investigate and characterize the "new" microtubule targeting agent Laulimalide

Survivin

Microtubules are essential components of the cytoskeleton and play a critical role in a variety of cellular processes including cell division, cell motility, intracellular trafficking, and cell shaping. Composed of αβ-tubulin heterodimers, microtubules are intrinsically dynamic polymers, and their dynamic property is crucial for the assembly of the mitotic spindle, the attachment of chromosomes to spindle microtubules, and the movement of chromosomes along the spindle (221-224). Suppression of microtubule dynamics by microtubule-targeting drugs such as the *Vinca* alkaloids and taxanes can engage the mitotic spindle checkpoint, arresting cell cycle progression at mitosis and eventually leading to apoptosis (115, 128, 225, 226). We have previously established a model of Taxol resistance consisting of a Taxol sensitive human ovarian cancer cell line 1A9 and two Taxol-resistant derivative cell lines, namely PTX10 and PTX22 (115). These two derivative cell lines are 25-fold resistant to Taxol due to acquired β-tubulin mutations in the Taxol binding site. Despite the 25-fold resistance, these Taxol-resistant cells undergo apoptosis when treated with higher, physiologically relevant, concentrations of Taxol. Herein we report that unlike the parental 1A9 cells, these Taxol-resistant cells have defective mitotic response to even high concentrations of Taxol that are sufficient to induce apoptosis. We also show that the defective mitotic response to Taxol in the Taxol-resistant cells is mediated by the dysregulation of the mitosis regulator and inhibitor of apoptosis protein survivin (227).

High Concentrations of Taxol Induce Apoptosis in the Absence of Mitotic Arrest in Taxol-resistant, β-Tubulin Mutant Cancer Cells — The Taxol-resistant, β-tubulin mutant human ovarian cancer cell line PTX10 exhibits 25-fold resistance to Taxol as compared to the parental Taxol-sensitive 1A9 cells (226). Cell cycle analysis (FACS) revealed that while 1A9 cells underwent mitotic arrest when treated for 16 h with as little as 10 nM of Taxol, PTX10 cells failed to arrest in mitosis even when treated with 100-fold higher concentrations of Taxol (1 μM) (**Figure 25A**). Nevertheless, both 1A9 and PTX10 cells exhibited apoptotic cell death in response to Taxol, as indicated by caspase 9 and PARP cleavage (**Figure 25B**).

To better understand the mechanism by which Taxol induced apoptosis in PTX10 cells without prior mitotic arrest, we performed a time-course cell cycle analysis of 1A9 and PTX10 cells treated with 10 and 250 nM of Taxol, respectively. These concentrations were selected based on the fact that PTX10 cells are 25-fold resistant to Taxol as compared to 1A9 cells. As shown in **Figure 25C**, 1A9 cells showed mitotic arrest as early as 12 h following Taxol treatment; however, no obvious mitotic arrest was observed in PTX10 cells even after 48 h of Taxol treatment. **Figure 25D** shows the percentages of mitotic and apoptotic cells in response to the treatment of Taxol (10 nM for 1A9 and 250 nM for PTX10). For example, almost complete mitotic arrest (82%) was observed in 1A9 after 24 h of treatment with Taxol; in contrast, a very modest mitotic arrest (8%) was observed in PTX10 cells following Taxol treatment. Nevertheless, after 48 h of treatment, 1A9 and PTX10 cells exhibited similar extent of apoptosis, 61% and 67% respectively. The lack of mitotic arrest prior to apoptosis in PTX10 cells was further confirmed by time-lapse video microscopy (**Figure 25E**). In this experiment, living 1A9 and PTX10 cells were visualized in the presence of 10 and 250 nM of Taxol, respectively. An obvious mitotic arrest was observed in 1A9 cells (cells rounding up) as early as 120 min of drug treatment. In contrast, no mitotic arrest was observed in PTX10 cells even after 400 min of drug treatment. PTX10 cells exhibited apoptotic figures after 240 min of Taxol exposure while 1A9 cells underwent apoptosis clearly following mitotic arrest (**Figure 25E**).

PTX10 Cells Undergo Very Transient Mitotic Arrest in Response to Taxol — To further investigate the molecular mechanism underlying the lack of Taxol-induced mitotic arrest in PTX10 cells, we synchronized cells by serum starvation and examined their cell cycle progression by BrdU incorporation assay. As shown in **Figure 26A**, both 1A9 and PTX10 cells exhibited a peak of BrdU positive cells 9.5 h after serum add back indicating S phase, when cells are active in DNA synthesis. We asked at which stage of the cell cycle Taxol-induced apoptosis occurred, by treating cells with Taxol (10 nM for 1A9 and 250 nM for PTX10) at 4, 9.5, or 15 h after serum add back. These time points correlated with G1, S, or G2 phase of the cell cycle, respectively. As shown in **Figure 26B**, 1A9 and PTX10 cells both showed the highest mitotic indices at 19 h after serum add back indicating mitosis. In addition, 1A9 and PTX10 cells treated with Taxol at any phase of the cell cycle (G1, S, or G2) entered mitosis (**Figure 26C**).

However, while 1A9 cells exhibited a prolonged (more than 18 h) mitotic arrest prior to apoptosis, PTX10 cells showed only a transient (less than 3 h) mitotic arrest (**Figure 26C-D**). The differential mitotic responses of 1A9 and PTX10 cells were also observed when higher concentrations of Taxol were used. For example, 1A9 cells remained able to arrest at mitosis for more than 15 h in response to even 1 μM of Taxol. However, PTX10 cells never exhibited mitotic arrest for more than 3 h. These data collectively indicated that Taxol-induced apoptosis occurred after entry to mitosis in both 1A9 and PTX10 cells, regardless of the time they spent in mitosis. A similar pattern of transient mitotic arrest in PTX10 cells was observed following treatment with additional microtubule-targeting drugs, including the microtubule-stabilizing drugs Taxotere and epothilone B, and the microtubule-destabilizing drug vinblastine (**Figure 26D**). These results therefore suggested that the mitotic response was severely impaired in these Taxol-resistant ovarian cancer cells as compared to the parental Taxol-sensitive cells.

Dysregulation of Survivin in Response to Taxol Treatment in the Taxol-resistant Cancer Cells — To study the mechanism by which the Taxol-resistant cells exhibited defective mitotic response to Taxol, we investigated several major proteins involved in the control of mitotic progression, including the mitotic spindle checkpoint proteins Mad2, Bub1 and BubR1 (115), and the mitosis regulator and inhibitor of apoptosis protein survivin (228). We compared the levels of these proteins between 1A9 and

PTX10 cells in three groups: cycling cells, mitotic cells derived from serum starvation and added back, and mitotic cells derived from serum starvation and added back plus Taxol treatment (**Figure 27A**). For all the three groups, there was no significant difference between 1A9 and PTX10 cells in Mad2, Bub1 and BubR1 expression levels. In addition, there was no obvious difference between 1A9 and PTX10 cells in the basal level of survivin in cycling or mitotic cells. However, PTX10 cells exhibited a much lower survivin level compared to the parental 1A9 cells in the group of mitotic cells derived from serum starvation and add back plus Taxol treatment (**Figure 27A**). The dysregulation of survivin in response to Taxol in PTX10 cells was further confirmed at different time points after serum added back plus Taxol treatment (**Figure 27).** For example, survivin expression was increased up to 7.4-fold in 1A9 cells after 20 h of serum add back. In contrast, there was no obvious increase in survivin expression in PTX10 cells at any time points (**Figure 27**).

To examine whether in PTX10 cells the dysregulation of survivin was due to incorrect intracellular localization, we stained cellular survivin and examined with confocal fluorescence microscopy **(Figure 28**). No difference was observed in survivin localization patterns between mitotic 1A9 and PTX10 cells. However, this experiment further demonstrated a lack of survivin induction in PTX10 cells in response to Taxol treatment (**Figure 28**).

Survivin Plays an Important Role in the Mitotic Response to Taxol — To test whether the dysregulation of survivin in the Taxol-resistant cells contributed to their defective mitotic response to Taxol, we introduced exogenous wild-type survivin in PTX10 cells and examined the percentages of mitotic and apoptotic cells after Taxol treatment (**Figure 29A**). We found that exogenous expression of wild-type survivin restored the mitotic response of PTX10 cells to Taxol treatment (the peak mitotic arrest was 62% at 24 h of Taxol treatment) (**Figure 29A**). In contrast, expression of dominant-negative survivin had no effect in their mitotic response (**Figure 29A**). In addition, exogenous expression of wild-type survivin had no obvious effect in the Taxol-induced mitotic response in 1A9 cells (**Figure 29B**). However, when 1A9 cells were transfected with dominant-negative survivin, their mitotic response to Taxol was significantly suppressed to a level comparable to that observed in PTX10 cells (**Figure 29B**). We also

observed that exogenous expression of survivin could enhance the mitotic arrest of PTX22 cells to Taxol treatment. These results thus demonstrated the importance of survivin in the control of mitotic response to Taxol treatment.

Figure 25. Differential mitotic response to Taxol in Taxol-sensitive and Taxol-resistant ovarian cancer cells.

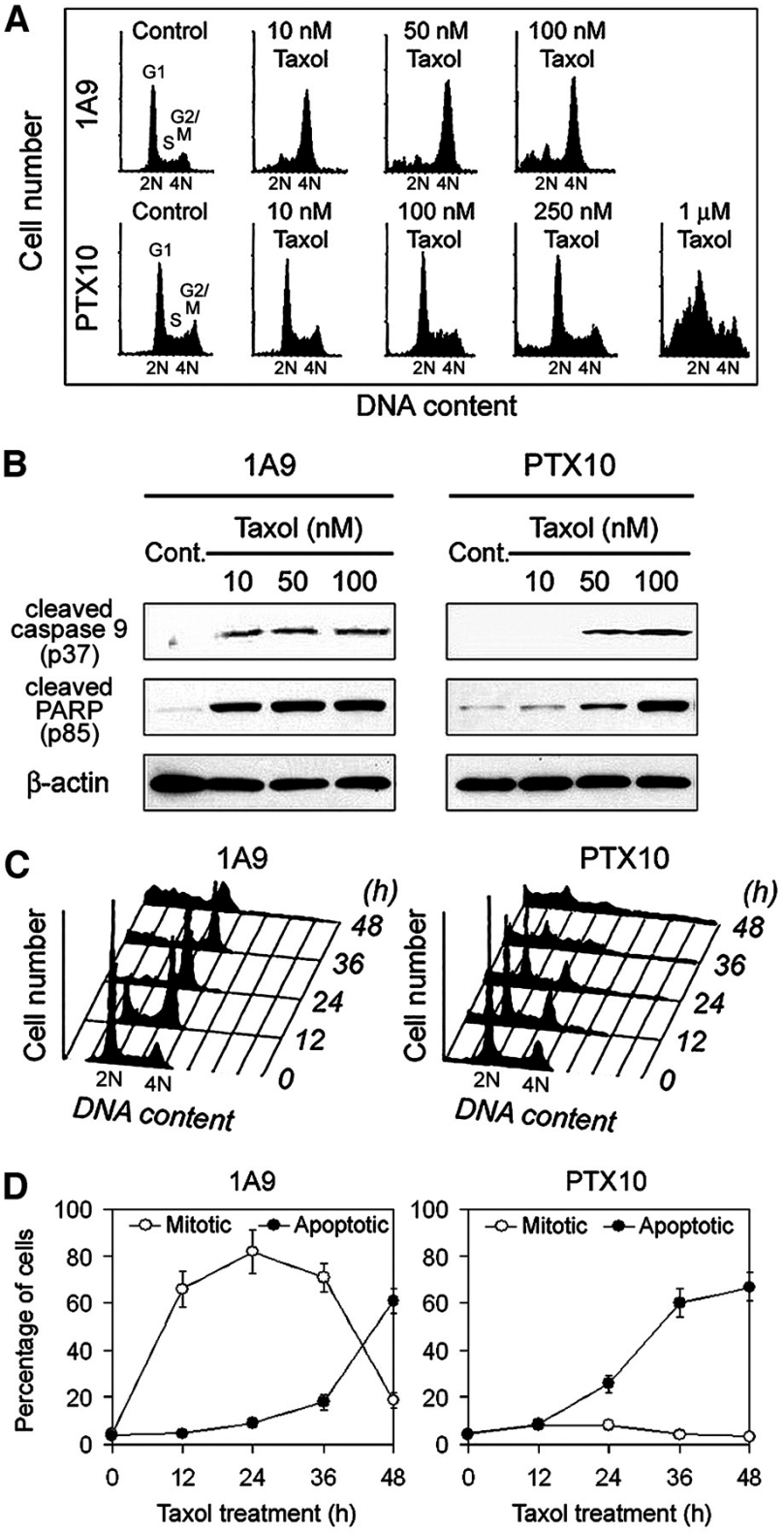

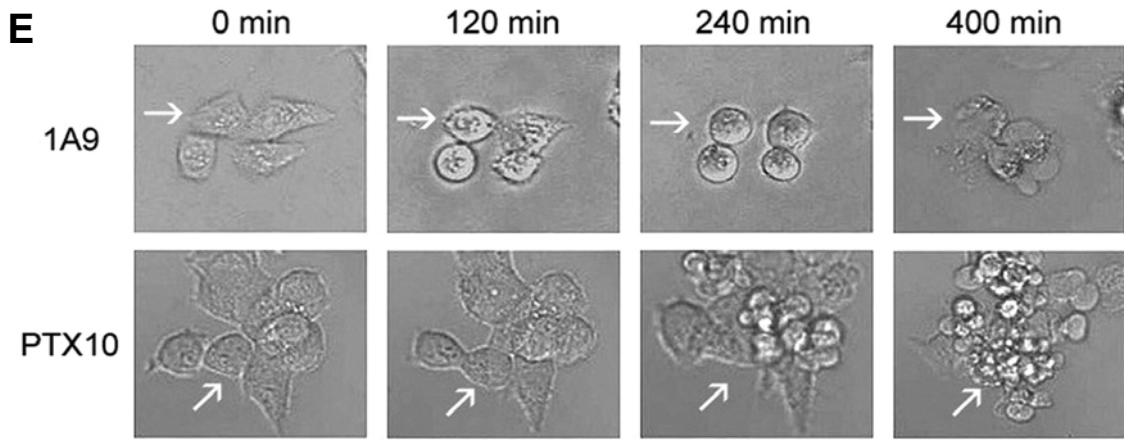

Figure 25. Differential mitotic response to Taxol in Taxol-sensitive and Taxol-resistant ovarian cancer cells. A) *Fluorescence-activated cell sorting analysis of DNA content in the Taxol-sensitive cell line 1A9 and in the Taxol-resistant derivative cell line PTX10. Cells were treated for 16 hours with the indicated concentrations of Taxol or with the solvent DMSO as control. Cells with 2 N DNA content are in G1 phase, 2 to 4 N in S phase, and 4 N in G2-M phase.* ***B)*** *Western blot analysis of cleaved caspase 9 (p37) and cleaved poly(ADP-ribose) polymerase (p85) in 1A9 and PTX10 cells treated with Taxol for 16 hours.* ***C)*** *Time course fluorescence-activated cell sorting analysis of DNA content in 1A9 and PTX10 cells treated with 10 and 250 nmol/L Taxol, respectively.* ***D)*** *Percentages of mitotic and apoptotic cells measured by DNA staining. 1A9 and PTX10 cells were treated with 10 and 250 nmol/L Taxol, respectively, for the indicated time. The values and error bars shown in this figure and in the following figures represent the averages and SDs, respectively, of three independent experiments.* ***E)*** *Time-lapse video microscopy of 1A9 and PTX10 cells treated with 10 and 250 nmol/L Taxol, respectively.*

Figure 26. PTX10 cells undergo very transient mitotic arrest in response to Taxol. A) *1A9 and PTX10 cells were synchronized by serum starvation, and the percentage of cells in S phase after serum add back was determined by BrdUrd incorporation at the indicated time points.* ***B)*** *Cells were synchronized by serum starvation, and the mitotic indices after serum add back were subsequently measured by DNA staining at the indicated time points.* ***C)*** *Cells were synchronized by serum starvation, and 4 hours after serum add back, they were treated with 10 and 250 nmol/L Taxol, respectively. The mitotic indices were then measured at the indicated time points.* ***D)*** *1A9 and PTX10 cells were processed as in C, and the duration of mitotic arrest in response to various microtubule-targeting drugs was measured by DNA staining.*

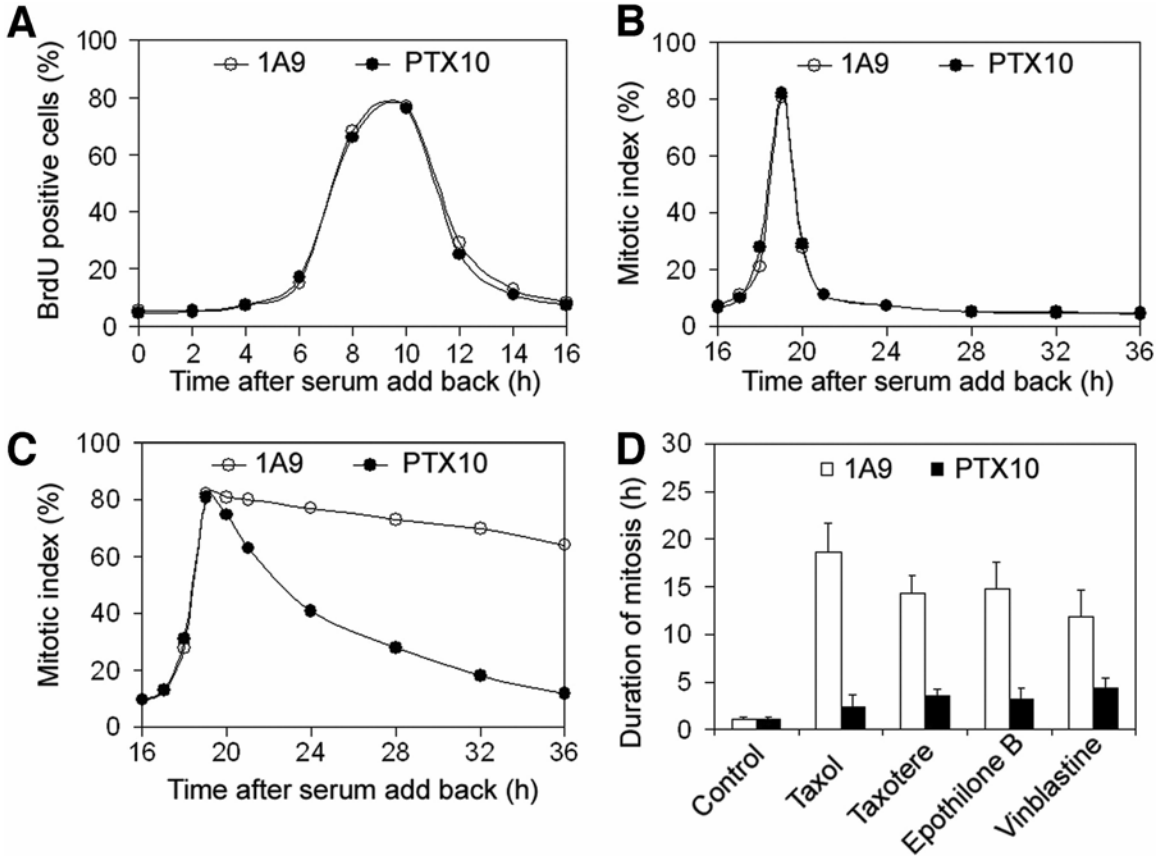

Figure 27. Deregulation of survivin in response to Taxol in PTX10 cells. A) *Survivin levels analyzed by Western blotting. 1A9 and PTX10 cells were synchronized by serum starvation, and 4 hours after serum add back, they were treated with 10 and 250 nmol/L Taxol respectively, for the indicated time. Actin was used as a loading control.* ***B)*** *Fold increase of survivin in response to Taxol. Experiments were done as in A, and survivin levels were determined by densitometric analysis of the protein bands on Western blots.*

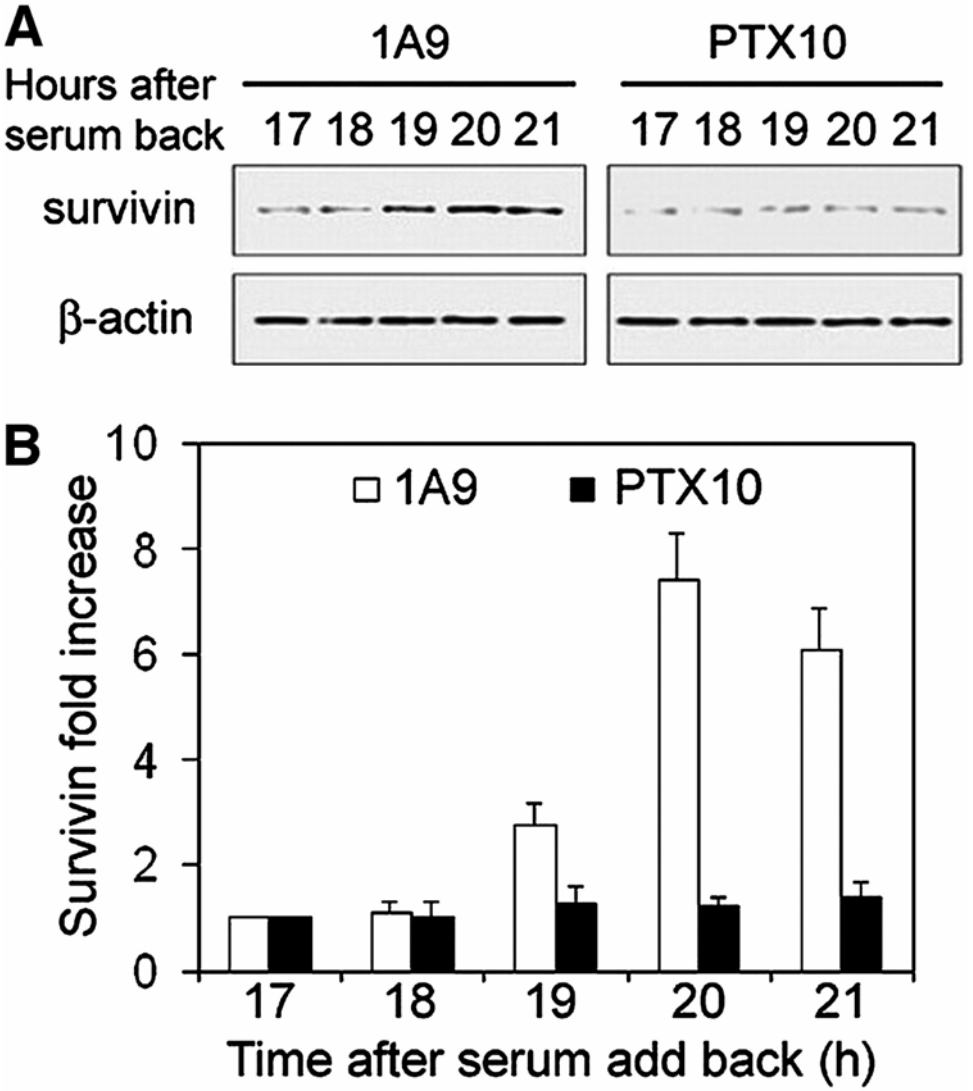

Figure 28. *Immunofluorescence images of microtubules (MT, red) and survivin (green) in 1A9 and PTX10 cells treated for 12 hours with 10 and 250 nmol/L Taxol, respectively. Arrows point at representative mitotic cells. Bar, 10 μm.*

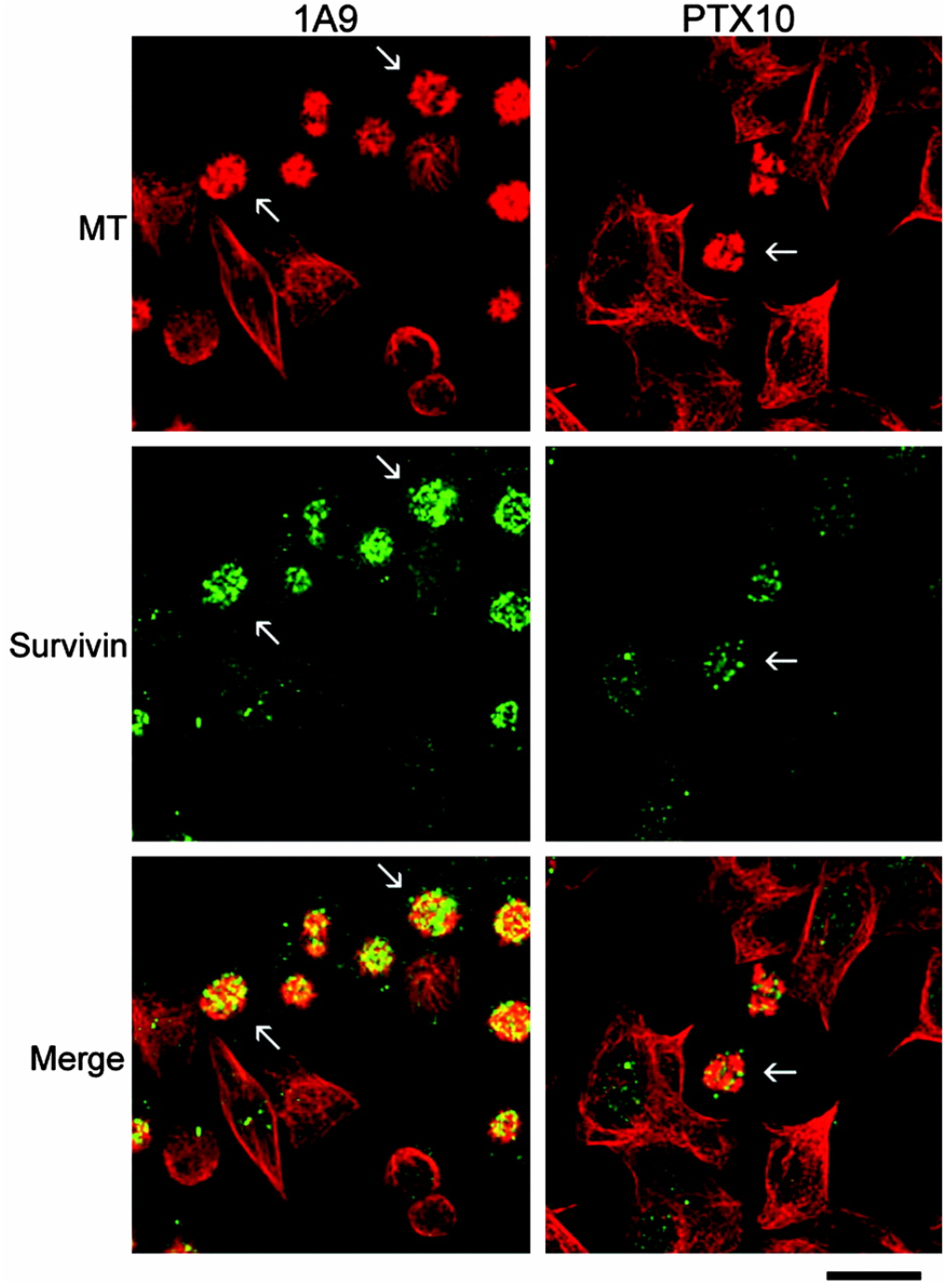

Figure 29. Survivin plays an important role in the mitotic response to Taxol*. PTX10 (**A**) and 1A9 (**B**) cells were transfected with plasmids expressing wild-type survivin (survivin-wt), dominant-negative survivin (survivin-dn), or an empty vector, and 24 hours later they were treated with 250 and 10 nmol/L Taxol, respectively. Percentages of mitotic and apoptotic cells were measured by DNA staining at the indicated time points after Taxol treatment.*

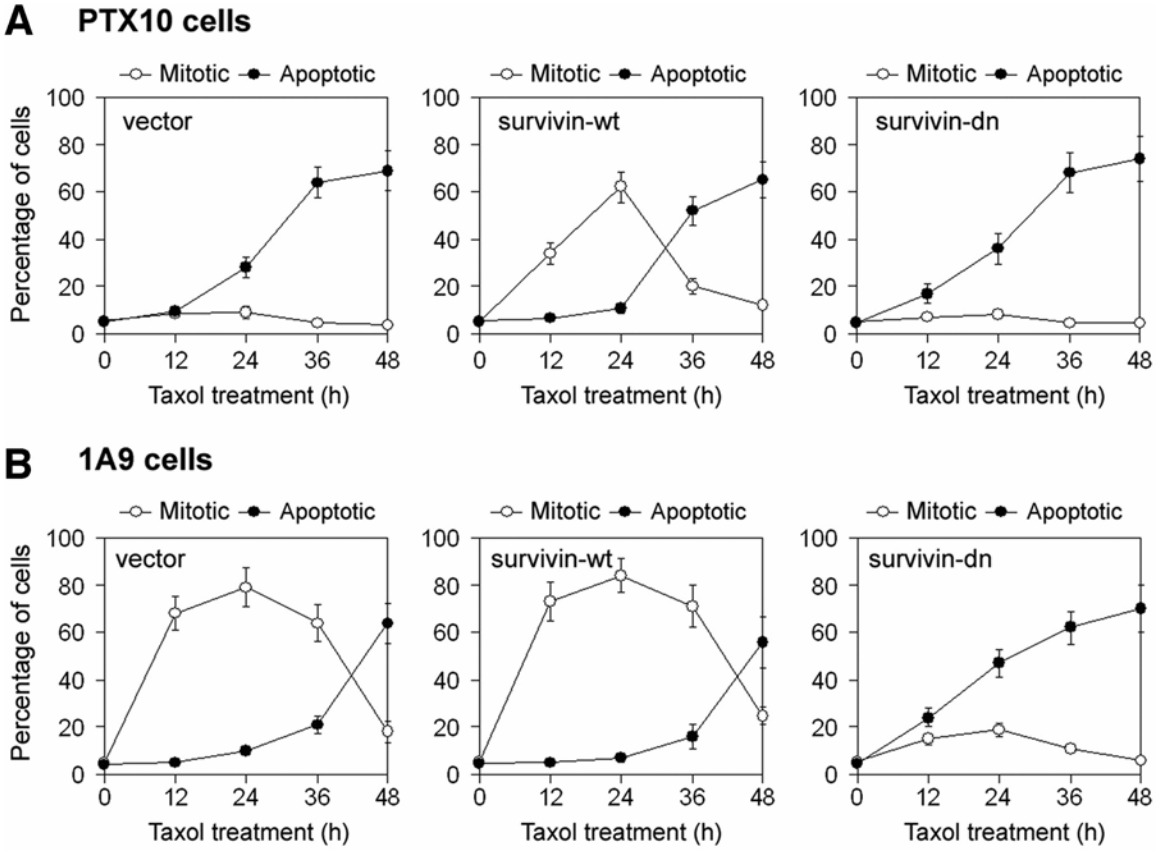

Discussion

In this study, we have shown that PTX10 and PTX22, were obtained exhibiting 25-fold resistance due to acquired β-tubulin mutations in the Taxol binding site (226) these Taxol-resistant cells undergo apoptosis when treated with higher, physiologically relevant Taxol concentrations, albeit without prior arrest in mitosis. These results are very intriguing since the relationship between Taxol-induced mitotic arrest and apoptosis remains largely unknown (229). Because mitotic arrest typically precedes apoptosis, a natural hypothesis is that mitotic arrest may provide a 'sensitive' state that prepares cells for subsequent apoptosis. Alternatively, mitotic arrest and apoptosis may represent two independent events resulting from the disruption of the normal physiological balance of microtubule dynamics. However, a conclusive answer to this important question is experimentally very challenging. Thus, the β-tubulin mutant Taxol-resistant cells provided us with a very useful experimental tool to approach this question. Here we show that Taxol-induced apoptosis requires prior entry to mitosis, even if transiently as in the case of PTX10 cells, suggesting that 1) cells go through mitotic entry, mitotic arrest and then mitotic exit to commit apoptosis in response to Taxol; 2) the duration of mitotic arrest provides a temporal determinant for the initiation of apoptosis.

Our results also suggest that there must be specific signals triggering apoptosis when cells are in a state of aberrant mitotic arrest (Taxol-induced), which is fundamentally distinct from the regular mitosis observed in cycling cells. To understand those signals, we have examined the potential involvement of proteins important for mitotic progression. Among the proteins examined, survivin appears to be the one critically involved in this pathway. Survivin has attracted considerable attention over the past years owing to its dual role in mitotic progression and apoptosis. Furthermore, this small protein (16 kDa) is highly overexpressed in many types of cancer but nearly undetectable in normal differentiated adult tissues, and thus seems to be a bona fide target for cancer specific therapy (230). At the cellular level, survivin is specifically expressed during the mitotic phase of the cell cycle (231). This cell cycle-regulated expression pattern of survivin has been documented by our studies with both 1A9 and PTX10 cells. It has been reported that the upregulated expression of survivin in mitosis can be further induced by microtubule-targeting drugs in a dose-dependent manner (80). We have also found that

Taxol can increase survivin expression in 1A9 cells, but not in the Taxol-resistant PTX10 cells even at high concentrations that compensate for the 25-fold resistance. Furthermore, exogenous expression of wild-type survivin is able to restore the mitotic response of PTX10 cells to Taxol treatment prior to their apoptosis. Exogenous expression of dominant-negative survivin, on the other hand, can abrogate the mitotic response of 1A9 cells to Taxol. These results therefore strengthen the critical role for survivin in the coordination of mitotic and apoptotic events in response to Taxol.

Laulimalide

The growing clinical usefulness of the taxoids (81) and the discovery of new natural products [epothilones (232), discodermolide (233), eleutherobin (234), laulimalide (74) and peloruside A (167)] with the same mechanism of action have occurred nearly simultaneously. The key feature of this mechanism is the binding of these compounds to microtubules, resulting in stabilization of these polymers (235-237) and quenching of their dynamic properties (233). Cells exposed to such drugs are unable to form a normal mitotic spindle, cannot divide after DNA replication, and soon undergo apoptosis. The epothilones, discodermolide, and eleutherobin inhibit the binding of [3H]- paclitaxel to tubulin polymer in a competitive manner (80, 235), suggesting that they bind to the same or overlapping sites on the protein.

Tubulin Assembly. In initial experiments, we confirmed the report of Mooberry et al. (218, 237, 238) that laulimalide appeared to be quantitatively similar to paclitaxel in its ability to induce microtubule assembly (239). Originally, we had planned to compare laulimalide with epothilone A because of the structural similarities between the two compounds (epoxide moiety, bulky side chain, lactone macrocycle) and because the effect of epothilone A on tubulin assembly is also quantitatively similar to that of paclitaxel (237). When we discovered that laulimalide had no apparent ability to inhibit taxoid binding to tubulin, it became important to include in the comparative studies, as controls, drugs less potent than laulimalide as stimulators of assembly that nonetheless were able to inhibit taxoid binding to tubulin. The polymerization studies presented in **Figure 30** were performed with a reaction system containing 10 μM tubulin, the drug usually at 10 μM, heat-treated MAPs, and GTP, with polymerization followed turbidimetrically. Temperature in these experiments was increased stepwise until relatively rapid assembly had occurred in each reaction mixture. Following assembly, the temperature was returned to 0 °C to evaluate polymer stability. In panel A, the reaction without drug (curve 0) is compared to reactions with 10 μM laulimalide, paclitaxel, or epothilone A (curves 1, P, and 2, respectively) and with 10 or 40 μM *trans*-desoxylaulimalide (curves 3L and 3H, respectively). The chief differences between the reactions induced by paclitaxel and laulimalide or epothilone A were that a greater

turbidity change occurred at warmer temperatures with paclitaxel and that the paclitaxel-induced polymer seemed less cold stable. The laulimalide analogue was distinctly less active than the parent compound, but its effect on assembly was enhanced by increasing the drug concentration. In panel B (**Figure 30**), assembly data is shown for three compounds clearly less active than laulimalide as inducers of tubulin assembly. These compounds, which had all been found to have relatively weak activity as inhibitors of the binding of [3H]paclitaxel to tubulin polymer (218, 235-237, 240), were sarcodictyin A (curve 5), the 2-ethoxyestradiol analogue (curve 6), and baccatin III (curve 7). Assembly induction by baccatin III is greater when higher concentrations of the compound are used. Assembly induced by eleutherobin, a more active congener of sarcodictyin A (238), is represented by curve 4, and assembly with laulimalide by curve 1.

Failure of Laulimalide to Inhibit Binding of Either [3H]-Paclitaxel or Flutax-2 to Tubulin Polymer. In previous studies (238), we had found that discodermolide, docetaxel, epothilones A and B, eleutherobin, and, to a lesser extent, sarcodictyins A and B, baccatin III, and the 2-ethoxyestradiol analogue had inhibited the binding of [3H]-paclitaxel to tubulin polymer. The inhibition patterns obtained with the more potent inhibitors all were of the competitive type, suggesting that they bind to the same or overlapping sites on tubulin. We examined laulimalide for its effect on this reaction, and neither laulimalide nor *trans*-desoxylaulimalide inhibited [3H]paclitaxel binding (**Table 3**). In at least 20 variations of this experiment, with laulimalide concentrations as high as 50 μM with 2 μM tubulin, this same negative result was obtained. Laulimalide failed to inhibit [3H]- paclitaxel binding even when laulimalide and tubulin polymer were incubated prior to addition of the paclitaxel, excluding slow binding of laulimalide relative to paclitaxel, or when polymer was generated in the presence of MAPs, excluding a binding site generated by the interaction of tubulin with MAPs, as might have occurred in the assembly reaction of **Figure 30**. In some experiments, in fact, laulimalide led to an increase in the amount of [3H]-paclitaxel bound to polymer, possibly indicating that the combination of laulimalide and paclitaxel caused an increase in the amount of polymer formed, and thus an increase in the number of available sites for paclitaxel. In the experiments presented in **Table 3**, weak inhibition was obtained with sarcodictyin A, while both epothilone A and eleutherobin potently inhibited the

binding of [3H]paclitaxel to the tubulin polymer. Because this result with laulimalide was so unexpected, we confirmed it with Flutax-2 (241) (**Figure 31**). The strength of the fluorescence polarization anisotropy signal permits the use of nanomolar concentrations of Flutax-2 and tubulin and consequently a much higher inhibitor-to-taxoid ratio than is usually possible with [3H]paclitaxel binding assays. In this assay, too, laulimalide was noninhibitory (**Figure 31**, solid circles), in contrast to the potent inhibition obtained with paclitaxel (open squares) or docetaxel (open circles). In these experiments, the maximum ratio of laulimalide to Flutax-2 was 400:1, versus 25:1 in the [3H]paclitaxel experiments. We had previously used this assay, with the high ratio of inhibitor to taxoid that it makes possible, to document convincingly the ability of baccatin III to bind in the taxoid site (238) despite the much weaker effect of baccatin III as compared with laulimalide on tubulin assembly (**Figure 30B**). As a further control, for contrast to the inability of laulimalide to inhibit Flutax-2 binding, we examined the effect of another weak inducer of assembly, the 2-ethoxyestradiol analogue, to inhibit Flutax-2 binding, and we found the steroid derivative to have an effect on Flutax-2 binding similar to that observed previously with baccatin III (**Figure 31**, open triangles).

Table 3: Laulimalide and *trans*-Desoxylaulimalide Are Unable to Inhibit the Binding of [^{3}H]Paclitaxel to Tubulin Polymer

drug added	**% inhibition ± SE**
30 μM laulimalide	0
30 μM *trans*-desoxylaulimalide	0
30 μM sarcodictyin A	41 ± 9
5 μM eleutherobin	75 ± 2
30 μM eleutherobin	89 ± 6
5 μM epothilone A	67 ± 3
30 μM epothilone A	91 ± 4

Table 3: *The potential inhibitor and [^{3}H]paclitaxel, in amounts sufficient to yield the indicated concentrations of the potential inhibitors and 2 μM paclitaxel, were mixed in a microfuge tube. Tubulin polymer (final tubulin concentration, 2 μM; at least 90% of the tubulin in polymer) was added to each tube. Following a 30 min incubation at 37° C, the reaction mixtures were centrifuged, and the amount of radiolabel present in an aliquot of each supernatant was determined in a liquid scintillation counter. The radiolabel content of uncentrifuged reaction mixtures*

was also determined. The pellet was assumed to contain the difference between the total radiolabel and the supernatant radiolabel. In the absence of an effective inhibitor, about 25% of the added radiolabel was recovered in the supernatant. The data presented are results from all determinations with each compound at the indicated concentrations. At least 20 experiments were performed with laulimalide and 3 with trans-desoxylaulimalide, and no inhibitory effect was ever observed. The inhibitory control drugs were each examined at least three times. SE, standard error.

Simultaneous Binding of Laulimalide and Paclitaxel to Microtubules. We next sought positive evidence that laulimalide and paclitaxel could bind to microtubules simultaneously by examining the ligand content of microtubule pellets by HPLC. We It has previously been shown by this technique that docetaxel and paclitaxel ((115)) or that baccatin III and paclitaxel (142) mutually excluded each other from binding to microtubules, consistent with the three compounds binding to the same site on polymer. **Figure 32** demonstrates that the opposite occurs with paclitaxel and laulimalide. When 35μM tubulin was polymerized in the presence of 37.5 μM paclitaxel, 92% of the tubulin was recovered in the polymer pellet, as well as paclitaxel in an amount equivalent to 1.04 mol/mol tubulin (**Figure 32A**). When 37.5μM laulimalide was used instead, 96% of the tubulin was in the polymer, along with an amount of laulimalide equivalent to 0.93 mol/mol tubulin (**Figure 32B**). When both drugs at 37.5 μM were used to induce assembly, 91% of the tubulin was in polymer with near stoichiometric amounts of both drugs: 0.96 mol paclitaxel/mol tubulin and 0.83 mol laulimalide/mol tubulin.

This result confirms the observations with [3H]paclitaxel and Flutax-2 that laulimalide does not interfere with the binding of taxoids to tubulin. The most straightforward interpretation of these data is that laulimalide does not bind in the taxoid site on β-tubulin. Instead, it must bind at an alternate location in the αβ-tubulin dimer.

Effects of Laulimalide on Drug-Resistant Cell Growth. The above biochemical findings made it particularly interesting to evaluate the effects of laulimalide on the growth of cells resistant to paclitaxel and the epothilones. We therefore examined a series of drug-resistant human ovarian carcinoma cell lines for their sensitivity to laulimalide in

comparison with paclitaxel and epothilones A and B (Table 4). 1A9/AD10 is a multidrug-resistant line that overexpresses Pglycoprotein. PTX10 and PTX22 were selected for resistance to paclitaxel (242) and A8 and B10 for resistance to epothilones A and B (233), respectively. The latter four lines were all found to have mutations in the M40 β-tubulin gene at amino acids near the binding site for taxoids (**Figure 11**), as derived from the electron crystallographic tubulin polymer model (80). As previously noted, laulimalide (235), like epothilones A and B (236), is not a good substrate for P-glycoprotein, and the 1A9/AD10 cell line retained sensitivity to laulimalide. All four lines with drug resistance based on mutations in the β-tubulin gene also retained their sensitivity to laulimalide. It is particularly interesting to note that the relative resistance values of the mutant lines relative to the parental line observed for laulimalide with the paclitaxel-resistant lines, especially PTX10, are lower than those obtained for either epothilone A or B; similarly, with the epothilone resistant lines, the relative resistance values for laulimalide are lower than those obtained for paclitaxel. This could derive from laulimalide binding to a distinct site on tubulin polymer, as strongly indicated by the biochemical evidence. At the same time, however, the paclitaxel-resistant lines (PTX10 and PTX22) retain significant sensitivity to the epothilones ((142), **Table 4**) and discodermolide (235), and the epothilone-resistant cells retain partial sensitivity to paclitaxel ((243), **Table 4**).

Table 4: Human Ovarian Carcinoma Cells Resistant to Paclitaxel or Epothilones Retain Sensitivity to Laulimalide

	cell lines[a]					
	IC_{50} (nM) ± SE[b]					
	(relative resistance[c])					
Compound	**1A9**	**PTX10**	**PTX22**	**A8**	**B10**	**1A9/AD10**
laulimalide	3.9 ± 0.4	6.0 ± 1	6.3 ± 1	9.2 ± 2	15 ± 0.2	31 ± 0.6
		(1.5)	*(1.6)*	*(2.4)*	*(3.8)*	*(7.9)*
epothilone A	1.7 ± 0.3	18 ± 7	4.3 ± 1	93 ± 30	125 ± 25	16 ± 0.6
		(11)	*(2.5)*	*(55)*	*(74)*	*(9.4)*
epothilone B	0.17 ± 0.08	0.70 ± 0.4	0.32 ± 0.2	6.4 ± 4	9.0 ± 5	2.6 ± 2
		(4.1)	*(1.9)*	*(38)*	*(53)*	*(15)*
paclitaxel	1.7 ± 0.3	50 ± 11	34 ± 3	13 ± 2	16 ± 4	4000 ± 900
		(29)	(20)	(7.6)	(9.4)	(2400)

Table 4. *[a]The parental cell line 1A9, a clone of line A2780, was used to select paclitaxel-resistant lines PTX10 and PTX22 and epothilone-resistant lines A8 and B10. These lines have four different mutations in the M40 β-tubulin gene (see legend of* ***Figure 11*** *for details). The multidrug-resistant, P-glycoprotein overexpressing line 1A9/AD10, selected in the presence of adriamycin, was also derived from A2780.[b] SE, standard error. IC_{50} values were determined at least 5 times.[c] The IC_{50} value of the resistant line divided by the IC_{50} value of 1A9*

The apparent binding of laulimalide at a new site on tubulin polymer raised the interesting possibility that this agent might have synergistic cytotoxic activity with compounds that bind at the taxoid site. This possibility particularly merited exploration in view of recent findings with discodermolide. Even though the kinetic evidence showed that discodermolide competitively inhibited the binding of [3H]paclitaxel to tubulin polymer (238), Martello et al. (79, 127, 242) found that paclitaxel and discodermolide had synergistic cytotoxic activity against several cancer cell lines. This finding could indicate that discodermolide and paclitaxel may bind at overlapping rather than identical sites on tubulin polymer. With the parental 1A9 cells, we were able to demonstrate synergistic cytotoxicity between paclitaxel and discodermolide at selected drug concentrations. Thus far, however, we have found no combination of laulimalide with paclitaxel, epothilone A or B, or discodermolide that indicates synergistic activity.

Figure 30. Drug-induced tubulin assembly in the presence of MAPs and GTP*. Reaction mixtures (final volume, 0.25 mL) containing all components except the drug were placed in cuvettes held at 0 C in Gilford model 250 spectrophotometers equipped with electronic temperature controllers. Baselines were established at 350 nm, and the drug was added in dimethyl sulfoxide (final concentration, 1%). Turbidity changes were followed, with the indicated temperature changes made at the time points indicated by the dashed lines to the left of the temperature. Reaction mixtures contained 0.1 M 4-morpholineethanesulfonate (pH 6.9 with NaOH in 1 M stock solution), 10mM (1.0 mg/mL) tubulin, 0.75 mg/mL heat-treated MAPs, and 0.1 mM GTP.* ***A)*** *Curve 0, no drug; P, 10mM paclitaxel; 1, 10mM laulimalide; 2, 10mM epothilone A; 3L, 10mMtrans-desoxylaulimalide; 3H, 40mM trans-desoxylaulimalide.* ***B)*** *Curve 0, no drug; 1, 10mM laulimalide; 4, 10mM eleutherobin; 5, 10mM sarcodictyin A; 6, 10mM 2-ethoxyestradiol analogue; 7, 10mM baccatin III.*

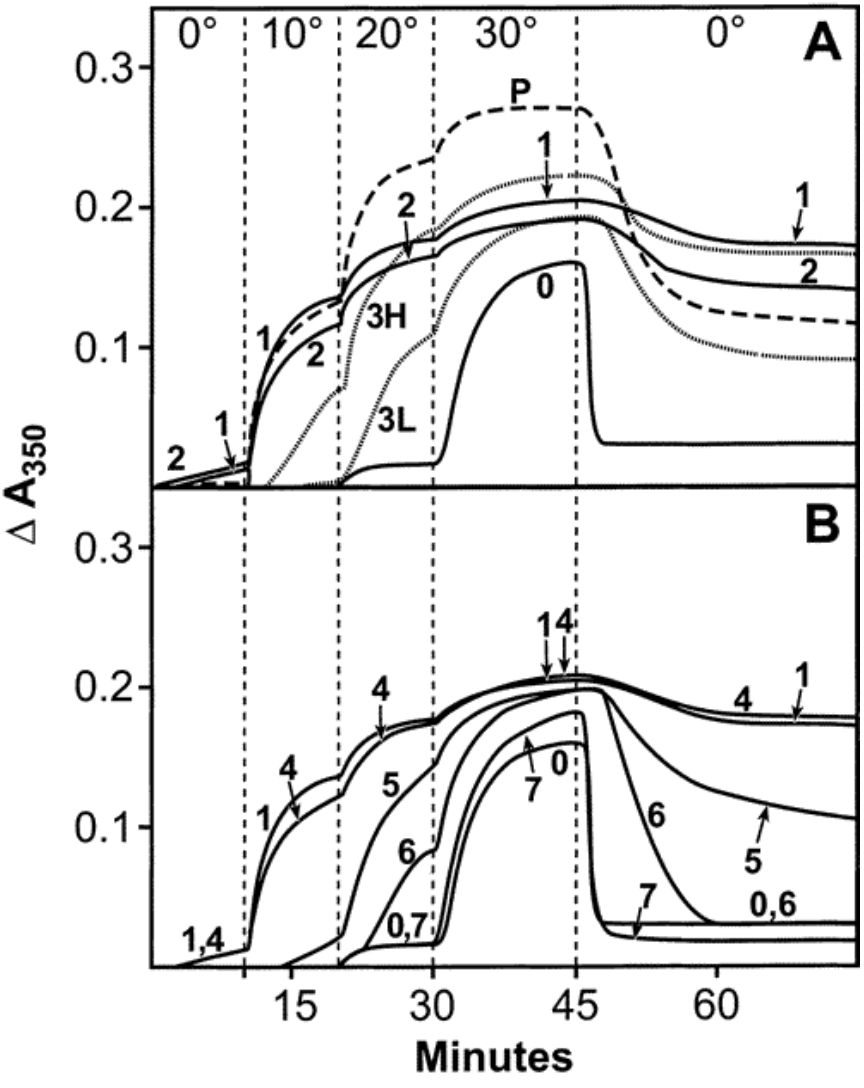

Figure 31. Inhibition of binding of Flutax-2 to tubulin polymer by paclitaxel, docetaxel, and the 2-ethoxyestradiol analogue but not by laulimalide*. **A)** The values shown are averages obtained in at least four independent experiments. These values are 2.2 ± 0.2 × 10^5 M^{-1} for the 2-ethoxyestradiol analogue, 1.5 ± 0.4 2 ×10^7 M^{-1} for paclitaxel, and 6.7 ± 1.2 2 ×10^7 M^{-1} for docetaxel. Standard errors for the data points are shown in the Figure, unless smaller than the symbol, and are also indicated for the apparent equilibrium binding constants. In the previous study Andreu 1998 at 25 oC, the average apparent binding constants obtained for paclitaxel, docetaxel, and baccatin III were, respectively, 3.7 2 ×10^7 , 6.0 2 ×10^7 , and 1.5 2 ×10^5 M^{-1} .**B) Binding of paclitaxel (a), laulimalide (b), or both laulimalide and paclitaxel to microtubules (c)**. Tubulin was polymerized, the polymer was harvested by centrifugation, the tubulin content of each pellet was determined, and bound ligand was extracted from the pellet protein and (244) analyzed by HPLC as described in the text. Each injection contained equivalent amounts of extract in terms of tubulin content of the pellets. (A) HPLC analysis of extract from microtubules formed in the presence of paclitaxel. (B) HPLC analysis of extract from microtubules formed in the presence of laulimalide. (C) HPLC analysis of extract from microtubules formed in the presence of both laulimalide and paclitaxel.*

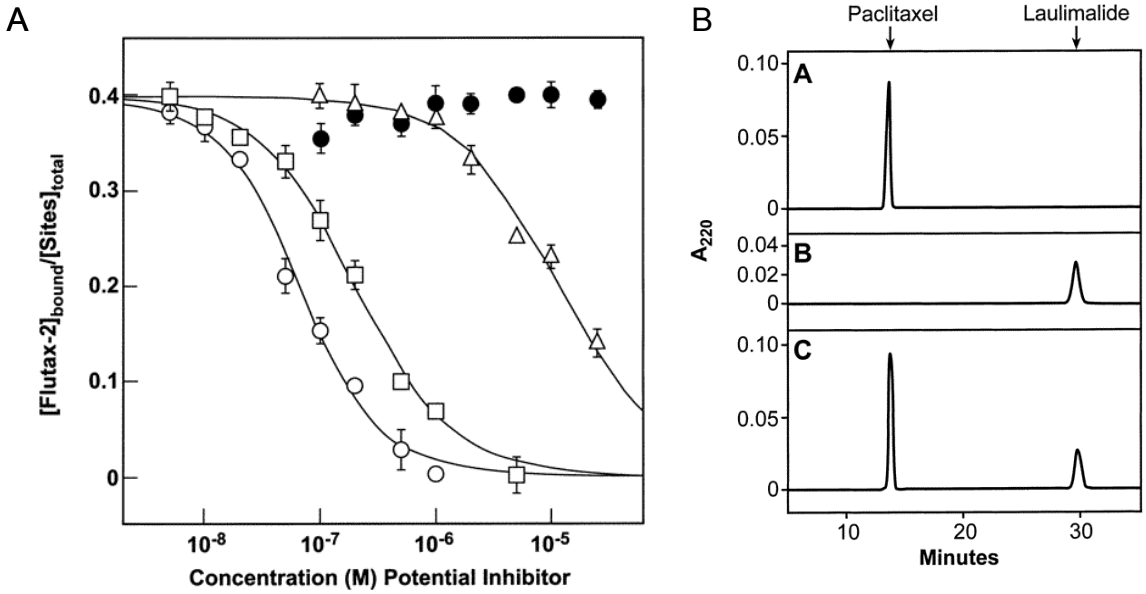

Discussion

In summary, while laulimalide has microtubule assembly promoting activity comparable to the activities of paclitaxel, epothilone A, and eleutherobin and much greater than the activities of sarcodictyin A, the 2-ethoxyestradiol analogue, and baccatin III, it is unable to inhibit the binding of either [3H]paclitaxel or Flutax-2 to tubulin polymer. In contrast, the relatively weak inducers of assembly sarcodictyin A, the 2-ethoxyestradiol analogue, and baccatin III all are able to interfere with taxoid binding to polymer. Even more compelling, when tubulin polymer was formed in the presence of both laulimalide and paclitaxel, it contained nearly molar equivalents of both drugs relative to the tubulin content. Laulimalide thus appears to bind at a previously unknown drug binding site on microtubules. The results with the paclitaxel- and epothilone-resistant ovarian cancer lines bearing mutated β-tubulin genes further support this conclusion from the biochemical experiments. Although the paclitaxel-resistant mutants remain sensitive to the epothilones and the epothilone-resistant mutants remain partially sensitive to paclitaxel, the relative resistance values for laulimalide are the lowest observed in all cases. It should be possible to locate the binding site of laulimalide on the αβ-tubulin dimer by the electron crystallographic technique (141), provided that the drug binds to zinc-induced sheets and remains bound during sample preparation.

MATERIALS AND METHODS FOR OBJECTIVE 2

Materials and Methods for Survivin

Materials — Taxol and vinblastine (Sigma-Aldrich), Taxotere (Aventis Pharmaceuticals), epothilone B (Novartis), and purvalanol A (Calbiochem) were from the indicated sources. All drugs were prepared as 100 mM stocks in dimethyl sulfoxide (DMSO) and stored in aliquots at -80oC. The following antibodies were used: rabbit anticleaved caspase 9, rabbit anti-cleaved poly (ADP-ribose) polymerase (PARP) from Cell Signaling; rabbit anti-survivin and goat anti- phosphorylated survivin from Santa Cruz Biotechnology; mouse anti-β-actin (Sigma- Aldrich); rat anti-α-tubulin, mouse anti-Bub1 and mouse anti-BubR1 from Chemicon; and rabbit anti-Mad2 from Abcam. The following secondary antibodies were used: horseradish peroxidase-conjugated anti-rabbit and anti-mouse antibodies (Sigma Aldrich), and rhodamine-conjugated anti-rat and fluorescein-conjugated anti-rabbit antibodies (Jackson ImmunoResearch).

Cell Culture and Synchronization — The human ovarian carcinoma cell line 1A9 and its Taxol-resistant derivative cell lines were cultured in RPMI 1640 medium (Invitrogen) supplemented with 10% fetal bovine serum (FBS) at 37oC in a humidified atmosphere with 5% CO2/95% air. For experiments involving synchronization, cells were grown in culture medium containing 1% FBS for 30 h (serum starvation) and then replaced with medium containing 10% FBS (serum add back). The percentage of cells in S phase at different time points after serum add back was determined using a 5-bromo-2'doxyuridine (BrdU) labeling and detection kit (Roche Applied Science).

Flow Cytometry — Analysis of the cell cycle by fluorescence-activated cell sorting (FACS) assay was performed as previously described (61). In brief, cells were centrifuged, washed twice with ice-cold phosphate-buffered saline (PBS), and fixed in 70% ethanol at -20oC. Cells were resuspended in 30 μl of phosphate/citrate buffer (0.2 M Na2HPO4/0.1 M citric acid, pH 7.5) at room temperature for 30 min, and then incubated with propidium iodide (20 μg/ml)/RNase A (20 μg/ml) in PBS for 30 min. Samples were analyzed on a Coulter Elite flow cytometer (Beckman Coulter).

Transient Transfection and Adenovirus Infection — The plasmid expressing survivin was kindly provided by Dr. Fengzhi Li (Roswell Park Cancer Institute). Transient transfections were performed using the Fugene 6 reagent (Roche Applied Science), as previously described (245).

Time-Lapse Video Microscopy — Cells grown in 35-mm dishes were examined with a Zeiss Axiovert microscope equipped with phase contrast, using a 20X objective. A stage heater was used to maintain the temperature at 37 ± 0.5°C. Images were taken using a Hamamatsu Orca II camera (Middlesex) every 4 min controlled by Metamorph image analysis software (Universal Imaging).

Fluorescence Microscopy — Cellular survivin and microtubules were examined by immunofluorescence microscopy as described (246). In brief, cells grown on 12 mm glass coverslips were fixed with PHEMO buffer (PIPES 68 mM, HEPES 25 mM, EGTA 15 mM, MgCl2 3 mM, 10% DMSO, pH 6.8) containing 3.7% formaldehyde, 0.05% glutaraldehyde, and 0.5% triton X-100 for 10 min at room temperature. Nonspecific sites were blocked by incubating with 10% goat serum in PBS for 10 min and processed for immunofluorescence staining with rat anti-α-tubulin and rabbit anti-survivin antibodies. The secondary antibodies were rhodamine-conjugated anti-rat and fluorescein-conjugated anti-rabbit antibodies. Coverslips were then mounted onto glass slides and examined with a Zeiss axioplasm laser scanning confocal microscope using a Zeiss 100X 1.3 oil immersion objective. For experiments involving quantification of mitotic and apoptotic cells, cells were stained with propidium iodide and the morphological changes in the nuclear chromatin of cells were then examined with a Zeiss Axiovert microscope.

Western Blotting — Proteins extracted from cells were resolved by SDS-PAGE and electrophoretically transferred onto PVDF membranes (Millipore). The membranes were blocked for 2 h in Tris-buffered saline containing 0.2% Tween 20 and 5% fat-free dry milk, and then incubated first with primary antibodies and then horseradish peroxidase-conjugated secondary antibodies for 2 and 1 h, respectively. Specific proteins were visualized with enhanced chemiluminescence detection reagent following the manufacturer's instructions (Pierce Biotechnology). The intensity of protein bands was determined by densitometric analysis with a Lynx video densitometer (Biological Vision).

Materials and Methods for Laulimalide

Materials. Synthetic laulimalide (247) and heat-treated MAPs from bovine brain (*14*) were prepared as described previously. Two preparations of bovine brain tubulin, with no significant MAPs content, were used in our experiments. The turbidimetry studies and [3H]paclitaxel binding studies were performed with tubulin prepared as described in ref (248). The Flutax-2 binding studies and the studies analyzing polymerbound drugs were performed with tubulin prepared as described in ref *15*. Paclitaxel, baccatin III, and [3H]paclitaxel were provided by the Drug Synthesis & Chemistry Branch, National Cancer Institute, and natural epothilones A and B by Merck Research Laboratories. Docetaxel was obtained from Aventis Pharmaceuticals. Synthetic eleutherobin (218) and sarcodictyin A (237) were generous gifts of Dr. K. C. Nicolaou, Scripps Research Institute. The 2-ethoxyestradiol analogue (115, 142) and Flutax-2 were generous gifts from Dr. M. Cushman, Purdue University, and Dr. F. Amat-Guerri, Consejo Superior de Investigaciones Cientificas, respectively. The synthesis of *trans*-desoxylaulimalide will be described elsewhere. The nuclear magnetic and mass spectroscopic data and elemental analysis of *trans*-desoxylaulimalide were in agreement with the assigned structure.

Methods. Details of the assays for microtubule assembly (115) and for isolation of the α-tubulin mutants (237) were described previously. Cytotoxicity assays on MCF-7 and ovarian cell lines were performed as described previously (240). The ovarian cells were grown for 72 h and the MCF-7 line for 48 h following drug addition in 96-well microtiter plates before measurement of cell protein with sulforhodamine B.

The assay for inhibition of binding of [3H]paclitaxel to tubulin polymer was described in detail previously (241). In this assay, 2.5 μM tubulin is initially assembled with 25 μM 2′,3′-dideoxyguanosine 5′-triphosphate, a potent inducer of microtubule nucleation, in 0.75 M monosodium glutamate. Mixtures of [3H]paclitaxel and potential inhibitors were added to the polymer for a final tubulin concentration of 2 μM and the desired drug concentrations. In developing this assay, we showed that over 90% of the tubulin was polymerized in the first phase of the incubation and that with 2.0 μM paclitaxel and no inhibitor, 71% of the added [3H]paclitaxel bound to the polymer in the second phase of the incubation. (Binding was stoichiometric with 4.0 *í*M [3H]paclitaxel.) The polymer

was harvested by centrifugation at 14 000 rpm for 20 min in 1.5 mL microfuge tubes in an Eppendorf model 5417C centrifuge. The amount of radiolabel in both the total reaction mixture and the supernatant was determined in a scintillation counter, and pellet radiolabel was obtained by subtraction. Inhibition of binding of Flutax-2 to microtubules was measured in microtiter plates by fluorescence polarization anisotropy as described previously (241), except that the glutaraldehyde-stabilized microtubules were stored frozen in liquid nitrogen and drug binding was at 37 °C. The microtubules (50 nM in terms of taxoid binding sites; the stoichiometry of binding of the fluorescent derivative relative to the tubulin content was about 90%) and 50 nM Flutax-2 were mixed prior to addition of varying concentrations of potential inhibitor. For analysis of the experiments presented here, we used the *K*a obtained previously for the binding of Flutax-2 to microtubules. This was 2.2 $\times 10^7$ M^{-1} (240). The glutaraldehyde-fixed microtubules methodology was originally developed to permit more accurate measurement of the binding parameters of taxoids to tubulin polymer (249) using fluorescence techniques, since the binding affinities of more active members of the taxoid class is so high. Without fixation, microtubules with picomoles of binding sites per milliliter would rapidly disassemble, since the concentration of tubulin would be so far below the critical concentration. The methodology also made it possible to obtain quantitative measures of the binding of low-affinity ligands for the taxoid site, since high ratios of ligand to fluorescent probe (i.e., Flutax-2) could be used (80, 235). In the experiments presented here, 50 nM Flutax-2 bound to an equivalent number of taxoid binding sites with a stoichiometry of about 0.4. To obtain higher stoichiometries, the sensitivity of the assay for weaker ligands would be greatly reduced. With 175 nM Flutax-2, saturation of the taxoid sites is about 75%, and 90% saturation is reached with 0.5 μM Flutax-2.

The cobinding of laulimalide and paclitaxel to microtubules was evaluated by isolating polymer by centrifugation, extracting the pellet, and analyzing the extracted bound ligands by HPLC. Calf brain tubulin (3.5 mg, final concentration, 35 *í*M) was mixed into reaction mixtures (1.0 mL) containing 3.4 M glycerol, 10 mM phosphate (pH 6.5), 6 mM MgCl2, 1 mM EGTA, 1 mM GTP, and 37.5 *í*M laulimalide and/or 37.5 *í*M paclitaxel. The reaction mixtures were warmed to 37 °C for 30 min and centrifuged for 10 min at 50 000 rpm in a prewarmed Beckman TL120.2 rotor. The microtubule pellets were

resuspended in 1.0 mL of 10 mM phosphate buffer (pH 7.0), and the tubulin concentration was determined spectrofluorometrically (142). The pellets, as well as the supernatants, were extracted 3 times with 1.0 mL of CH2Cl2. This procedure quantitatively separates the drugs, which enter the organic phase, from the tubulin, which precipitates at the organic-aqueous interface. After evaporation of the CH2Cl2, the residues were each dissolved in 100 íL of 70% (v/v) methanol. Standard solutions of paclitaxel and laulimalide were processed analogously. HPLC analysis was performed on a C-18 column (Supercosil, LC18 DB, 250 _ 4.6 mm, 5 mm bead size) developed isocratically with 70% methanol at a flow rate of 1.0 mL/min. Drug concentrations in the pellet were determined by integration of eluted peaks in comparison to the areas produced by known quantities of the drugs from the standard solutions.

OBJECTIVE 3: Understand the timeline of events that takes place during the development of drug resistance to microtubule-targeting agents.

a. To investigate the genetic differences between cells undergoing drug selection that have a low level of drug resistance and cells that have high levels of drug resistance.
b. To establish a temporal model for the development of drug resistance

Tubulin LOH

The epothilones are novel microtubule-stabilizing natural products of soil bacteria origin, that compete with Taxol for the same binding site on β-tubulin but maintain activity against Pgp-expressing MDR cells (142). In an effort to better understand how the epothilones interact with MTs and in order to ascertain the mechanism of resistance cancer cells may develop towards this new class of agents, we have isolated two epothilone-resistant human ovarian cancer cells, namely the 1A9-A8 and 1A9-B10 cells, that were selected with epothilone A and B respectively (129). These epothilone-resistant sublines exhibit impaired epothilone-and Taxol-driven tubulin polymerization, caused by the following acquired β-tubulin mutations in each clone: β274 (Thr->Ile) in 1A9-A8 cells and β282 (Arg->Gln) in 1A9-B10 (115, 116, 131, 136, 142-144). Interestingly, these mutations are located at the Taxol-binding site in the atomic model of αβ-tubulin, thus providing a clear explanation of the drug resistance mechanism (250, 251).

It has now become evident that acquired tubulin mutations represent the main mechanism by which cancer cells become resistant to drugs that target microtubules (142). However, the temporal sequence of the molecular events that occur during the development of drug resistance to microtubule-targeting drugs is not known.

We have recently showed that during the development of drug resistance to both taxanes and epothilones, the first genetic event is acquisition of a β-tubulin point mutation at the drug's binding site in one of the two β-tubulin alleles, followed by a second genetic event involving the loss of the other (wild-type) β-tubulin allele, which occurs only after prolonged exposure to the selecting agent (142). This loss of heterozygosity for β-tubulin

gene M40 in the presence of the protective mutant β-tubulin allele then confers still higher levels of both epothilone and Taxol resistance to these human ovarian cancer cells. Thus, loss of heterozygosity in the β-tubulin gene appears to be integral to the development of the highest level of resistance by cancer cells to these anticancer drugs

Description of Drug Resistance Model. In order to understand the molecular events that occur during the development of drug resistance, as well as the adaptive temporal stages in the development of a stable resistance phenotype, we used a model of epothilone resistance that was previously created in our laboratory (79, 129). This model consists of a pair of cell lines: the parental, drug-sensitive human ovarian carcinoma cell line, 1A9, and the epothilone A-resistant clone, namely 1A9-A8. Previous characterization of 1A9-A8 cells revealed that the epothilone-resistant phenotype is due to an acquired β-tubulin mutation at residue β274 (Thr to Ala) (142). Mutation of this residue, located within the taxane-binding pocket on β-tubulin (252) confers a 40-fold resistance to epothilone A (Epo A). In an effort to gain insight into the molecular evolution leading to this 40-fold drug resistance phenotype, we examined an earlier isolate of 1A9-A8 clone, which we call 1A9-A8^{E}. This 1A9-A8^{E} early-step isolate is a precursor of the 1A9-A8 late-step isolate, as it was only exposed to the selecting agent for six months, while 1A9-A8 cells endured a 15-month selection process. Growth inhibition assays revealed that this early-step isolate was only 10-fold resistant to the selecting agent, epothilone A, unlike the 40-fold resistance displayed by its later-step successor, the 1A9-A8 clone (**Table 5**).

Table 5. Cytotoxicity Profile of Epothilone A Resistant Cells

	1A9 IC50	1A9-A8^{E} IC50	**Relative Resistance**	1A9-A8 IC50	**Relative Resistance**
Epothilone A	3.2	32	**10**	125	**39**
Epothilone B	0.9	8	**9**	29	**32**
Paclitaxel	1.5	9	**6**	15	**10**

Table 2. Cytotoxicity profile of Epothilone A resistant cells to drugs acting on MTs. *The IC50 values, expressed in nM, are obtained following 72-hour exposure to the drug. Relative Resistance is calculated as the ratio of the IC 50 of each respective drug against the resistant clone divided by that obtained against the parental 1A9 cells.*

The β-tubulin gene status correlates with extent of drug resistance. To examine whether alterations in the tubulin gene status could account for the differential drug sensitivity displayed by these clones, we sequenced cDNA from the predominant β-tubulin isotype (gene M40) from 1A9-A8^{E} cells. The results of this analysis, shown in **Figure 32,** clearly demonstrate that both the wild-type and mutant $^{Thr}\beta274^{Ile}$ tubulin alleles are expressed in the 1A9-A8^{E} cells. In contrast, the 1A9-A8 cells express only the mutant β-tubulin, consistent with our previous observations (115). Furthermore, the heterozygous tubulin gene status appears to correlate with reduced levels of drug resistance to the microtubule-stabilizing drugs epothilone A, epothilone B, and Taxol (PTX); while significantly higher-fold resistance values are observed in the 1A9-A8 cells containing only the mutant tubulin gene (**Table 5**). Thus, intermediate levels of drug resistance are observed with 1A9-A8^{E} cells, as compared with both the 1A9 wt cells and the 1A9-A8 mutant cells.

Impaired drug-induced tubulin polymerization correlates with tubulin gene status. In order to examine whether the tubulin gene status correlates with the ability of epothilone to induce tubulin polymerization in the three related cell lines (1A9, 1A9-A8, and 1A9-A8^{E}) we performed cell-based tubulin polymerization assays, shown in **Figure 33**. After treating the cells with escalating doses of Epo A, the cells were harvested in a low salt buffer and then centrifuged to separate the pellet fraction containing the polymerized form of tubulin, from the supernatant that contains the soluble form of tubulin. Under our experimental conditions, the untreated controls from all three cell lines contained most of the cellular tubulin in the supernatant fraction, thus in the soluble or unpolymerized form. In the parental cell line (1A9), treatment with Epo A led to a dose-dependent increase in tubulin polymerization, as indicated by the shift of total tubulin from the supernatant to the pellet fractions. In sharp contrast, Epo A had almost no effect

on tubulin polymerization in the late-step 1A9-A8 cells, with the majority of the tubulin remaining in the soluble form even at the highest drug concentration (1500 nM), as expected due to the mutant-only tubulin gene status. Interestingly, the intermediate selection step, represented by the 1A9-A8^{E} cells, showed an intermediate degree of tubulin polymerization following drug treatment, consistent with both the wild type and the mutant allele being expressed. Treatment with 150 nM of Epo A resulted in 90% of polymerized parental cell tubulin (**Figure 33A**), 70% of polymerized tubulin from the early-step 1A9-A8^{E} cells and only 3% of polymerized tubulin from the late-step 1A9-A8 cells (**Figure 33B**). Thus, the effects of Epo A on tubulin polymerization from these three cell lines correlate well with their respective tubulin gene status.

Impaired drug-induced G2/M Arrest correlates with Tubulin Gene Status. Microtubule-targeting drugs are known to induce G2/M arrest as a result of their binding to tubulin or microtubules, blocking cell division at mitosis. Thus, we wanted to determine epothilone's ability to induce mitotic arrest in our cell model consisting of isogenic human ovarian cancer cell lines harboring wt, wt/mut or mut only β-tubulin genes status. As shown in **Figure 34,** Epo A treatment resulted in a complete G2/M arrest in the parental 1A9 cells. As expected, no change was observed in the cell cycle profile of the 1A9-A8 cells upon treatment with Epo A, while a modest G2/M arrest was achieved in the 1A9-A8^{E} clone. Drug treatment with 10 nM of the microtubule-destabilizing drug vincristine, resulted in G2/M arrest in all three cell lines, consistent with the different binding site of this drug on tubulin. Since FACs analysis cannot discriminate between G2 arrest and mitotic arrest, we also tested the ability of epothilone ability to induce mitotic arrest in these cells lines (**Table 6**). The results of the mitotic index analysis fully corroborate the cell cycle analysis data as they show minimal mitotic arrest in the 1A9-A8 clone even at the highest epothilone concentration (100 nM). Collectively, these data reflect the tubulin gene status and the ability of the drug to affect tubulin polymerization (**Figure 33**).

Mitotic Index (%)			
Epothilone A (nM)	**0**	**10**	**100**
1A9	6.3	82	96
1A9-A8^{E}	5.2	39	47
1A9-A8	3.2	2.7	6.1

Table 6. **Mitotic Index of Epothilone A Resistant Cells** *Mitotic Index of cells treated with the indicated drug concentrations for 24 hr. Approximately 150 cells are scored per drug treatment.*

Genomic DNA sequencing indicates that wt β-tubulin gene was lost in 1A9-A8. Our data presented in **Figure 32**, clearly show that a tubulin mutation in one of the two alleles is acquired early on during drug selection, while following continuous selection pressure, only the mutant tubulin is expressed. Furthermore, the presence of only mutant tubulin appears to confer higher levels of drug resistance. To examine whether methylation of wt β-tubulin was responsible for the lack of wt β-tubulin expression in 1A9-A8 cells, we treated the 1A9-A8 cells with the DNA demethylating agent 5'-azacytidine and did not detect re-expression of the wild-type β-tubulin sequence (data not shown). We next examined the promoter methylation status of β-tubulin by methylation-specific PCR (142) and found it to be unmethylated (data not shown). To examine whether the gene encoding wt β-tubulin gene was present in 1A9-A8 cells, we sequenced β-tubulin M40 genomic DNA from the three cell lines. The 1A9 cell line displayed a wildtype β-tubulin sequence, as expected. The 1A9-A8 cells displayed only the mutant $^{Thr}\beta274^{Ile}$ sequence, while the intermediate clone 1A9-A8^{E} had both the wild type and mutant sequences (data not shown). These results suggest that the loss of wt β-tubulin in 1A9-A8 cells is a genetic event.

Loss of Heterozygosity for TUBB at 6p25 results in increased Taxol and epothilone resistance. To further examine the molecular mechanism leading to loss of wt β-tubulin gene in the late-step 1A9-A8 cells, we performed loss of heterozygosity analysis (LOH).

using single nucleotide polymorphic (SNP) markers. We selected forty-five SNP markers spanning 41.5 mega base pairs along 6p25, to assess the biallelic M40 status of 1A9 parental cells. The heterozygosity status of the 45 selected SNP markers was examined in 1A9 parental cells by PCR amplification of genomic DNA and sequencing. As shown in Table S1 only four from the 45 tested SNP markers were heterozygous in 1A9 cells. The remaining 41 markers that were tested in 1A9 cells and deemed uninformative by being homozygous are listed in table S1 in the supplement along with their location on contig NT_003488. Two of these SNP markers from within the TUBB gene were not heterozygous in 1A9 cells so they could not be informative in our analysis. These four informative SNP markers were then tested in the early-step 1A9-A8^{E} and late-step 1A9-A8 epothilone-resistant cell lines, as well as in the late-step Taxol-resistant cells 1A9-PTX10 and 1A9-PTX22, harboring only mutant β-tubulin alleles at residues β270 and β364, respectively (253). These results are summarized in **Figure 35** The parental 1A9 and the early-step isolate 1A9-A8^{E} cells contain both alleles, while the late-step isolate clones 1A9-A8, 1A9-PTX10 and 1A9-PTX22 contain only one allele for all 4 SNP markers. All SNPs were located within contig NT_003488, and the deletion encompasses all of the SNP markers in this region. These results indicate that one of the wild type TUBB allele is lost in 1A9-A8, 1A9-PTX10 and 1A9-PTX22 by chromosome loss, which are consistent with our DNA sequencing analysis.

Fluorescence *In Situ* Hybridization at region 6p25. To corroborate our LOH results and to determine whether this LOH event involves the entire chromosome, we performed fluorescence i*n situ* hybridization **(FISH)** using the BAC clone RP11-506K6 containing M40 at 6p25 (see scheme in **Figure 35**). Before hybridization, sequence analysis confirmed the presence of M40 in this BAC clone. As observed in **Figure 36A** the metaphases of the parental 1A9 and the early-step 1A9-A8^{E} cells show the presence of two copies of chromosome 6 (green centromeric chrom. 6 probe), each displaying BAC hybridization (orange staining).

In contrast, FISH results from the late-step 1A9-A8 cells, depict the presence of a mixed population. Approximately 25% of 1A9-A8 cells display a pattern where the BAC probe hybridized to only one copy of chromosome 6, while the second copy of chromosome 6

is devoid of BAC hybridization (**Figure 36A**, left panel). In these cells, the LOH event probably involves partial chromosome loss. This result is consistent with the loss of heterozygosity for 6p25 as we previously observed. The remaining 75% of 1A9-A8 cells exhibited BAC hybridization to both copies of chromosome 6 (**Figure 36A**, right panel). Based on the LOH analysis showing loss of heterozygosity for 6p25, this result indicates that during drug selection the 1A9-A8 cells led to the loss of the entire chromosome containing the wt β-tubulin allele followed by duplication of the chromosome containing the mutant β-tubulin allele.

Figure 32. Sequence analysis of β-tubulin M40 cDNA from 1A9 parental and Epo A resistant cells*. A portion of the sequence chromatogram of β-tubulin M40 cDNA exon 4 from 1A9 parental and both EpoR cell lines is shown. The 1A9 parental cell line displays wild type sequence for the M40 β-tubulin amino acid Thr274 (ACC) (top panel), while a homozygous point mutation at this residue β274 (ThrACC to IleATC) is seen in the late-step Epo-resistant clone 1A9-A8 (middle panel). A heterozygous point mutation for the same residue β274 (ThrACC to ThrACC/IleATC) is observed in the early-step Epo-resistant clone 1A9-A8E (lower panel).*

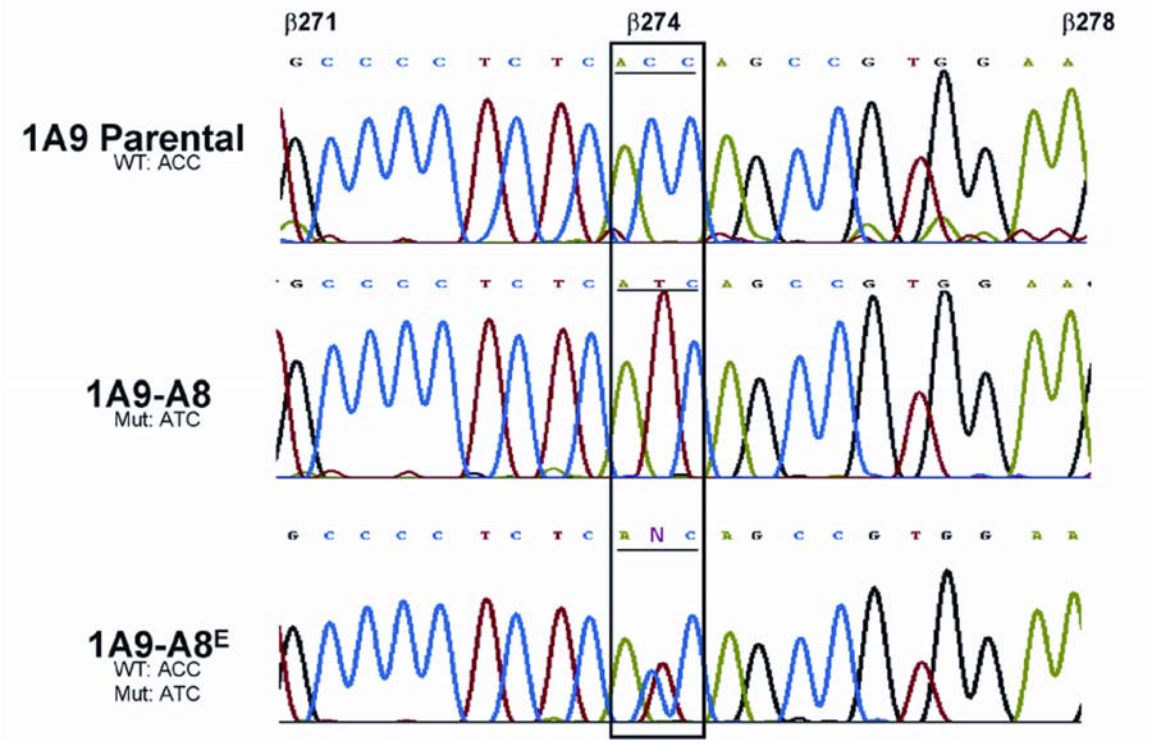

Figure 33. 1A9/A8 and 1A9/A8E cells exhibit impaired in vivo drug-induced tubulin polymerization compared with their parental 1A9 cells. *Drug-sensitive parental 1A9 (panel A) and the Epo AR clones, 1A9-A8 and 1A9-A8E (panel B), were treated for 5h with or without (0) various concentrations of Epo A as indicated. After cell lysis, the polymerized (P) and the soluble (S) protein fractions were separated by centrifugation, resolved by SDS/PAGE, and immunoblotted with an antibody against alpha-tubulin. The percent of polymerized tubulin (%P) was determined by dividing the densitometric value of polymerized tubulin by the total tubulin content (the sum of P plus S). The results shown are from a representative experiment of four independent observations.*

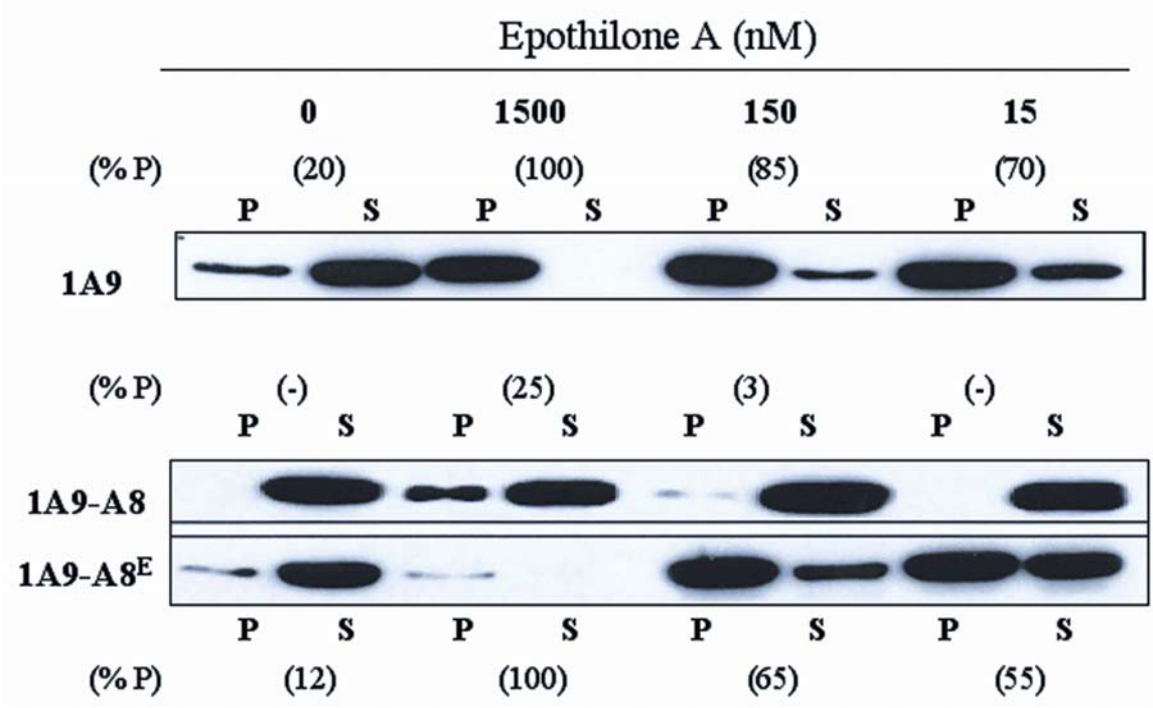

Figure 34. Impaired Epothilone-induced G2/M arrest in the 1A9-EpoR cells. *Cell cycle analysis by flow cytometry was performed in the parental 1A9 and the 1A9-EpoR clones, following overnight treatment with Epo A or Vincristine as indicated. The parental 1A9 cells readily arrested in G2/M, after treatment with either microtubule-stabilizing or destabilizing agents. The early step isolate 1A9-A8E was partially arrested in G2/M following Epo A treatment; while the late-step isolate 1A9-A8 failed to arrest in mitosis after treatment with Epo A even at the highest concentration. Both EpoR clones were arrested in G2/M after e treatment with 10 nM Vincristine. 10000 events were recorded for each condition, the histogram is representative of three independent experiments.*

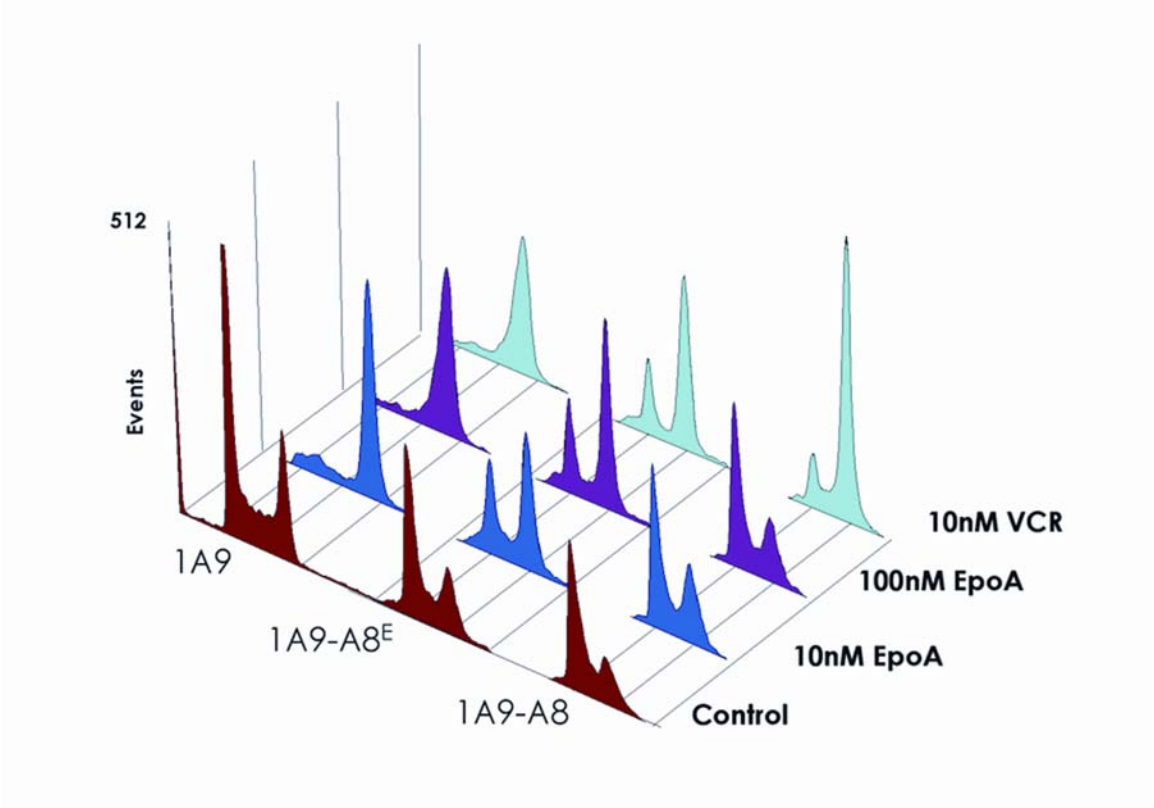

Figure 35. SNP marker analysis of 1A9 and 1A9-Resistant Cells. Left Panel*: Diagram of chromosome 6p displaying the location of the SNP markers within the 9.5Mb contig NT_003488. The β-tubulin gene M40 is highlighted within the BAC clone RP11-506k6 located within this contig at 6p25. The location of the four informative SNP markers is displayed.* ***Right Panel****: table showing the corresponding SNP nucleotides by DNA sequencing analysis in the parental 1A9 cells, and the four drug-resistant clones, as indicated.*

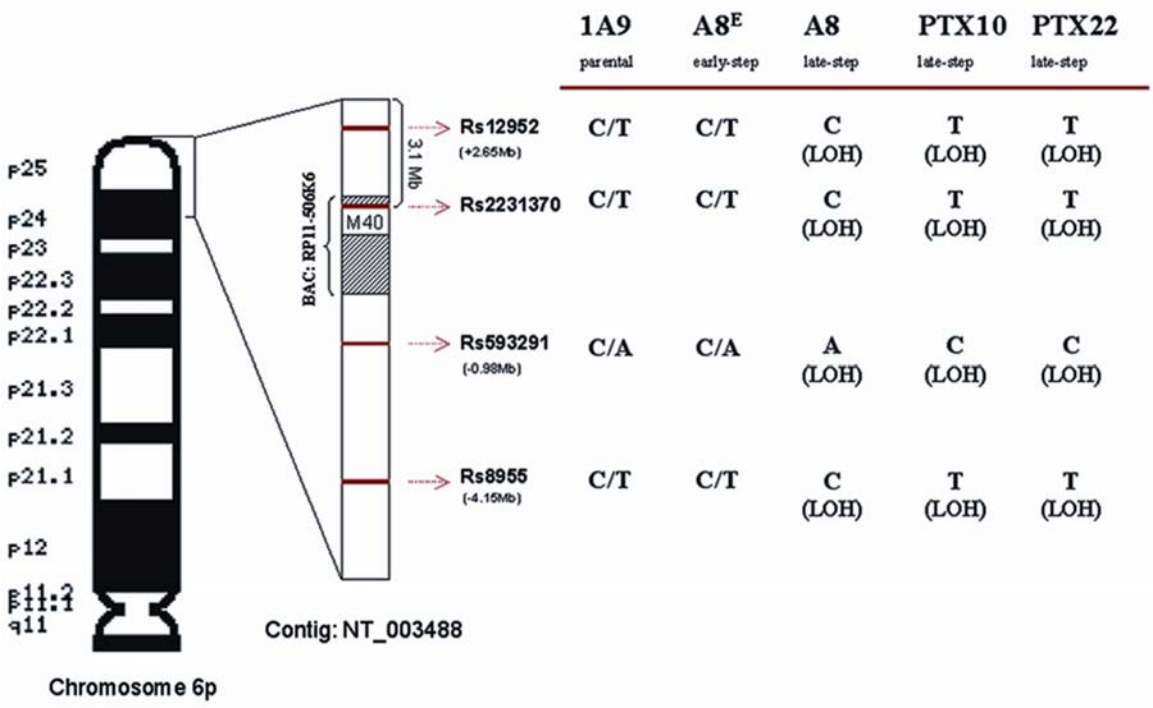

	1A9 parental	A8^{E} early-step	A8 late-step	PTX10 late-step	PTX22 late-step
Rs12952 (+2.65Mb)	C/T	C/T	C (LOH)	T (LOH)	T (LOH)
Rs2231370	C/T	C/T	C (LOH)	T (LOH)	T (LOH)
Rs593291 (-0.98Mb)	C/A	C/A	A (LOH)	C (LOH)	C (LOH)
Rs8955 (-4.15Mb)	C/T	C/T	C (LOH)	T (LOH)	T (LOH)

Figure 6. A) FISH analysis of 1A9, 1A9-A8^{E} and 1A9-A8 cells. *Metaphase spreads from all three cell lines were hybridized with BAC clone RP11-506k6 (orange) containing the β-tubulin gene M40, and a centromeric probe for chromosome 6 (green), followed by counterstaining with nucleic acid stain Sytox Blue (blue). The parental 1A9 cells display two copies of chromosome 6 (white arrows) as evidenced by the chromosome 6 centromeric probe staining. Both 6 chromosomes displayed staining for the BAC clone indicating two copies of the β-tubulin gene M40. The early-step clone 1A9-A8^{E} presented a similar karyotype as the parental cells, with two copies of chromosome 6 each containing the β-tubulin BAC clone. In the late-step 1A9-A8 cells however, only one chromosome 6 stained for the BAC clone, although both copies of the chromosome 6 were present (left panel). The white arrows indicate chromosomes 6, as evidenced by the green centromeric staining, and the BAC hybridization at the tips of the chromosome. In 1A9-A8 the yellow dashed arrow indicates the chromosome 6 that has lost the chromosomal region of 6p25. Insets display either a magnification of chromosome 6 in metaphase, or interphase. DNA in interphase cells and individual chromosomes in the metaphase plate are stained in blue. Scale bar indicates 5μm.* ***B) Temporal model for the development of drug resistance to Epothilone A.***

Figure 6. A) FISH analysis of 1A9, 1A9-A8^{E} and 1A9-A8 cells.

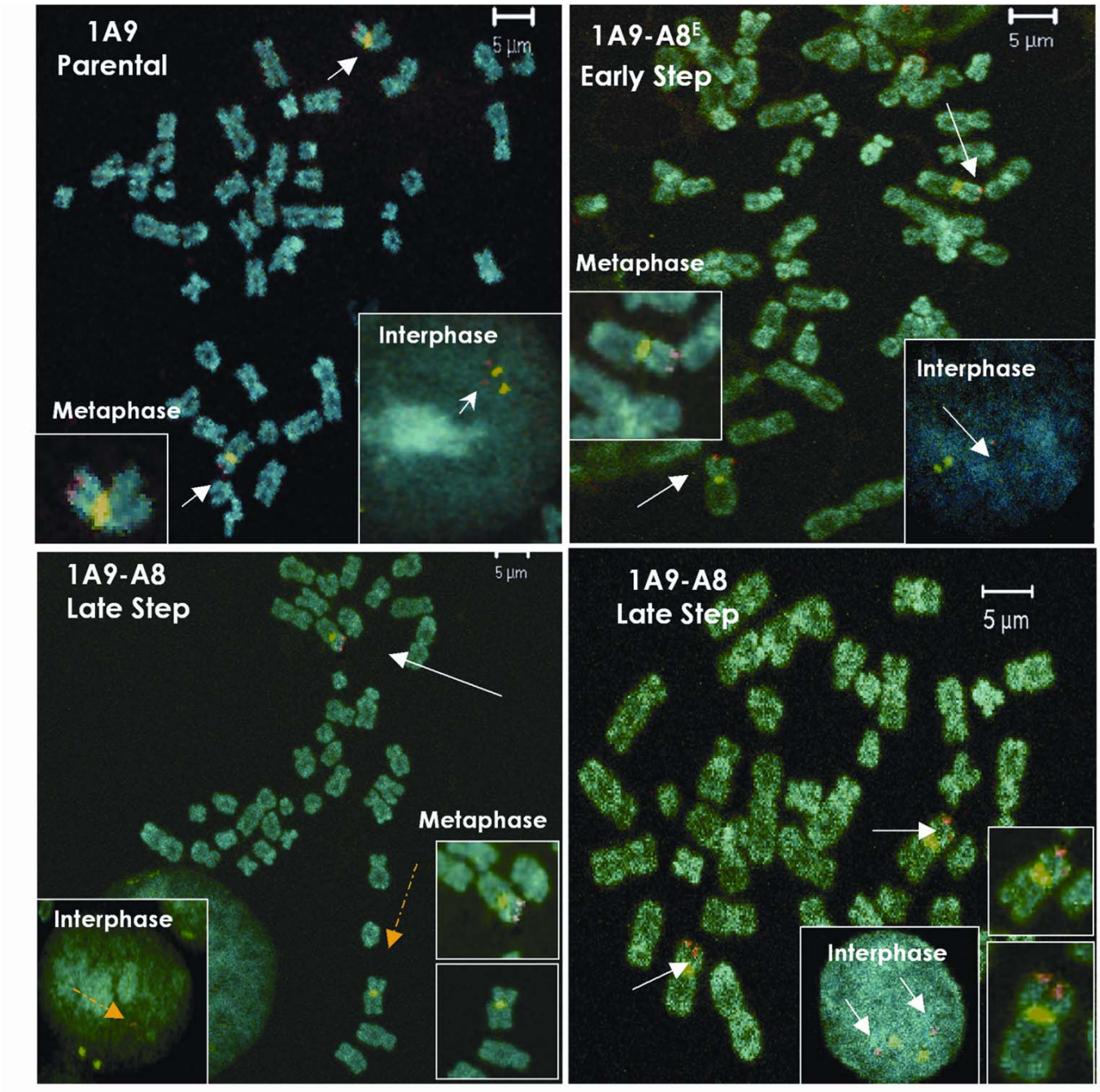

Figure 36B. Temporal model for the development of drug resistance to Epothilone A.

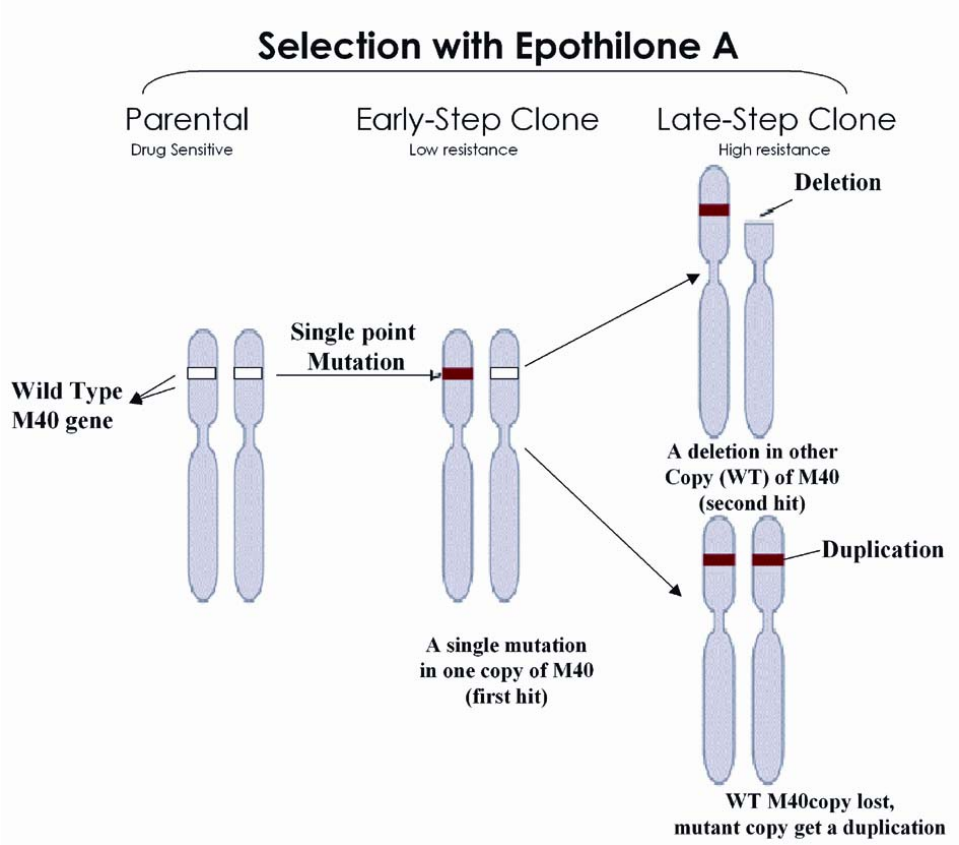

Discussion

Anticancer drugs select for drug resistance by killing drug-sensitive cells. Taxanes are very effective in the treatment of a wide variety of solid tumors; however, acquired resistance to taxanes limits their clinical efficacy. With continued exposure to the therapeutic drug, a cell develops a mechanism to further increase its chances of survival and expansion. We have presented the temporal mechanism by which the 1A9 ovarian carcinoma cells, upon exposure to Epo A, develop moderate drug resistance due to a mutation in one allele in the drug binding pocket domain of the target gene: β-tubulin; and subsequently lose the chromosomal area around 6p25 creating a cell type that is now highly resistant to the selecting agent albeit containing a similar, if not identical cellular background **(Figure 36B)**. The cells with an intermediate level of resistance are now called 1A9-$A8^{E}$ and have approximately a ten-fold degree of resistance to Epo A, the selecting agent. The above mentioned mutation is located residue β274 (Thr->Ile). This mutation changes the binding pocket and does not allow the drug to bind as efficiently (117, 118, 130, 131, 136, 137, 143-145). Nevertheless, the cell is still producing the wild type allele gene and protein therefore the drug can bind there and exert its effect. At some point after the acquisition of the β-tubulin mutation, 1A9-$A8^{E}$ cells lose the chromosomal area encompassing 6p25 resulting in the loss of the wild type allele and consequently a higher degree of resistance to Epo A (40 fold). The phenomenon of acquiring a point mutation in one allele and LOH in the other allele is frequently seen in various tumor suppressor genes.

The best known example is LOH of p53. In cancer cells that lost p53 function, one p53 allele is usually mutated and the other allele is lost due to chromosomal deletion (117, 118, 131, 144). Most strikingly, a similar event: mutation of one β-tubulin allele and then loss of the other allele has been observed during evolution of resistance to Taxol. Thus, the taxane-driven selection for mutant tubulin mirrors the process of inactivation of tumor suppressors. This is consistent with the idea the genetic instability in human cancers is responsible not only for tumorigenesis but also for the development of drug-resistant clones. Our model for the development of epothilone resistance in 1A9 cancer cells foresees the acquisition of a β-tubulin mutation in one allele. As the mutation is located

within the taxol-binding site, epothilone is now unable to bind to some of the M40 β-tubulins. Therefore, the cells are conferred with a moderate degree of resistance to the selecting agent, as long as the other wild-type allele is still expressed. Upon continued selection with Epo A, the expression of the wild type allele disappears, due to loss of the wild-type β-tubulin allele. Thus, Epo A is unable to effectively bind to any of the M40 β-tubulins, thus providing the cancer cells with significant growth advantage in the presence of the drug.

Several other groups have reported acquired β-tubulin mutations in response to drug selection with taxanes, epothilones and other microtubule-targeting drugs (254). In a number of these reports, only the mutant β-tubulin gene appears to be expressed (8). It would be interesting to know whether the inactivation of wild-type β-tubulin allele is due to LOH or promoter methylation in these cases. In either case, tubulin mutations followed by the inactivation of the remaining wild-type tubulin allele seems to be a general mechanism of acquired resistant to microtubule targeting agents.

Most of late stage 1A9-A8 cells still have two copies of 6p25 even though our LOH analysis suggest that one of the parental allele is lost. This is probably due to the duplication of the chromosome containing the mutant β-tubulin allele after the loss of the chromosome containing the wild-type β-tubulin allele. This phenomenon has been frequently observed in association with LOH in human cancers (115).

To date, there are eight β-tubulin isotypes described in mammalian cells (10). Although the exact role of each of these isotypes has yet to be defined, it seems that all of them are incorporated into the microtubule polymer and contribute to the overall cellular microtubule function. Interestingly, however, all tubulin mutations identified so far occur at the major β-tubulin isotype (class βI/gene HM40) (117, 118, 130, 131, 136, 137, 143-145), the expression of which accounts for 80-95% of total tubulin mRNA in a subset of cancer cell lines from the NCI60 human cancer cell collection (254). From a mechanistic standpoint, one wonders why the other β-tubulin isotypes in their wild-type sequence do not “take over” expression-wise, in order for the cell to escape the toxic effects of

microtubule-targeting drugs that use class I β-tubulin as a target isotype. Our own experience, together with recurring data in the literature (255-261), suggests that the cell's first response is to adapt to the otherwise lethal effects of the drug by acquiring tubulin mutations in sites that are important for drug-tubulin interactions. This cellular behavior of acquiring mutations *versus* substituting isotypes suggests that the class I β-tubulin isotype is not functionally redundant and its role in the cell simply cannot be replaced by the other isotypes. The latter constitutes a compelling hypothesis for why this is the single isotype identified in which sequence alterations occur to block the action microtubule-targeting drugs.

Losses of heterozygosity are the most common genetic alterations observed in human cancers (257) and are often associated with loss of tumor suppressor genes leading to tumorigenesis. However, no studies have correlated the occurrence of LOH with drug resistance. The results reported herein, reveal a new mechanism of taxane resistance that could be clinically important given the fact that LOH in chromosome 6p is frequently encountered in human tumors (142). In addition, LOH analysis of the 6p25 region in cervical cancer has revealed two as yet unidentified tumor suppressor genes (115). Therefore, some of these tumors may lose one copy of 6p during tumorigenesis, and they may only contain one intact copy of β-tubulin gene. Based on our model, we predict that these tumors may have a high likelihood of acquiring a second β-tubulin mutation and become resistant to microtubule-polymerizing agents. This in conjunction with the unstable human cancer genome that could mutate tubulin in response to treatment with taxanes could provide a rational basis for clinical drug resistance

MATERIALS AND METHODS FOR OBJECTIVE 3

Materials and Methods for Tubulin LOH

Cell Lines, Antibodies, and Drugs. The epothilone A resistant cell line, 1A9-A8, was selected from the human ovarian carcinoma 1A9 cells as previously described (115). The 1A9-$A8^E$ clone (expressing both WT and mutant alleles) was an intermediate isolate in the selection process of 1A9-A8 (mutant allele only) cells. These cells were cultured in RPMI 1640 medium (Cellgro) supplemented with 10% fetal bovine serum (Gibco BRL) and 1% Penicillin-Streptomycin (Cellgro), and grown as monolayers at 37°C in a 5% CO_2 tissue culture incubator. The mouse monoclonal anti-α-tubulin (DM1α) antibody used is from Sigma. Both epothilones A and B were a generous gift from the laboratory of K.C. Nicolaou (The Scripps Research Institute, La Jolla, CA). Paclitaxel (Taxol) was purchased from Sigma and vincristine from Eli-Lilly.

Drug Sensitivity Assay. Cytotoxicity assays using the protein-staining sulforhodamine B (SRB) method were performed in 96-well plates, as described previously (262-264)

Tubulin Polymerization Assay. Quantitation of the degree of *in vivo* tubulin polymerization in response to Epothilone A was performed as previously described (265).Briefly, cells were plated in 24-well plates. The following day, they were exposed to increasing concentrations of Epothilone A for a period of 6 h. Cells were then lysed in a hypotonic buffer [1 mM $MgCl_2$, 2mM EGTA, 0.5% Nonidet P-40, 20 mM Tris-HCl, pH 6.8 containing protease inhibitors (Boehringer-Mahneim)]. The lysed, cells were incubated for 5 min at 37^0 C, and cytoskeletal and cytosolic fractions (containing polymerized (p) and soluble (s) tubulin, respectively) were separated by centrifugation. Equal loading of the fractions was resolved by electrophoresis through 10% SDS polyacrylamide gels, and immunoblotted with an antibody against α-tubulin.

Beta-tubulin sequencing. Total cellular RNA was isolated with the RNeasy Mini Kit (Qiagen) and the M40 β-tubulin isotype was amplified by RT-PCR using One-Step RT-PCR (Qiagen). Genomic DNA was isolated using the QIAamp DNA Mini Kit (Qiagen).

For PCR amplification and sequencing of the M40 β-tubulin isotype, four overlapping sets of primers were used, as summarized below. The primers were designed to be specific for M40, using GenBank™ accession numbers AP000512 for genomic DNA and AF070600 for cDNA. PCR products were purified using the PCR Purification Kit (Qiagen) and then sent to the sequence core lab of the University of Michigan for DNA sequence analysis.

Position	Sequence	Orientation	Use
M40-250	CTCCGCAAGTTGGCAGTCAAC	Forward	PCR-T_a 58°C
M40-340	GGGGATCCATTCCACAAAGTA	Reverse	
M40-253	TTGGCAGTCAACATGGTCC	Forward	Sequencing
M40-324	CGTTAAGCATCTGCTCATCGACCTCC	Reverse	

Cell Cycle Analysis. Cells were plated in 6-well plates. The following day, they were treated with various concentrations of epothilone A and vincristine for 18 hours. Following treatment, both adherent and floating cells were harvested and pelleted by centrifugation. Cell pellets were suspended in 1 ml of 0.1 mg/ml propidium iodide containing 0.6% NP40 (ICN Pharmaceuticals, Costa Mesa, CA) with 1 mg/ml RNase A (Sigma Chemical Co), then incubated in the dark at room temperature for 30 min. Data acquisition and analysis were performed on a FACScan instrument equipped with CellQuest software (Becton Dickinson Immunocytometry Systems). Cell cycle analysis was performed with Flowjo (Treestar). All cell cycle experiments were performed at least three times.

Mitotic Index Analysis. Cells were plated on glass coverslips and treated with drugs for 24 hrs. Cells were fixed with ice-cold methanol and DNA was stained with Sytox Green (Molecular Probes, Oregon). Epifluorescence microscopy was used to count a minimum of 500 cells per drug treatment and mitotic figures were scored.

Loss of Heterozygosity Analysis. Loss of heterozygosity for M40 β-tubulin was examined using PCR primers that amplify single nucleotide polymorphism markers (selected from the human SNP database) around the β-tubulin M40 gene (TUBB) location. A total of 45 SNPs were tested. The PCR products were purified using the PCR Purification Kit (Qiagen) and then sequenced (Sequencing Core, University of Michigan, Ann Arbor, MI) to determine if heterozygosity was present. Each PCR reaction was performed at least twice.

Fluorescence *in situ* Hybridization (FISH) Analysis. The three cell lines (1A9, 1A9-A8 and 1A9-A8^{E}) were induced to be in metaphase by treatment with 0.1 μg/ml colcemid (KaryoMax, Life Technologies) for 4 hours at 37^{o}C. These metaphase cell preparations were harvested and fixed in a 3:1 solution of methanol/acetic acid. One or 2 drops of this cell suspension were added onto each slide and allowed to air-dry. The BAC clone RP11-506k6 (β-tubulin, 6p25: from the RCPI-11 Human BAC Library of the Children's Hospital Oakland Reach Institute BACPAC resources) was labeled by nick translation with digoxigenin-12-dUTP (spectrum-orange, Vysis, Downers Grove, IL). Hybridization and immunodetection were performed following the manufacturer's recommendation. For the detection of chromosome 6 we used a green chromosome 6 centromeric probe (Vysis, Downers Grove, IL) Chromosomes were counterstained with Sytox Blue (Molecular Probes) and analyzed by laser scanning confocal microscopy (Zeiss LSM510 axioplasm laser scanning Confocal microscope) using a Zeiss X100 1.3 oil-immersion objective. More than 20 metaphases from each cell line were analyzed.

OBJECTIVE 4: Characterize alternate drug regimens that are active in anti-mitotic drug-resistant cells.

a. To understand the effect on microtubules of farnesyltransferase inhibitors.
b. To investigate the molecular mechanism underlying the synergy between farnesyltransferase inhibitors and taxanes

Farnesyltransferase Inhibitors

Farnesyl transferase inhibitors (FTIs) are a novel class of anti-neoplastic agents that have high anti-tumor activity and are currently in clinical trials (266, 267). These agents inhibit the farnesyl transferase (FT) enzyme, whose function is to post-translationally modify proteins by the addition of a 15-carbon farnesyl group. The initial driving force behind FTI development was based on the finding that oncogenic Ras, a low molecular weight GTPase, induces malignant transformation upon the addition of a farnesyl group to its C-terminus by the FTase. This in turn allows it to localize to the plasma membrane and act as a relay switch by transducing biological information from extracellular signals to the nucleus (for review see (268, 269)).

Since Ras farnesylation is required for Ras membrane localization, FTase became an attractive target for new anti-cancer agents (270). Furthermore, based on the finding that oncogenic Ras mutations are found in 30% of all human cancers (271-273), it was hypothesized that tumor growth could be inhibited by preventing Ras farnesylation. Thus, FTIs were developed as targeted agents against Ras and were shown to inhibit Ras function (274), as well as possess potent anti-tumor activity in multiple cancer cell lines and animal models. Despite the initial hypothesis that FTIs inhibit tumor growth by inhibiting Ras farnesylation, it was later shown that FTIs demonstrate anti-tumor activity independent of Ras status (275), suggesting that the mechanism of FTI activity extends beyond the inhibition of Ras farnesylation (71, 128).

To probe the molecular mechanisms of FTI action, previous works have focused on the relationship between FTIs and microtubule-targeting agents. Microtubules are dynamic polymers, composed of α- and β-tubulin subunits that elongate and shorten. In the cell, they function in a variety of processes including cell division, cell signaling, and

intracellular trafficking (reviewed in (72, 225, 276)). Since microtubules are essential components of the cell division machinery, they are attractive and validated targets for anti-cancer therapy (277) as evidenced by the clinical success of microtubule-targeting drugs such as the taxanes (274, 278-280). More recently, epothilones, a new class of microtubule-targeting drugs, are in clinical development and show very positive preliminary results (281). Notably, FTIs in combination with paclitaxel or epotholines act synergistically to inhibit cell growth in numerous human cancer cell lines and xenograft models (282-284) . In addition, a combination clinical study of the FTI, lonafarnib (SCH66336 or sarasar; LNF) with paclitaxel yielded impressive preliminary results, with partial responses in eight of twenty evaluable patients, including patients whose disease had previously progressed while on taxanes alone (285). Despite these promising results, the molecular mechanism of the synergistic interaction of FTIs with taxanes is unknown.

The synergy between taxanes and FTIs, suggests that there may be a link between microtubules and the mechanism of FTI action. This is further supported by studies showing that FTI-2153 inhibited normal bipolar microtubule spindle formation, suggesting that spindle microtubules may have been affected by this treatment (286). These FTI-treated cells were arrested in early mitosis and this effect was independent of p53 and Ras status. Nevertheless, the effects of FTI treatment on interphase microtubules have not been examined.

Here we investigated the effects of LNF (21), on interphase microtubules in lung and breast cancer cells (61, 287). Our results demonstrate that exposure to LNF resulted in microtubule bundle formation, and stabilized interphase microtubules. Moreover, we show that the combination of LNF and paclitaxel for16 hr synergistically enhanced tubulin acetylation, mitotic arrest, and cell death; furthermore this effect correlated with FT inhibition. In addition, the combination of LNF and paclitaxel inhibits the deacetylating activity of HDAC6 *in vitro*, whereas either drug alone does not. Importantly, we show that the LNF/taxane combination is synergistic only in cells lines expressing the wild-type tubulin deacetylase, HDAC6, but not a catalytic-mutant HDAC6, revealing that functional HDAC6 is required for the synergy of LNF with taxanes. Taken together, these data suggest a relationship between FT inhibition, HDAC6

function, enhanced tubulin acetylation and cell death, providing a putative molecular basis for the LNF/taxane anti-proliferative combination.

Lonafarnib treatment alters microtubule structure. To examine the effects of LNF on interphase microtubules, we performed live cell microtubule imaging using MCF-7 breast cancer cells stably expressing GFP:α-tubulin. This cell line allows for the visualization of microtubules in living cells and eliminates the possibility of artifacts associated with fixed tissue analyses. Cells were treated for 48 hrs with 5 and 10 μM LNF (mean 72 hr IC_{50} of LNF was 8 μM in seven cancer cell lines tested; data not shown) and microtubules were observed using live-cell epi-fluorescence microscopy (Fig. 1A). Nearly all untreated control cells observed had an extensive, fine, and organized microtubule network. In contrast, LNF treatment led to a dose-dependent increase in microtubule bundling compared to control cells ($p < 0.05$; **Figure 37B**). Treatment with 5 μM and 10 μM LNF led to nearly 10% and 25% of cells harboring extensive microtubule bundling, respectively. Similar microtubule bundles were observed in nearly 60% of cells treated with paclitaxel, while cells treated under the same condition with the non-microtubule targeting, DNA-intercalating agent, adriamycin (ADR) had identical microtubule morphologies as control cells.

Lonafarnib treatment increases tubulin acetylation and microtubule stability. The appearance of microtubule bundles after LNF treatment in A549, H1299, and MCF-7 cells raises the possibility that LNF can affect microtubule stability in a manner similar to paclitaxel. To validate this hypothesis, indirect immunofluorescence using an antibody against acetylated α-tubulin was performed. Acetylation of α-tubulin at lysine 40 is an established marker of microtubule stability (281). Thus, the amount of acetylated tubulin is thought to be proportional to the stability of the microtubule. As shown in **Figure 37C**, LNF treatment for 48 hr resulted in a marked dose-dependent increase in acetylated α-tubulin, in contrast to the low basal levels of acetylated tubulin in untreated cells. This effect was similar to paclitaxel-induced tubulin acetylation, suggesting that LNF may also affect microtubule stability similar to paclitaxel.

To further probe the effects of LNF treatment on microtubule stabilization, a cell-based tubulin polymerization assay was performed (288). This quantitative tubulin polymerization assay is based on the fact that drug-stabilized microtubule polymers

remain detergent-insoluble when extracted in a hypotonic buffer, and therefore, remain in the pellet after centrifugation. Conversely, the pool of soluble tubulin dimers remains in the supernatant. LNF treatment resulted in a dose-dependent increase in tubulin polymerization, as shown by the increase in the percentage of tubulin found in the pellet fraction, as compared with untreated control cells (**Figure 37D**). Specifically, untreated cells contain almost no stabilized tubulin (0% tubulin in the pellet) under our experimental conditions, whereas LNF treatment (5-20 μM) led to a dose-dependent increase in tubulin polymerization (25-60% of total tubulin in the pellet fraction). Similarly, treatment with 5 nM paclitaxel resulted in about 80% tubulin polymerization. The same blot was reprobed with an antibody against acetylated α-tubulin. A similar dose-dependent increase in acetylated α-tubulin in the pellet was observed upon LNF treatment and this shift of acetylated-tubulin towards the polymerized (P) fraction was greater than total tubulin. Thus, the majority of tubulin polymers in the pellet fraction represent stabilized acetylated microtubules rather than random microtubules trapped in this fraction.

Combination of LNF with paclitaxel synergistically increases acetylated tubulin, mitotic arrest, and cell death. FTIs have been shown to synergize with microtubule stabilizing drugs in numerous preclinical models as well as in a phase I clinical trial (288). These observations were confirmed in our laboratory by performing combination index analysis assays of 10 different human cancer cell lines treated with paclitaxel and LNF. These assays revealed a marked synergy (CI = 0.2-0.7) between the two drugs and is consistent with previous findings. Our results, together with the reported literature, prompted us to hypothesize that the synergy of LNF with taxanes may in part be due to their combined effects on cellular microtubule acetylation and stability.

To test this hypothesis we quantitated acetylated tubulin levels using flow cytometry in cells treated for 16 hr (unlike the 48 hr treatment in **Figure 37B**) with LNF and paclitaxel, both alone and in combination. As shown in Figure 4A there was not a significant difference in acetylated tubulin levels between control untreated cells and cells treated for only 16 hr with LNF (1, 5, and 10 μM) or paclitaxel(2, 5 and 10 nM) alone. In contrast, the combination of 1, 5, and 10 μM LNF with as low as 2 nM paclitaxel resulted in a marked increase of acetylated tubulin similar to that observed with

100 nM of paclitaxel alone (**Figure 38A**). Notably, non-microtubule-targeting chemotherapy drugs, such as adriamycin (DNA-intercalating antibiotic) and U89 (anti-metabolite) had no effect on acetylated tubulin levels; whereas, the microtubule-destabilizing drug vincristine led to a slight decrease of acetylated tubulin levels compared to untreated cells (**Figure 38A**). To further explore the synergistic combination of LNF with paclitaxel, immunofluorescence analysis of acetylated tubulin at two different time points was performed (**Figure 38B**). This analysis confirmed the marked increase in acetylated tubulin levels after 16 hr when low doses of LNF (at 0.5, 1, and 5 μM) were combined with low doses of 2nM paclitaxel. At 32 hr of treatment similar effects on acetylated tubulin were observed, suggesting that this effect is maintained for at least 32 hr. Since tubulin acetylation is associated with microtubule stability, we examined whether the increased levels of acetylated tubulin observed with the combination of LNF and paclitaxel resulted in increased mitotic arrest and cell death. Flow cytometry analysis of DNA content revealed that the combination of LNF and paclitaxel led to a synergistic increase in G_2/M arrest as compared to each drug alone (**Figure 38C**). Specifically, 16 hr treatment with as low as LNF 0.5 μM + taxol 2 nM resulted in a dramatic increase in G_2/M arrested cells as compared to untreated cells or cells treated with each drug alone.

Longer treatment (32 hr) with the same drug combinations resulted in a dose-dependent increase in apoptotic cell death that is likely due to cells previously arrested in mitosis becoming apoptotic (**Figure 38C**). The percentage of apoptotic cells in the combination treatments was similar to that achieved with taxol at 100 nM, whereas either drug alone at low dose produced minimal apoptotic cells. Overall, these results show that the LNF/paclitaxel-mediated increase in tubulin acetylation correlates with a synergistic increase in mitotic arrest and cell death.

The synergistic increase in tubulin acetylation correlates with farnesyl transferase inhibition. Since LNF inhibits the farnesyl transferase enzyme, we wanted to determine if the increase in tubulin acetylation observed with the combination of LNF and paclitaxel correlates with farnesyl transferase inhibition in cells. If so, it would suggest that the observed increase in tubulin acetylation may be a consequence of FTase inhibition. To do this, HDJ-2 was used as a readout for farnesyl transferase inhibition,

since FTI treatment inhibits HDJ-2 farnesylation resulting in the appearance of a slower-migrating nonfarnesylated HDJ-2 form. As shown in **Figure 39A**, 1μM LNF alone and in combination with paclitaxel inhibited HDJ-2 farnesylation in a time-dependent manner, as assessed by the increase of the non-farnesylated (upper band) and concomitant decrease of the farnesylated HDJ-2 band (lower band). As expected, paclitaxel alone had no effect on HDJ-2 farnesylation. When the same blots were reprobed for acetylated α-tubulin, we observed a correlation between inhibition of HDJ-2 farnesylation and tubulin acetylation beginning at 3 hr treatment with the LNF/paclitaxel combination. In contrast, minimal effect on tubulin acetylation was observed with either drug alone. Taken together, these results show a positive temporal correlation between farnesyl transferase inhibition and tubulin acetylation, when LNF and paclitaxel are combined.

Next, we wanted to determine if there is also a correlation between tubulin acetylation and mitotic arrest. Therefore, in parallel with the time course experiment described above, we quantitated the percentage of cells in mitosis after treatment with the combination of LNF and paclitaxel. This result is represented in the bar graph in **Figure 39B** showing that there is about a 3 hr delay between the increase in microtubule acetylation (starting at 3 hr) and the first indication of mitotic arrest (at 6hr). Furthermore, the percentage of cells in mitosis increased with longer exposures to the combination of the two drugs, peaking at 12 hr of treatment. Overall, this result shows that when LNF and paclitaxel are combined, microtubule acetylation occurs prior to mitotic arrest and suggests that there is a correlation between tubulin acetylation/stability and mitotic arrest.

LNF in combination with paclitaxel inhibits the tubulin deacetylating activity of HDAC6 . Our observation that LNF and paclitaxel synergistically enhance tubulin acetylation (**Figure 38**) prompted us to explore the possibility that this effect is due to the functional inhibition of the only known tubulin specific deacetylase (286), histone deacetylase 6 (HDAC6). To determine the effect of LNF on HDAC6 function we transfected A549 cells with FLAG-tagged HDAC6 (wild-type or catalytic subunit mutant) and these proteins were immunoprecipitated with an anti-FLAG antibody. The tubulin deacetylase activity of HDAC6 in the presence of LNF and paclitaxel was assayed *in vitro* by co-incubating the immunoprecipitants with purified bovine brain

microtubule protein. Western blot analyses of acetylated tubulin levels were used as a read-out for HDAC6 activity (**Figure 40B**), such that HDAC6 functionality is evidenced by tubulin deacetylation. As a positive control we used trichostatin A (TSA), which inhibits the function of all HDACs including HDAC6. As expected bovine brain tubulin is heavily acetylated (lane 1) and co-incubation with wt-HDAC6 almost completely deacetylated tubulin (lane 3). In contrast, co-incubation with the catalytically inactive mutant HDAC6 had no effect on tubulin acetylation (last lane). The addition of LNF or paclitaxel alone to the purified wild-type HDAC6-tubulin complex had no effect on HDAC6 activity, since tubulin was heavily deacetylated indicating normal HDAC6 activity. In contrast, when LNF (variable doses) and paclitaxel (kept constant at 10 ∝M) were combined *in vitro*, there was a dose-dependent increase of tubulin acetylation, suggesting that the combination of these agents inhibits tubulin deacetylating HDAC6 activity. Paclitaxel alone had no effect on HDAC6 activity even at 100 μM. We also tested the microtubule depolymerizing agent colchicine for HDAC6 inhibitory activity, and like paclitaxel, it did not inhibit HDAC6 function.

To probe the importance of HDAC6 inhibition in the mechanism of synergy between LNF and paclitaxel, we combined the specific HDAC6 inhibitor, tubacin, with paclitaxel. This experiment allows us to determine whether the combination of a specific HDAC6 inhibitor with paclitaxel leads to a synergistic increase in tubulin acetylation, similar to the LNF/paclitaxel combination. Western blot analysis of A549 cells treated with the combination of tubacin and paclitaxel at low doses (beginning at 0.3 μM tubacin and 1 nM paclitaxel) led to a synergistic increase in acetylated tubulin, as compared to either drug alone (**Figure 40B**). These findings were confirmed with acetylated tubulin immunofluorescence. Thus, specific inhibition of HDAC6 (e.g., with tubacin) in combination with paclitaxel leads to a synergistic increase in acetylated tubulin, further suggesting that the LNF/paclitaxel inhibition of HDAC6 activity provides a mechanistic basis for the enhanced tubulin acetylation. To further explore the functional importance of HDAC6 in the synergy between LNF and paclitaxel we tested this drug combination in a pair of cell lines engineered to stably express either wild-type HDAC6 (HDAC6-wt) or a catalytic mutant HDAC6 (HDAC6- mut). These cells lines will allow us to determine if a functional HDAC6 protein is required for the observed effects on acetylated tubulin. In

agreement with previously published data (278)**,** HDAC6-wt cells had lower baseline levels of acetylated tubulin relative to HDAC6-mut cells, consistent with the presence of a functional *versus* a nonfunctional HDAC6 (**Figure 40C,** untreated). Upon treatment with the LNF/paclitaxel combination, there was a synergistic increase in acetylated tubulin in HDAC6-wt cells as expected; however the LNF/paclitaxel combination had no effect on tubulin acetylation in the HDAC6-mut cells. This result indicates that the synergistic increase in acetylated tubulin induced by the LNF/paclitaxel combination is dependent upon the presence of a functional HDAC6. To extend these observations, we used another taxane, docetaxel (DTX), in combination with LNF.

Next, we wanted to determine if functional HDAC6 is required not only for the synergistic increase in acetylated tubulin with the LNF/taxane combination (**Figure 40C**), but also for the synergistic anti-proliferative activity of the drugs. Thus, we performed cytotoxicity assays employing the routinely used combination index analysis to assess synergy between the two drugs against cells with HDAC6-wt and HDAC6-mut genetic background. Our results show that the combination of LNF with DTX resulted in a robust synergistic anti-proliferative effect in HDAC6-wt cells (mean CI=0.4 indicating strong synergy; **Figure 40D**). In stark contrast, the combination of LNF and DTX was antagonistic in the HDAC6-mut cells (mean CI=2.5), suggesting that the lack of functional HDAC6 in these cells not only precludes increased levels of acetylated tubulin with this drug combination but also abolishes their anti-proliferative synergy. To confirm that the combination of DTX with LNF inhibits the tubulin deacetylase activity of HDAC6 *in vitro,* similar to our previous results with paclitaxel (**Figure 40A**), we used cells stably expressing wild-type HDAC6 to immunoprecipitate HDAC6, and performed another *in vitro* tubulin deacetylase assay. Our data show that the combination of 10 μM LNF with 10 μM DTX resulted in a synergistic inhibition of HDAC6 function, as evidenced by the appearance of acetylated tubulin, whereas either drug alone had no effect on HDAC6 functionality (**Figure 40E**). Collectively, these data provide a mechanistic link between HDAC6 inhibition, tubulin acetylation and the synergistic interaction of these drugs (281).

Although the precise mechanism of FTI action remains unclear, FTIs have shown promise in combination therapies, especially with the microtubule stabilizing agent,

paclitaxel (PTX). In cell lines, the FTI/Taxol combination results in a robust anti-proliferative and anti-mitotic synergy (289). Importantly, the combination of one FTI, lonafarnib (LNF), and paclitaxel (Taxol) resulted in durable partial responses in 8 out of 21 evaluable patients, whereby patients were administered continuous lonafarnib plus paclitaxel every 3 weeks (a total of 24 patients with solid tumors of whom 50% had non-small cell lung cancer (286). Notably, these partial responses were observed in 3 of 7 patients who had failed prior taxane-containing therapies. Furthermore, a follow-up phase II study of 29 evaluable patients has shown similar results, whereby 48% of patients with non-small cell lung cancer who experienced disease progression while on prior taxane therapy or who relapsed within 3 months following taxane therapy cessation, showed clinical benefit from the lonafarnib (100 mg PO BID) and paclitaxel combination (unpublished). Lastly, a recent phase I study showed that the combination of the FTI, BMS-214662 with paclitaxel and carboplatin in patients with advanced cancers had broad activity in solid tumors, where one patient had a measurable partial response with taxane-resistant esophageal cancer (290). Taken together, the FTI/paclitaxel combination has clinical potential and appears to maintain efficacy in subset of patients resistant to paclitaxel alone.

This clinical data prompted us to test the hypothesis that FTIs can reverse resistance to taxanes by restoring the enhanced anti-proliferative activity of the FTI/taxane combination (115). To do this, we employed a model of taxane resistance to determine if cells resistant to paclitaxel alone still show an enhanced response to the FTI/taxane combination. Our results show that the FTI/taxane combination retains potent anti-proliferative, apoptotic, and anti-mitotic activity in cells that are 22-fold resistant to taxol and 14-fold resistant to docetaxel alone. To probe the mechanism behind these observations, we show that FTIs increase the levels of Flutax (fluorescently-conjugated taxol) bound to the microtubule in both taxol-resistant and taxol-sensitive cell lines, leading to enhanced microtubule stabilization. Furthermore, the mechanism by which this occurs is dependent on farnesyl transferase (FT) inhibition and the functionality of the tubulin deacetylase, HDAC6. These results support previously published data showing that the synergy between FTIs and taxanes is HDAC6-dependent (278, 280) as well as

complement clinical data showing that the FTI/Taxane combination is effective in taxol-resistant cells.

Farnesyl transferase inhibitors restore FTI/taxane anti-proliferative activity in paclitaxel-resistant cancer cells. Our laboratory has established a model of paclitaxel resistance comprised of the 1A9 taxol-sensitive human ovarian carcinoma cell line and its taxol-resistant derivative line, 1A9/PTX10 (termed PTX10). Taxol-resistance in this model is due to an acquired tubulin mutation at the taxol binding site and results in ~ 25-fold and 10-fold resistance to paclitaxel (PTX) and docetaxel (DTX), respectively (278, 280). We used this model to test the hypothesis that FTIs can restore the anti-proliferative activity of the FTI/taxane combination in these resistant cells. To do this, the mean IC_{50} of both 1A9 and PTX10 cells was determined after a 72 hr exposure to either an FTI or taxane alone (**Figure 41A**). In agreement with previous studies, PTX10 cells had a mean IC_{50} of 100 nM when treated with PTX, compared to the parental 1A9 cells, whose IC_{50} was only 4 nM; thus, PTX10 cells were 25-fold resistant to taxol treatment. Similarly, when PTX10 cells were treated with DTX alone, 10-fold relative resistance was observed. Neither 1A9 nor PTX10 cells had any significant resistance to either LNF or FTI-277, since similar IC50s were observed in both cell lines. Next, we treated cells with the FTI/taxane combination for 72 hr and again determined the IC_{50}s. As previously described for other taxane-sensitive cancer cell lines (278), the FTI/taxane combinations in 1A9 cells resulted in a significant decrease in IC_{50} relative to each treatment alone. PTX10 cells were then treated with the various FTI/taxane combinations, and although these cells are resistant to taxanes, all FTI/taxane combinations still resulted in a significant anti-proliferative synergy. Specifically, PTX10 cells were only 1.5 and 3.5-fold resistant to the LNF/PTX and LNF/DTX combination, respectively. Moreover, the FTI-277/PTX and FTI-277/DTX combination in PTX10 cells resulted in 4.3 and 4.6-fold resistance, respectively. Thus, the FTI/taxane combination still retains significant anti-proliferative activity even in taxol-resistant PTX10 cells. It is also worth noting that a similar restoration of taxane resistance was observed with the FTI, tipifarnib..

To quantitate the interaction of FTIs and taxanes in taxol-resistant cell lines, combination index analysis was employed to determine to the degree of synergy between these two

agents in the different cell lines. To do this, the fractional cell growth inhibition (FA) was plotted as a function of the combination index (CI), whereby a CI less than 1 represents synergy, equal to 1 is additivity, and greater than 1 is antagonism. In the taxol-sensitive 1A9 cells the farnesyl transferase inhibitors (LNF and FTI-277) were synergistic with both PTX and DTX (**Figure 41B**; $p<0.05$ for all), which is consistent with previous studies in other cell lines (115, 287). In the Taxol-resistant PTX10 cells, which are ~25-fold resistant to paclitaxel, we observed additivity at most doses (CI around 1; $p > 0.05$) and synergism at doses around an FA of 0.5 (Fig. 1C). When LNF was given in combination with DTX in PTX10 cells, synergy was observed at almost all doses ($p<0.05$). Similarly, the combination of FTI-277 with PTX or DTX, resulted in synergy at nearly all doses (**Figure 41C**; $p <0.05$). Similar experiments with tipifarnib and a taxane were performed and also resulted in a similar synergistic pattern. Overall, these data show that an FTI/taxane combination is synergistic in Taxol-sensitive 1A9 cells and results in additivity or synergy (depending upon the dose) in taxol-resistant PTX10 cells.

The FTI/taxane combination causes enhanced apoptosis and mitotic arrest in Taxol–resistant cells. Western blot analysis for the apoptotic marker PARP p85 was performed to confirm that the FTI/taxane combination induces apoptosis in taxol-resistant cells, and is not just cytostatic. Both 1A9 and PTX10 cells were subjected to various FTI/taxane treatments for 24 hr. In 1A9 cells, 5 nM PTX results in a slight induction of PARP cleavage whereas the combination of LNF (1 μM) with PTX at 2 and 5 nM causes a significant dose dependent increase of PARP cleavage compared to either LNF alone (1 μM) or 5 nM PTX (**Figure 42A**). Likewise, the combination of PTX with FTI-277 also resulted in a synergistic increase of PARP cleavage compared to either agent alone. In PTX10 cells, PARP cleavage was not induced even at 50 nM PTX as expected, however addition of LNF (1 μM) to increasing doses of PTX starting at 5 nM did induce significant PARP cleavage, compared to either agent alone. Thus, the FTI/taxane combination, relative to either agent alone, causes enhanced apoptosis in both taxol-resistant and –sensitive cells.

Taxol is known to be a potent anti-mitotic, however, in PTX10 cells, even high doses of taxol leads to little or no mitotic arrest (291). Furthermore, it is also known that the combination of an FTI and taxol leads to enhanced mitotic arrest (286). Our results in 1A9 cells are consistent with this finding and we show that in 1A9 cells the FTI/Taxol combination led to a potent increase in mitotic arrest relative to either treatment alone (**Figure 42B**; $p < 0.05$) Thus, we wanted to determine if the LNF/taxane combination still retains its anti-mitotic activity in PTX10 cells. In PTX10 cells, LNF alone resulted in a slight increase in mitotic arrest, whereas paclitaxel alone at 25 nM caused no mitotic arrest and only at a dose of 250 nM is a slight increase in mitotic arrest observed. In contrast, when an FTI (either LNF or FTI-277) was combined with paclitaxel, the anti-mitotic synergy of these two agents was present such that even low doses of Taxol (beginning at 2 nM) with 1 μM LNF led to a synergistic increase in mitotic arrest (**Figure 42C**). This effect was dose dependent whereby increasing doses of PTX with FTI (1 μM) increased the number of cells arrested in mitosis.

Confocal images of mitotic 1A9 and PTX10 cells treated with the various agents are shown in Fig. 2D. In both cell lines untreated cells have a bipolar microtubule spindle with chromosomes aligned along the spindle equator. After treatment with LNF (1 μM), both cell lines show a slight increase in the number of mitotic cells having a monopolar spindle, accompanied by a ring of chromosomes. As expected, PTX-treatment (2 nM) had no affect on the spindle architecture in PTX10 cells but did induce multi-polar spindles and dispersed chromosomes in 1A9 cells, as expected. Furthermore, the combination of LNF and PTX in 1A9 cells resulted in more "taxol-like" spindle, since the microtubules were in a multi-polar configuration and chromosome were dispersed. On the other hand, in PTX10 cells the LNF/PTX combination resulted in more monopolar spindles that are reminiscent of LNF treatment alone. Overall, these data show that although these PTX10 cells do not undergo mitotic arrest with paclitaxel alone, the combination of an FTI/PTX combination restores the synergistic anti-mitotic activity of these agents.

FTIs increase the affinity of Flutax (fluorescently-conjugated taxol) for the microtubule in taxol-resistant and –sensitive cells. The data presented herein describe

the observation that FTIs can restore the anti-proliferative, apoptotic, and anti-mitotic activity of the FTI/taxane combination in taxol-resistant cells. Thus, we sought to determine the mechanistic basis of these results by monitoring taxol behavior in taxol-resistant and -sensitive cell lines with and without FTIs. To do this, we used live-cell confocal microscopy with Flutax, a fluorescently conjugated taxol molecule. Flutax is approximately 100 fold less cytotoxic than unconjugated taxol (data not shown), therefore we adjusted the dose of Flutax accordingly. In 1A9 cells 16 hr treatment with Flutax alone (75 nM) resulted in a clearly filamentous microtubule pattern (**Figure 43A**), indicating that Flutax was bound to microtubules. To test the effect of LNF on Flutax, LNF (1μM) and Flutax (75 nM) were given in combination to cells for 16 hr. Interestingly, this resulted in a significant increase in the intensity of Flutax along the microtubule as well as the number of Flutax labeled microtubules (**Figure 43A**), suggesting enhance Flutax's affinity for the microtubule.

In conjunction, we performed a similar experiment in PTX10 cells; however the Flutax concentration was raised to 10-fold to 750 nM. In PTX10 cells treated with 750 nM Flutax alone, we observed little Flutax on the microtubules relative to 1A9 cells and very few Flutax-labeled microtubules (**Figure 43A**). This result is consistent with the fact that these cells are resistant to taxol and that taxol is incapable of binding to microtubules in these cells. In contrast, the addition the combination of LNF (1 μM) and Flutax resulted in a marked increase in the Flutax signal intensity on the microtubules as well as a substantial increase in the number of Flutax labeled microtubules (**Figure 43A**). A similar experiment was performed with FTI-277 and a similar increase in Flutax-microtubule labeling was observed upon addition of the FTI (**Figure 43A**). Taken together, these results show that FTIs can increase the affinity of Flutax for the microtubule in both taxol-resistant (PTX10) and taxol-sensitive cells, resulting in an increase in the signal intensity of bound Flutax and the number of Flutax-labeled microtubules.

To determine if this scenario holds true in other cancer cell lines, we performed similar analysis in the lung cancer cell line, A549 (**Figure 43B**). In these cells, Flutax (75 nM)

treatment alone, resulted in a relatively greater Flutax signal intensity than 1A9 and PTX10 cells; nevertheless, the combination of LNF (1 μM) with Flutax (75 nm) still resulted in a significant increase in Flutax signal intensity and the number of Flutax-labeled microtubules. Thus, this data is consistent with that observed in 1A9 and PTX10 cells, and suggests that LNF increases the affinity of Flutax for the microtubule. Quantitative analysis of the Flutax signal intensity on the microtubule is depicted in a bar graph in **Figure 43C**.

To further probe this observation we wanted to determine if the enhancement of Flutax binsing on the microtubule is a consequence of FT inhibition or rather independent of the FT inhibitory active of the FTI. Thus, we used the inactive LNF enantiomer, SCH66337, which has at least 100-fold less inhibitory activity of FT in vitro (personal communication. Robert Bishop, Schering-Plough). To confirm this we performed western blot analysis of HDJ-2, which is used as readout for FT status, since HDJ-2 has a clear farnesylated (lower band) and non-farnesylated (upper band) band on a SDS-PAGE gel. Time course analysis of HDJ-2 farnesylation shows that LNF (1 μM) induces the non-farnesylated HDJ-2 band to begin to appear after 3 hr post-treatment and the intensity of this band steadily increases over time (**Figure 43D**). In contrast, the LNF enantiomer, SCH66337, induces a faint non-farnesylated band whose intensity remains constant over time. Thus, SCH66337 does not retain significant FT-inhibitory activity. We used SCH66337 to determine if FT inhibition is required for the enhancement of taxol binding to the microtubule in PTX10 cells. Cells were treated for 16 hr with both Flutax alone (750 nM) and Flutax + SCH66337 (1μM; **Figure 43E**). Unlike the combination of LNF with Flutax, the combination of SCH66337 and Flutax did not result in an increase of Flutax on the microtubule, indicating that FT inhibition is required for enhancing the affinity of Flutax for the microtubule.

FTIs enhance the microtubule stabilizing effects of taxol in taxol-resistant and –sensitive cells. These results show that LNF causes enhanced Flutax binding in all cell lines tested, including cells that are resistant to PTX alone. If this scenario is true, one would predict that enhanced taxol binding on the microtubule should result in increased microtubule stability. Thus, we used a microtubule stability assay to determine if FTI-

induced taxol binding leads to an enhancement of microtubule stability. This quantitative cell-based tubulin polymerization assay (21) is based on the fact that stabilized microtubules remain detergent-insoluble when extracted in a hypotonic buffer, and therefore are found in the pellet after centrifugation, whereas dynamic microtubules remains in the supernatant. In taxol-sensitive 1A9 cells, untreated control cells had 8% of tubulin found in the pellet and upon LNF treatment alone there was a slight increase such that 19% of tubulin was in the pellet, indicating a small increase in microtubule stability by LNF alone (**Figure 43F**, top). Treatment with PTX 2 and 5 nM also led to a small increase in microtubule stability (9 and 15%, respectively), whereas treatment with PTX at 10 nM led to a significant increase in microtubule stability, with 41% of tubulin in the pellet. The combination of LNF (1 μM) with PTX at 2 and 5 nM caused a large increase in percentage of tubulin found in the pellet relative to either drug alone (41 and 43%, respectively. Moreover, even the combination of LNF (1 μM) and PTX at 10 nM also resulted in an increase over PTX alone, such that 51% of tubulin was found in the pellet.

In taxol-resistant PTX10 cells, LNF treatment at 1 μM and PTX treatment at 10 and 50, and 100 nM had no significant affect on microtubule stability as expected, since similar levels of tubulin is detected in the pellet relative to untreated cells (**Figure 43F**, bottom). In contrast, the combination of 1μM LNF with as little as 10 nM PTX led to 41% of tubulin found in the pellet, and 43 and 51% with LNF and PTX at 50 and 100 nM, respectively. Thus, the combination of LNF with PTX synergistically increases microtubule stability in taxol-sensitive and –resistant cell lines.

HDAC6 functionality is required for FTI-induced taxol binding

We have previously shown that functional HDAC6 is required for the synergy of LNF and taxanes (21, 286). Thus, we wanted to further test this scenario and determine whether a functional HDAC6 is required for LNF to enhance the affinity of Flutax for the microtubule. To do this, two stable transfected NIH-3T3 cell lines were used; the HDAC6-wt cell lines overexpress wild-type HDAC6 and the HDAC6-mut cell line overexpress a catalytically inactive HDAC6 (271-273). Thus, in the HDAC6-mut cell line HDAC6 function is compromised and high levels of acetylated tubulin is observed

(21). Both cell lines were treated for 16 hr with either Flutax (75 nM) or the Flutax (75 nM)/LNF (1 μM) combination. In both cell lines, Flutax alone was bound to the microtubules, whereby HDAC6-mut cells had a greater signal intensity than HDAC6-wt cells (**Figure 44A**). Interestingly, when LNF was combined with Flutax in HDAC6-wt there was a significant increase in microtubule-bound Flutax as observed with other cell lines in Fig. 3. However, in contrast to any other cell line tested, the addition of LNF had no effect on microtubule bound Flutax (**Figure 44**). Thus, these results suggest that a functional HDAC6 is required for LNF's ability to enhance the affinity of taxol for the microtubule.

Figure 37. Lonafarnib treatment alters microtubule structure and increases tubulin acetylation. ***A)*** *MCF-7 breast cancer cells stably expressing GFP: -tubulin were observed using live-cell fluorescence microscopy following the indicated drug treatments for 48 hours. Solid arrows, microtubule bundling. Bottom row displays higher magnification of microtubules shown in the top row. Bar, 10 µm.* ***B)*** *number of cells containing microtubule bundles following drug treatments shown in A. Asterisks denote a significant difference in the percentage of cells having microtubule bundles compared with control (P < 0.05). Bars, ±SD.* ***C)*** *A549 cells were treated with lonafarnib (LNF) for 48 hours and microtubules were visualized by immunofluorescence labeling using an antibody against acetylated -tubulin. Treatment with paclitaxel (PTX) is included as a positive control. Bar, 10 µm.* ***D)*** *Western blot analysis against total -tubulin (top) and acetylated tubulin (bottom) on the polymerized (P) and soluble (S) fractions of protein lysates from A549 cells treated with the indicated drug concentrations for 48 hours. %P, relative percentage of polymerized tubulin for each drug treatment.*

Figure 37. Lonafarnib treatment alters microtubule structure and increases tubulin acetylation.

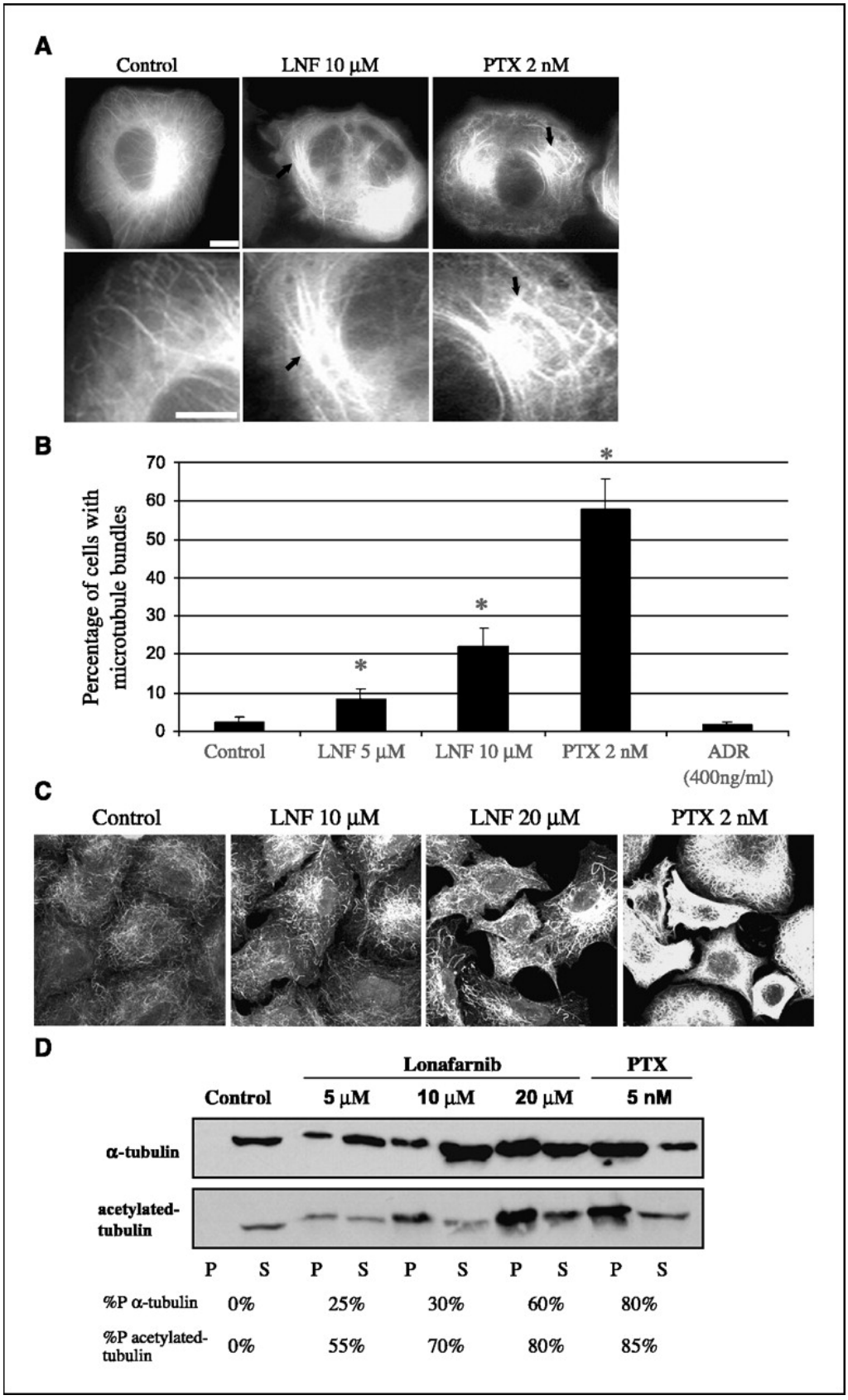

Figure 38. Lonafarnib and paclitaxel synergistically increase acetylated tubulin, mitotic arrest, and apoptosis*. A) flow cytometry was done with an acetylated tubulin antibody in A549 cells treated with the indicated drugs. Representation of acetylated tubulin levels after 16 hours of drug treatment. Columns, mean fluorescence for acetylated tubulin relative to that of control untreated cells (FTI: lonafarnib).* ***B)*** *acetylated tubulin immunofluorescence of cells treated with lonafarnib and paclitaxel, both alone and in combination, for 16 and 32 hours****. C)*** *cell cycle analysis for 16 and 32 hours of treatment with the combination of lonafarnib and paclitaxel.*

Figure 38. Lonafarnib and paclitaxel synergistically increase acetylated tubulin, mitotic arrest, and apoptosis

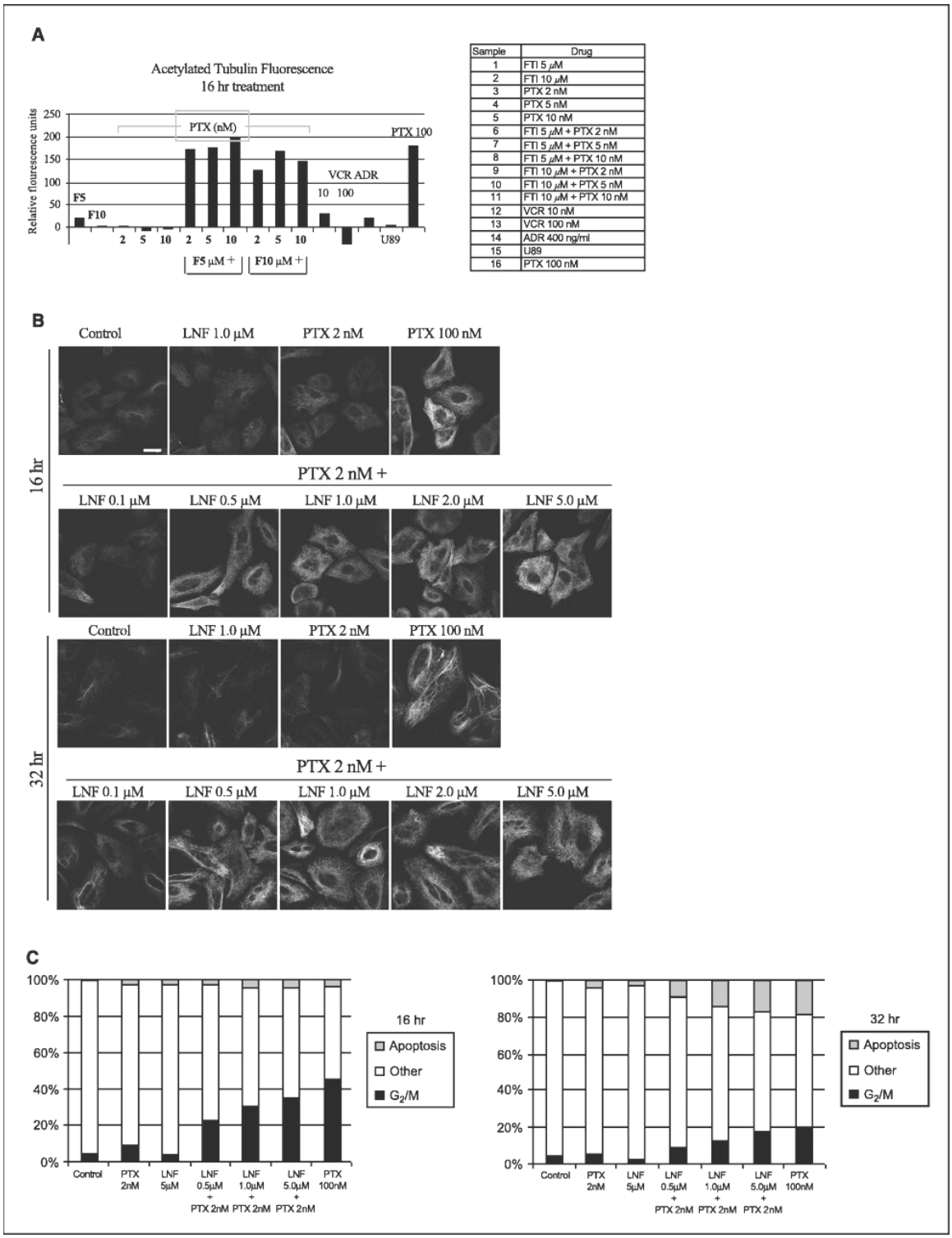

Figure 39. The synergistic increase in acetylated tubulin caused by lonafarnib and paclitaxel treatment correlates with FT inhibition and mitotic arrest. A) *Western blot analysis for acetylated tubulin, HDJ-2 (N, non-farnesylated band; F, farnesylated band), and total tubulin following lonafarnib and/or paclitaxel treatment over time.* ***B)*** *Percent mitosis assessed by DNA staining, done in parallel and with the same drug treatments over time as in* ***A****. Bars, SD.*

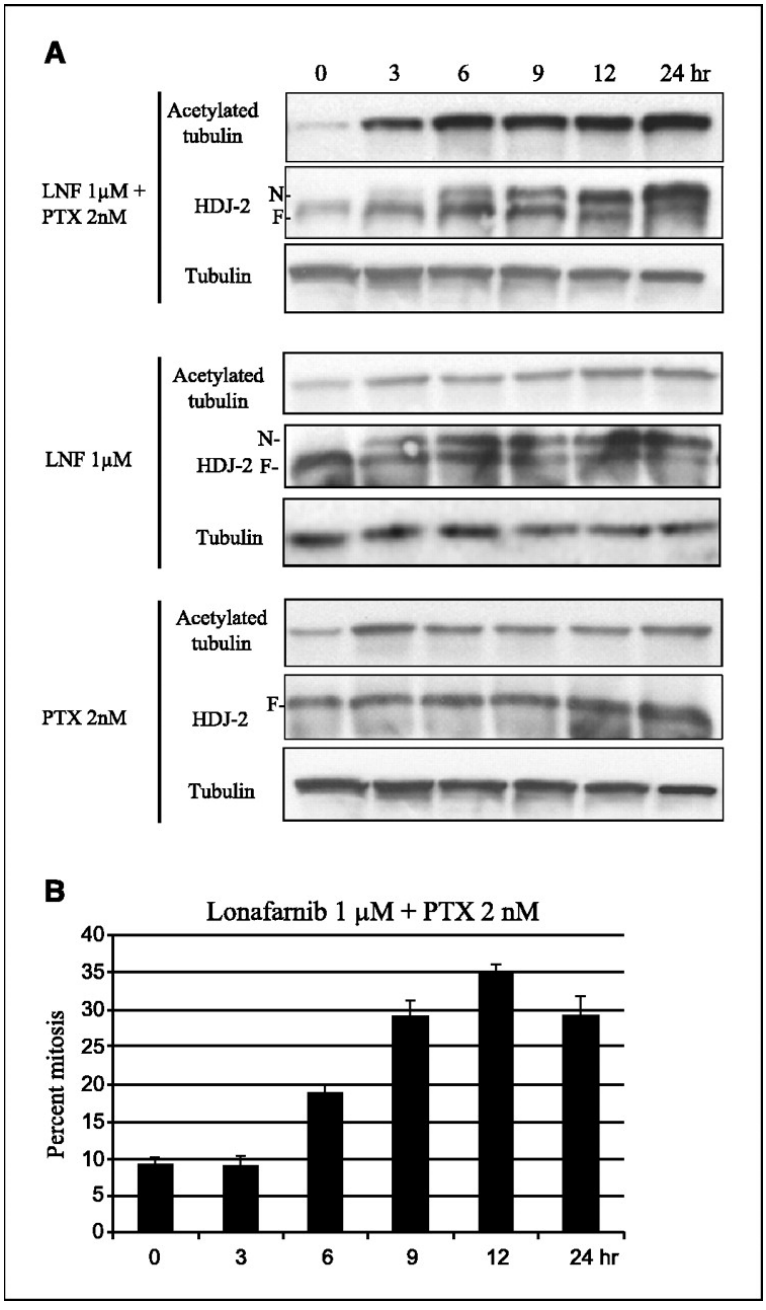

Figure 40. The synergistic combination of lonafarnib and taxane prevents HDAC6 tubulin deacetylation in vitro and is dependent on HDAC6 functionality. A) *Representative Western blots of acetylated a-tubulin, total tubulin, and Flag, following immunoprecipitation (IP) from A549 cells transfected with either Flag-HDAC6-WT or Flag-HDAC6-mut. Before Western blotting the Flag-IP complexes were incubated in vitro with preassembled purified bovine brain microtubule protein in the presence of various drugs to determine the tubulin deacetylase activity of HDAC6 (left-hand blot).* ***B)*** *Western blotting of acetylated tubulin after treatment with tubacin, a specific HDAC6 inhibitor, both alone and in combination with paclitaxel. Trichostatin A (TSA) was used as additional positive control for pan-HDAC inhibition. As a control for total tubulin levels, blots were reprobed for a-tubulin.* ***C)*** *Immunofluorescence analyses of acetylated tubulin in NIH-3T3 cells stably expressing either HDAC6-wt or HDAC-mut, following 16-hour drug treatments as indicated.* ***D)*** *Assessment of synergy between lonafarnib and docetaxel in HDAC6-wt and HDAC6-mut using combination index analysis. The lonafarnib/docetaxel combination is synergistic in HDAC6-wt (combination index < 1) but is antagonistic in HDAC6-mt cells (combination index > 1). Bars, SD. E, representative Western blots of acetylated -tubulin, total tubulin, and HDAC6 following immunoprecipitation (IP) from NIH-3T3 cells stably expressing Flag-HDAC6-WT. Before Western blotting the Flag-IP complexes were incubated in vitro with preassembled purified bovine brain microtubule protein in the presence of various drugs to determine the tubulin deacetylase activity of HDAC6. The in vitro effects of trichostatin A (pan-HDAC inhibitor), lonafarnib, and docetaxel (DTX) on acetylated a-tubulin are shown.*

Figure 40. The synergistic combination of lonafarnib and taxane prevents HDAC6 tubulin deacetylation in vitro and is dependent on HDAC6 functionality

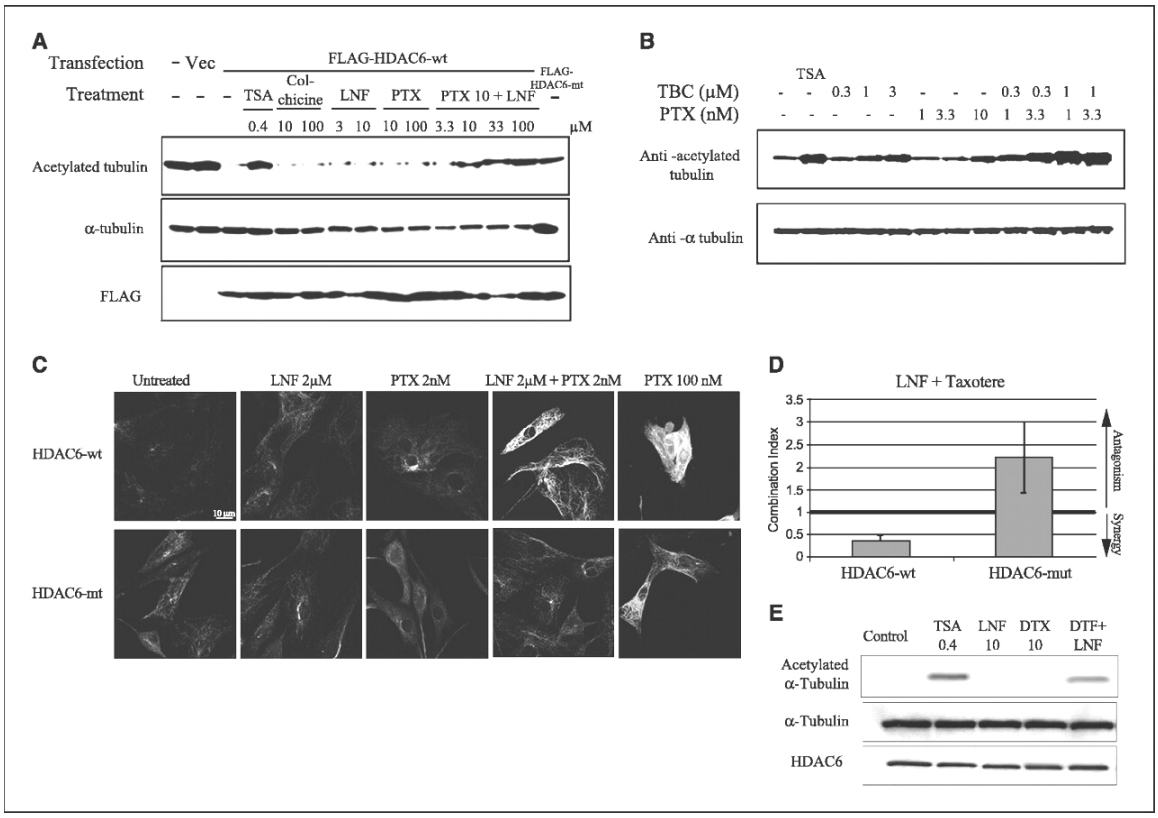

Figure 41. Farnesyl transferase inhibitors restore the anti-proliferative activity of the FTI/taxane combination in taxol-resistant cancer cells. A) *A bar graph displaying the mean IC50 with the various treatments in 1A9 and PTX10. The IC50 units are nM for PTX and DTX, and μM for LNF and FTI-277. Values are a mean ± SE.* ***B and C)*** *Combination index (CI) analysis is plotted as a function of fractional cell growth inhibition (FA) in 1A9 paclitaxel-sensitive cells* ***B)*** *and PTX10 taxol-resistant cells* ***C)****. A CI > 1 indicates antagonism, ~1 is additivity, and <1 is synergy. The mean combination index on each graph and a p-value determining significance compared to a CI of 1, are also shown.*

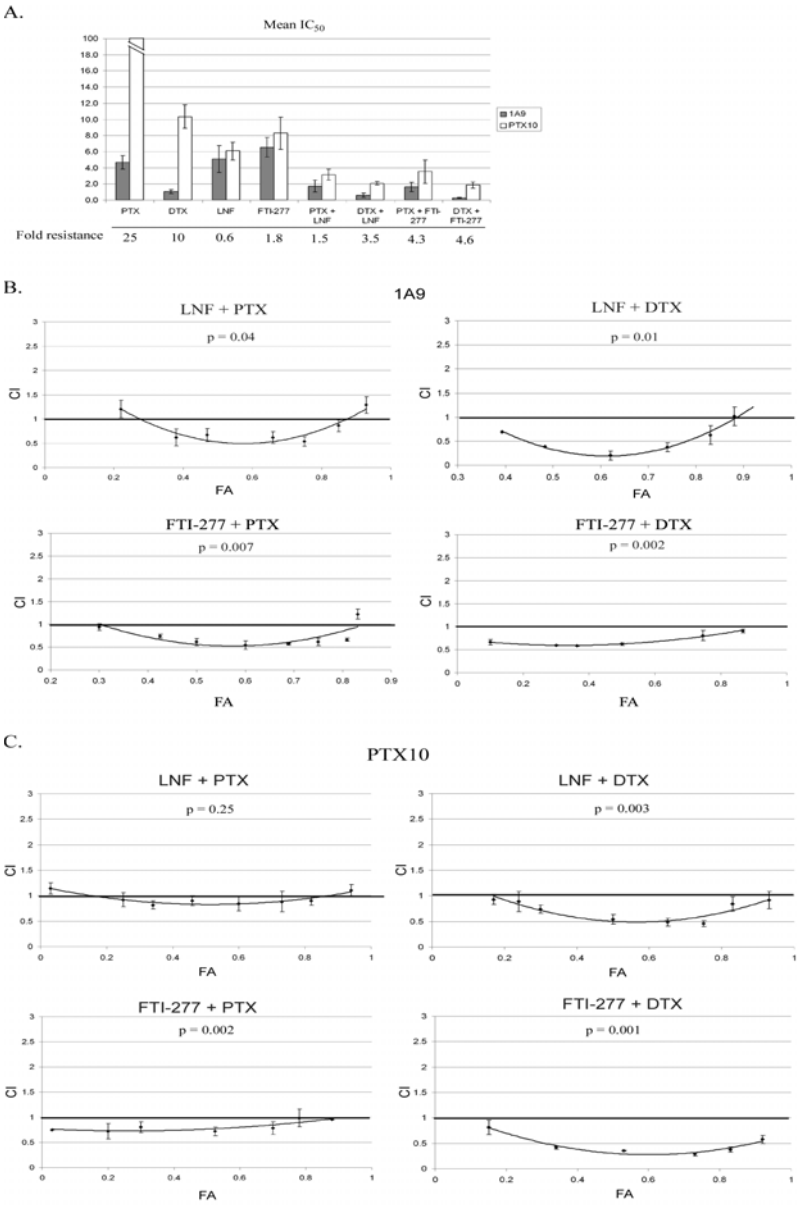

Figure 42. The FTI/PTX combination enhances apoptosis and mitotic arrest in paclitaxel-sensitive and –resistant cells. A) *Western blot assessing apoptosis using an antibody to the apoptotic marker, PARP p85. Both 1A9 (top blot) and PTX10 (bottom blot) cells were treated for 30 hr with varying doses of PTX and an FTI, both alone and in combination. Tubulin is used as a protein loading control.* ***B)*** *A bar graph showing the percentage of 1A9 cells in mitosis after the various treatments for 16 hr. Values are a mean ± SE and asterisks show values that are statistically significant from control (P< 0.05)* ***C)*** *A bar graph showing the percentage of PTX10 cells in mitosis after the various treatments for 16 hr. Values are a mean ± SE and asterisks show values that are statistically significant from control (P< 0.05)* ***D)*** *Confocal images of mitotic 1A9 and PTX10 cells with an antibodies against tubulin (red) and a DNA stain (green). Cells were treated for 16 hr with LNF and PTX, both alone and in combination. Scale bar is 10 µm.*

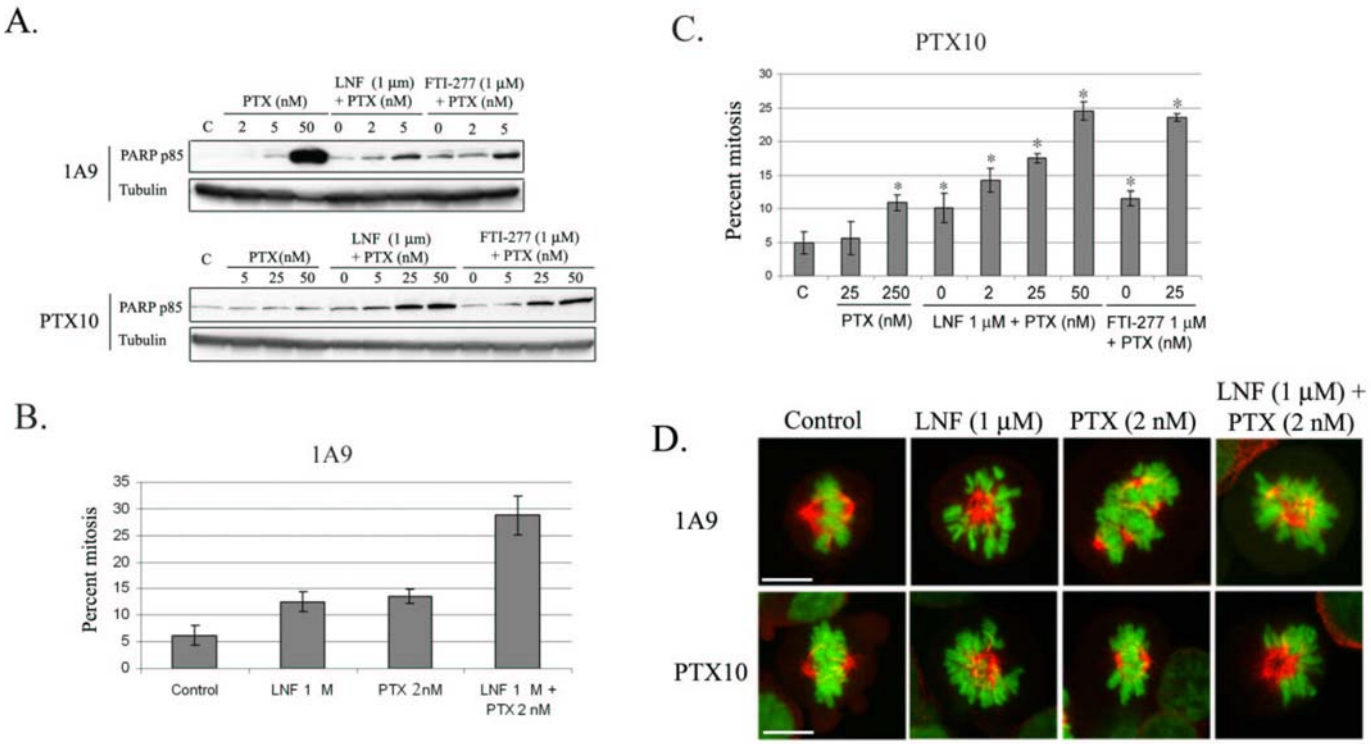

Figure 43. FTI treatment increases the affinity of Flutax for the microtubule. ***A)*** *Live cell imaging of Flutax fluorescence in 1A9 and PTX10 cells treated for 16 hr with the various drug combinations. The left column shows cells treated with Flutax alone at 75 nM or 750 nM for 1A9 and PTX10, respectively. The same cell lines were treated with Flutax (same doses as in left-hand column) and LNF or FTI-277 (both at 1 μM). Scale bar is 10 μm* ***B)*** *A549 cells were treated for 16 hr with either 75 nM Flutax or Flutax in combination with LNF or FTI-277 (both at 1μM). Scale bar is 10 μm.* ***C)*** *Bar graphs displaying the average pixel intensity of at least ten thresholded images of each cell line treated with Flutax alone or Flutax with an FTI. Values are means ± SE and asterisks show values that are statistically significant from treatments with Flutax alone (P< 0.05)* ***D)*** *Western blot of HDJ-2 farnesylation. Top band represents non-farnesylated HDJ-2 (n) and the bottom band is farnesylated HDJ-2 (f). Actin is shown as a loading control.* ***E)*** *Live-cell imaging of Flutax fluorescence in PTX10 cells treated for 16 hr with either Flutax alone (750 nM) or Flutax plus the inactive LNF enantiomer, SCH66337 (1 μM).* ***F)*** *Microtubule stability assay showing a western blot of tubulin either in the pellet (P) or supernatant (S) fraction in both 1A9 and PTX10 cells with the indicated treatments.*

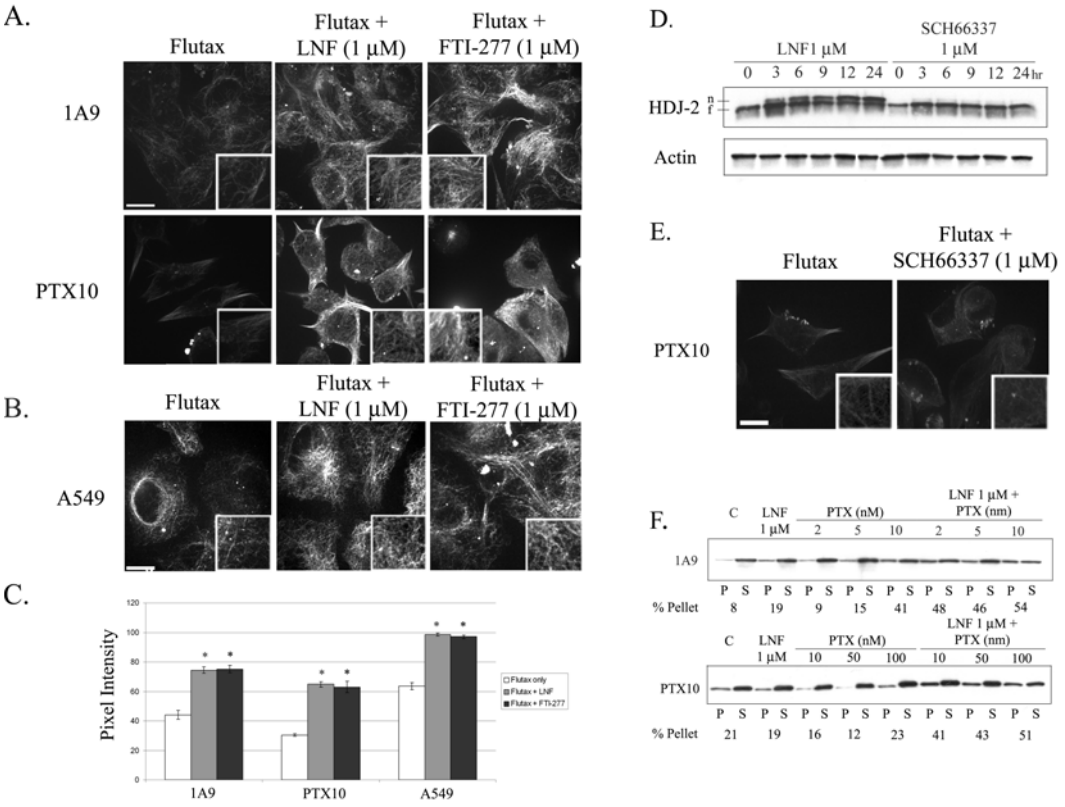

Figure 44. HDAC6 functionality is required for FTIs to enhance the affinity of taxol for the microtubule. ***A)*** *Live cell imaging of Flutax fluorescence in HDAC6-WT and HDAC6-mut cell lines. Cells were treated for 16 hr with Flutax alone (75 nM; left hand column) or Flutax (75 nM) plus LNF (1μM; right hand column).* ***B)*** *Bar graphs displaying the average pixel intensity of at least ten thresholded images of each cell line treated with Flutax alone or Flutax and LNF. Values are means ± SE and asterisks show values that are statistically significant from treatments with Flutax alone ($p < 0.05$).*

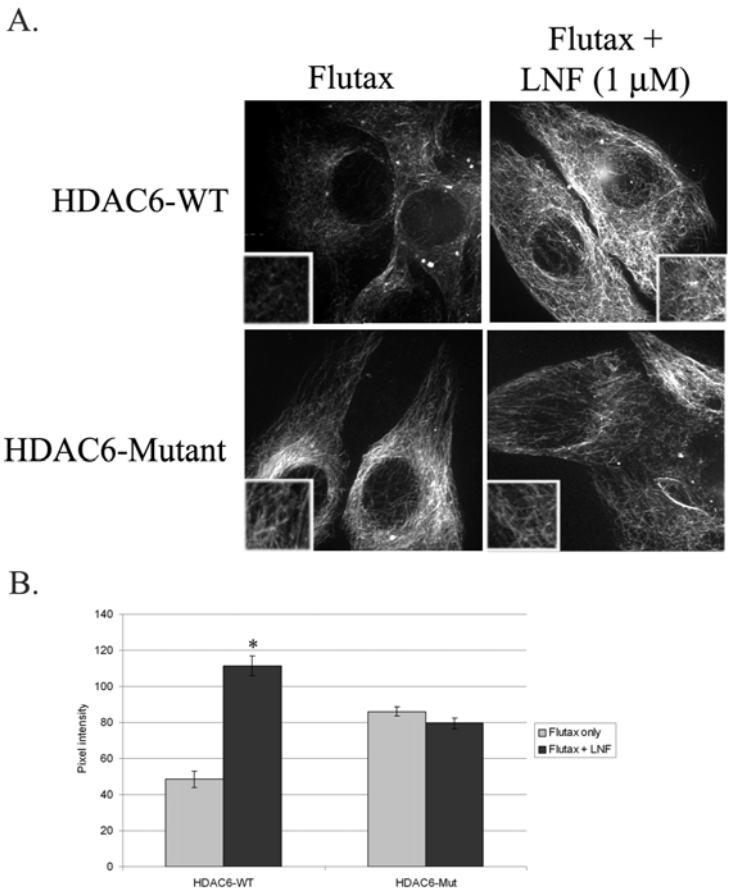

Discussion:

Analyzing the effects of LNF as a single agent on microtubules. The farnesyl transferase inhibitors were developed as targeted therapies against cancers with oncogenic Ras mutations, however, FTIs were shown to retain their activity independently of Ras status(278, 280) Here we examined the effects of the FTI, lonafarnib (LNF), on interphase microtubules in human cancer cells. Our results demonstrate that prolonged exposure (48 hr) to LNF alone leads to microtubule stabilization as evidenced by increased tubulin acetylation, and bundle formation (**Figures 37-38**). Since tubulin acetylation is an established marker of microtubule stability (283), we believe that the LNF-induced microtubule stabilization may contribute to its anti-proliferative effects, similar to the taxanes and epothilones.

However, it is important to note that the microtubule-stabilizing capacity of LNF is weak relative to other established microtubule stabilizing agents, which stabilize microtubules at low nanomolar concentrations. This suggests that the mechanism by which LNF induces microtubule stabilization may differ from traditional microtubule-stabilizing agents (e.g. the taxanes).

Microtubule acetylation and the mechanism of synergy between LNF and the taxanes. Previous reports have shown that FTIs synergize with taxanes and epothilones in a variety of human cancer cell lines *in vitro* and *in vivo* (278-280); however, the mechanism underlying this synergy is unknown. Our results show that the combination of low doses of LNF (beginning at 0.5 μM) and paclitaxel (2nM) resulted in a dramatic increase in tubulin acetylation (**Figure 38A-C**), compared to untreated cells or each drug treatment alone. Importantly, the mean C_{max} of LNF achieved in patients dosed twice daily with 200 mg of LNF is 4.4 μM (unpublished) and therefore the doses (LNF beginning at 0.5 μM) at which we observed synergistic enhancement of acetylated tubulin are within the C_{max}.

Furthermore, the effect of LNF/PTX on acetylated tubulin was observed in as little as 3 hr of drug treatment (**Figure 39**) and preceded the synergistic increase in mitotic arrest (**Figure 38C, 39B**), suggesting that increased microtubule acetylation/stability is associated with aberrant mitotic arrest and cell death. Nevertheless, it remains unclear if

LNF/PTX induced microtubule acetylation only serves as marker for cell death or instead is the catalyst, and therefore studies are underway addressing this issue.

Mechanistically, we show that the synergistic increase in microtubule acetylation is due to the effect of the combination of LNF and paclitaxel on the tubulin deacetylase HDAC6 (**Figure 40**). We propose that the enhanced tubulin acetylation we observe is due to the inhibition of HDAC6 function. We provide four lines of evidence to support this claim. First, we show that the combination of LNF and paclitaxel inhibit HDAC6 tubulin deacetylating activity *in vitro,* whereas either drug alone had no effect (**Figure 40A**). Second, we can reproduce the LNF/paclitaxel-induced increase in tubulin acetylation by using tubacin, a specific HDAC6 inhibitor, in combination with paclitaxel (**Figure 40B**). This suggests that pharmacologic inhibition of HDAC6 in combination with paclitaxel synergistically increases tubulin acetylation. Third, cells expressing a catalytically inactive HDAC6 (HDAC6-mt) fail to show an increase in acetylated tubulin when LNF and paclitaxel are combined (**Figure 40C**), suggesting that this drug combination requires functional HDAC6 to retain efficacy. Fourth, the robust cytotoxic synergy of LNF and docetaxel is lost in these cells expressing mutant HDAC6, whereas potent synergy remains in their wild type HDAC6 counterparts (**Figure 40D**). This observation provides evidence that the deacetylating activity of HDAC6 is required for the LNF/taxane synergy, providing a mechanistic link between functional HDAC6, tubulin acetylation and cell death. However, it is still unknown whether the effect of the LNF/taxane combination on HDAC6 function is due to direct binding of these drugs to this enzyme or due to their effects on microtubule stability, which in turns alters the affinity of HDAC6 for the microtubule. We favor the latter scenario, since either drug alone does not alter HDAC6 function, reducing the likelihood that these drugs bind HDAC6 directly.

Is there a biological link between FTase inhibition and microtubule acetylation?

Since all FTIs tested to date synergize with paclitaxel, it is likely that they share a common mechanism of synergy related to farnesyl transferase inhibition. In Fig. 4A, we show that the increase in tubulin acetylation observed with the low dose LNF/paclitaxel combination, correlates with farnesyl transferase inhibition. This result suggests that inhibition of farnesyl transferase may be biologically linked with enhanced tubulin

acetylation. Currently, there are no reports of a link between the FTase enzyme and interphase microtubules.

Preliminary data from our laboratory in 50 human cancer cell lines used in the NCI Anticancer Drug Screen (http://dtp.nci.nih.gov) have revealed that acetylated tubulin protein levels negatively correlated with FTase gene expression and protein levels (COMPARE analysis http://itbwork.nci.nih.gov/CompareServer/CompareServer; unpublished data). Thus, it may be possible that proteins regulating microtubule stability are farnesylated by FTase; consequently, inhibition of FTase by LNF may in turn affect microtubule stability. In fact it is already known that the mitotic microtubule associated protein, CENP-E, is farnesylated and its association with microtubules during mitosis is altered in mitotic cells (281). Thus, further investigation of a putative link between FTase and interphase microtubules is warranted.

The FTI/Taxane combination has shown potent anti-proliferative synergy in cell lines and pre-clinical models (115, 142). Results from a phase I (286) and Phase II clinical trial (unpublished) in solid tumors showed that a subset of patients previously refractory/resistant to Taxol, still responded to LNF/Taxol combination, suggesting that combining Taxol with an FTI may reverse acquired taxol resistance. Our data supports this hypothesis and shows that in Taxol-resistant cells the FTI/taxane combination retains potent anti-proliferative and anti-mitotic activity (**Figure 41, 42**). We observed this with all FTI tested, but not the inactive LNF enantiomer, suggesting that this mechanism is FT-dependent. We believe there are at least two possible explanations for this occurrence. First, since our cell lines are taxol-resistant due to a mutation in the M40 allele β-tubulin in the taxol binding pocket, taxol is thought to have a low affinity for the microtubule (286); therefore it is possible that the high levels of free taxol (i.e, the Taxol that is not bound to the microtubule) has a weak affinity for a non-microtubule substrate, which is enhanced when an FTI is present. This off-target effect of taxol in combination with an FTI could then lead to the observed synergy in the taxol-resistant cells, and possibly even taxol-sensitive cells, albeit the percentage of free taxol would presumably be less. Although we cannot rule out this possibility, the scenario seems unlikely since we observed enhance microtubule stability in the drug combination (**Figure 43F)** and increased mitotic arrest (**Figure 42**), both of which are associated with a microtubule-

targeting effect. Furthermore, anti-proliferative synergy (286) and enhancement of taxol binding by an FTI (**Figure 44**) is dependent on the functionality of the tubulin deacetylase, HDAC6, which is intimately associated with microtubule function.

An alternative possibility is that FTIs increase the affinity of taxol for microtubules in both taxol-resistant and sensitive cells, resulting in increased microtubule stability and subsequent mitotic arrest and cell death. Our results support this scenario since we show in Figure 3 that FTIs increase the amount of Flutax bound on the microtubule and that the drug combination leads to a synergistic increase in microtubule stability, in both taxol-resistant and –sensitive cells. Furthermore, in Figure 41 and 42 we show that the drug combination also enhances mitotic arrest and cell death, again in both taxol-resistant and –sensitive cells. Thus, the ability of FTIs to induce taxol binding on the microtubule may enhance microtubule stabilization consequently precluding normal bipolar spindle formation. As a result, the cell arrests in mitosis and eventually undergoes apoptosis.

Although this scenario is possible, the question still remains, how would FTIs increase taxol's affinity for the microtubule, especially in taxol-resistant cells? It is already known that Taxol has greater affinity for the microtubule polymer over the tubulin dimer (74, 249, 292-294), thus it is possible that FTI's induce microtubule polymer formation themselves, leading to an increased affinity of taxol for the polymerized microtubules. In fact, it was previously shown that longer exposures to FTIs (48hr) suppress microtubule dynamics, induce bundle formation, and increase microtubule stability (9, 128), and causes extensive microtubule networks in K-*ras* transformed NRK cells (295); therefore, in these relatively shorter time periods of FTI treatment (16hr), FTIs may have a subtle but significant affect on microtubule polymer formation, resulting in an increased affinity of taxol for the microtubule. Thus, in the taxol-resistant cells, the inability of taxol to bind to the microtubule is overcome, at least in part, by FTI-induced microtubule polymer formation, resulting in an increase in taxol's affinity for the microtubule.

Importantly, we believe that the ability of FTIs enhance Flutax binding on the microtubule is dependent of FT inhibition, since all FTI tested retain this property, except

for the inactive LNF enantiomer SCH66337 (**Figure 43D-E**). Thus, perhaps, FT inhibition has a downstream effect on microtubule function. It is already known that the microtubule-associated proteins CENP-E and CENP-F are farnesylated (284, 296) as well as CNP, a membrane-associated microtubule binding protein that promotes microtubule assembly (297, 298). Therefore, there could be an intermediary event whereby inhibition of farnesylation alters microtubule dynamics. One key player in this scenario could be the tubulin deacetylase HDAC6, which we show is critical for LNF/taxane synergy; however, the consensus FT targeting motif (CAAX) is not found on HDAC6. Nevertheless, it still remains possible that an upstream farnesylation event could downregulate HDAC6 activity (leading to increase microtubule acetylation) and consequentially effect microtubule stability. In fact, we have previously shown that the combination of LNF and taxol inhibits HDAC6 activity, in vitro, leading to increased tubulin acetylation (299).

These studies support clinical data showing that the FTI/Taxane combination is effective in taxol-resistant cells and can potentially impact the design of future clinical trials in Taxol-resistant/refractory patients. The mechanism by which taxane resistance occurs in the clinic is still under debate (61); however overcoming taxane resistance by combining it with an FTI could prove useful in the treatment of several solid tumors. Still, another challenge would be to determine in which patients this treatment would prove beneficial; thus our future experiments will focus on determining which molecular markers (e.g. HDAC6, basal acetylated tubulin levels) could predict response to drug treatment with the FTI/taxane combination. Overall, these results provide a putative mechanism of synergy between FTIs and taxanes in both taxol-resistant and –sensitive cancer cells. Thus, FTIs in combination with taxanes will likely prove to be a beneficial chemotherapeutic strategy, especially in patients resistant/refractory to taxol alone.

MATERIALS AND METHODS FOR OBJECTIVE 4

Materials and Methods for Farnesyltransferase Inhibitors

Cell Culture --The human non-small cell lung cancer cell lines, A549 and H1299, were maintained in RPMI 1640 supplemented with 5% fetal calf serum, nonessential amino acids and 0.1% penicillin/streptomycin at 37°C in 5% CO2. Live cell microscopy was performed with MCF-7 breast cancer cells stably transfected with GFP:α-tubulin and maintained in DMEM supplemented with 5% fetal calf serum, nonessential amino acids and 0.1% penicillin/streptomycin.. All lines were cultured at 37°C in a humidified atmosphere with 5% CO2. NIH-3T3 cells expressing various HDAC6 constructs were previously generated ((115, 142)) and were cultured in DMEM medium under the same conditions.

Reagents

Lonafarnib (SCH66336) was provided by Schering Plough Research Institute (Kenilworth, NJ). FTI-277 was purchased from EMD Biosciences, Inc (San Diego, CA). Both FTIs were dissolved in dimethyl sulfoxide (DMSO) at a concentration of 10 mM, and aliquots were stored at -80˚C. Stock solutions were diluted to the desired final concentrations with growth medium just before use.

Immunofluorescence analysis --Immunofluorescence microscopy was performed as previously described ((115, 142)). Cells were fixed in PHEMO buffer (68 mM PIPES, 25 mM HEPES, 15 mM EGTA, 3 mM MgCl2, 10% DMSO) with 3.7% formaldehyde, 0.05% glutaraldehyde, 0.5% Triton X-100. Cells were washed in PBS 3 times for 5 minutes then blocked in 10% goat serum for 15 minutes. The following primary antibodies were used: α-tubulin (Chemicon International, MAB1864; 1:500 dilution) and acetylated tubulin (Sigma T-6793, dilution 1:1000) with incubation times of 1 hr. The secondary antibodies used were Alexa 563 conjugated goat anti-rat IgG (1:500); Alexa 488 conjugated goat anti-mouse IgG antibody (1:500), both from Molecular probes. Cells were imaged using a Zeiss LSM 510 Meta (Thornwood, NY) confocal microscope using a either a 63X (N.A. 1.4) or 100X (N.A. 1.4) Apochromat objective. To stain DNA for

mitotic cell counting, we fixed cells as described above, and added Sytox Green (Molecular Probes; #S7020) to the Gel Mount mounting media (Biomeda Corp; Foster City, CA). All images were acquired using Zeiss LSM 510 software and processed in Adobe Photoshop 7.0

Cell tubulin polymerization assay --Quantitative drug-induced tubulin polymerization was performed as previously described(299). The percent pellet (%P) is calculated as the amount of polymerized tubulin (P), over the total amount of polymerized and soluble tubulin (P+S) times 100 {P/(P+S) x 100} based upon densitometric analysis.

FLOW cytometry analysis--To determine acetylated tubulin levels, cells were plated and on the following day treated with different concentrations of the drugs for 16 hr. After drug treatment, cells were fixed with PHEMO buffer for 10 minutes as previously described (300) and stained with an antibody against acetylated tubulin (1:500; Sigma T-6793) followed by secondary Alexa 488 goat anti-mouse IgG antibody (1:500). Finally, cells were scraped into 1 ml of PBS, and FLOW cytometry analysis was performed on a Becton Dickinson FLOW cytometer.

For cell cycle analysis, cells were scraped from plates, centrifuged at 1000 rpm for 5 minutes, and propidium iodide buffer containing 0.1 mg/ml propidium iodide and NP-40 (0.6%) in water was used to resuspend cells. Cell were incubated in this buffer for 30 minutes at room temperature in the dark, then passed through a filter to remove cell clumps and finally read in a Becton Dickinson FLOW cytometer

***In vitro* acetylated tubulin assay --**A549 cells were transiently transfected with Flag-tagged pBJ5-HDAC6 expression plasmids using FuGene (Roche) following the manufacturer's guidelines. Untransfected cells or cells transfected with an empty vector were used as controls. In Figure 6F, we used NIH-3t3 cells stably expressing FLAG tagged HDAC6-wt and HDAC6-mt proteins and therefore cells did not have to be transfected. Cell lysates were prepared 48 hours after transfection and then immunoprecipitated with anti-Flag M2 agarose beads (Sigma- FLAGIPT1). Tubulin acetylation assays were performed by incubating the immunoprecipitates with preformed MAP-stabilized microtubules at 37 oC, along with the appropriate drug, for 2 hours as described previously (301, 302). Reactions were then placed on ice for 15 minutes and centrifuged briefly at 14, 000 rpm to separate the supernatant from the agarose beads. The

supernatant was analyzed by Western blotting with antibodies against acetylated α-tubulin and against α-tubulin (as described below) and the beads were analyzed with an antibody against Flag M2 (Sigma- F3165; 1:1000).

Western blotting --Cells were plated in 6-well plates at 50% confluency and treated the next day with the appropriate drug and time interval. Cells were lysed, centrifuged at 15,000 rpm for 15 min, and electrophoresed on a 7.5% SDS-PAGE gel (BCA assay was used to determine protein concentration in a spectrophotometer). Proteins were transferred to a PVDF membrane (100V for 1 hr) using a Bio-Rad transfer apparatus and blotted with antibodies against acetylated tubulin (Sigma T6793; 1:1000), total tubulin (Sigma DM1α, 1:1000), HDJ-2, acetylated histone H3 (Cell Signaling; at 1:1000), actin, and HDAC6 (1:1000; Cell Signaling #2162).

Cell survival and Synergy Assays (Combination Index Analysis)-- Cells were plated in a 96-well plate at 2,000 cells/well and allowed to attach overnight. Cells were then treated with serial dilutions (1:3) of either LNF alone, PTX alone, or the combination of LNF and PTX for 72 hr. Cell were then fixed with 50% tri-chloro acetic
acid (TCA) for 30 min, washed 3 times with water, dried, and stained with 0.4% sulfurhodamine B (SRB; protein stain) for 30 min. Cell were then washed with 0.1% acetic acid, air dried, and the bound SRB was dissolved with 10mM unbuffered TRIS base (pH= 10.5). The plates were read in a microplate reader (OD564) and synergy was determined using CalcuSyn software, which calculates the combination index (CI) based upon the percent cell survival at vary doses of the drug treatments, both alone and in combination. A CI greater than 1 indicates antagonism, equal to 1 is additivity, and less than 1 is synergism.

Live-cell Flutax binding studies

Flutax was kindly provided by Dr. Fernando Diaz (CNEO Madrid, Spain). Cells were plated on live cell imaging chambers from World Precision Instrument (#500820) overnight. Prior to use Flutax was diluted to the proper concentration in media and centrifuged at 14K rpm in an Eppendorf 5415C centrifuge for 10 minutes. Cells were treated with Flutax or Flutax/FTI for 16 hr at the doses indicated. After treatment, the cells were washed 3X in PBS and a new media was added to the cells. Cells were imaged

using a Perkin Elmer Ultraview ERS spinning disc confocal microscope. This system was mounted on a Zeiss Axiovert 200m inverted microscope equipped with a 37 degree stage warmer, incubator, and CO_2 perfusion. A 63X or 100X Zeiss Apochromat oil objective (N.A. 1.4) was used for all images a Z-stack was created using the attached piezo electric z-stepper motor. The 488 nm laser line of an Argon ion laser (set at 60% power) was used to excite the Flutax and emission was detected with a Hamamatsu Orca-ER camera with exposure time from 200-400 ms. For each comparison, the exposure time and laser intensity was identical for accurate intensity measurement. Pixel intensity was quantitated using Metamorph 8.0 (Universal Imaging, Downingtown PA) by first thresholding the image and then calculating the mean pixel intensity using the Region Statistics feature on the software.